ISOTOPIC CHARACTERIZATION OF GROUNDWATER RECHARGE AND FLOW IN AN UPLAND BEDROCK AQUIFER, VERMONT

Thesis Presented

by

Michael David Abbott

to

The Faculty of the Graduate College

of

The University of Vermont

In Partial Fulfillment of the Requirements
for the Degree of Master of Science
Specializing in Geology

May, 1997

Accepted by the Faculty of the Graduate College, The University of Vermont, in partial fulfillment of the requirements for the degree of Master of Science, specializing in Geology.

Thesis Examination Committee:

Paul R. Bierman, Ph.D. — Advisor

Andrea Lini, Ph.D. — Co-Advisor

Stephen F. Wright, Ph.D. — Co-Advisor

David E. Dougherty, Ph.D. — Chairperson

Delcie R. Durham, Ph.D. — Dean, Graduate College

Date: March 14, 1997

ABSTRACT

This study characterizes groundwater flow and recharge mechanisms in an upland fractured bedrock aquifer. From July, 1995 to December, 1996, samples of rain, snow, meltwater and groundwater were collected on a weekly basis in the upper watershed of the Browns River, northwestern Vermont. The head of this basin is near the summit of Mount Mansfield (1339 m asl). The lowest point in the basin is near the town of Underhill Center (250 m asl). Groundwater was collected from residential wells and springs, most located between 250 m asl and 450 m asl, with the exception of a spring high on the slopes of the mountain, at 650 m asl. More than one thousand samples were analyzed for oxygen isotopic composition ($\delta^{18}O$). One hundred samples were analyzed for δD (deuterium) composition, and a group of nine groundwater samples, collected in June of 1996, were analyzed for ^{3}H (tritium) abundance.

Several trends were observed in the temporal $\delta^{18}O$ composition of precipitation and groundwater. Mean annual precipitation $\delta^{18}O$ values in the basin were depleted by 2.5 per mil (‰) per 1000 m gain in elevation. Annual precipitation $\delta^{18}O$ ranged over 25 ‰. Groundwater $\delta^{18}O$ was less variable. Most wells varied annually within 2 ‰, with the exception of the high spring, which varied over a range of 4.3 ‰. The mean $\delta^{18}O$ composition of each well and spring was used to estimate the locations of the upland recharge zone for each well.

Measurements of $\delta^{18}O$ in groundwater revealed that the nature of recharge to bedrock changes with elevation and season. The $\delta^{18}O$ record for the high spring mimicked the seasonal variations in precipitation $\delta^{18}O$. However, the least depleted measurements were from samples collected in September, two months after the warmest time of year, indicating a groundwater residence time in the order of 2 months above the high spring. The other wells varied significantly in their $\delta^{18}O$ composition only during the colder months (late November to early April). During the warmer months, the $\delta^{18}O$ record in these wells was very uniform, varying within a range of less than 0.4 ‰ for each well. This suggests that increased rain interception and soil water uptake by trees and other vegetation in the basin significantly reduces recharge at lower elevations during the warmer months. The stable isotopic signature of winter groundwater represents deeper, well-mixed groundwater recharged at higher elevations. The high spring does not exhibit this stable period, probably because it is located much higher in the basin than the other wells, in a relatively sparse coniferous forest typically exposed to colder temperatures.

A system dynamics model was developed in order to quantify the effects of mechanisms affecting recharge to bedrock temporally and spatially in the watershed. Use of this model with the $\delta^{18}O$ records as calibration tools, led to the derivation of equations describing recharge to bedrock. These equations incorporate all of the mechanisms influencing recharge (precipitation, melting, evaporation, vegetative uptake) and describe changes in the interrelationships of these mechanisms with elevation and season.

ACKNOWLEDGMENTS

This thesis is dedicated to my grandfather, Willard Abbott, who passed away during the course of my research. One of the last things he said to me was, "People are the stupidest goddamned things on the face of the earth." This is one of the reasons why the availability of clean drinking water is now a very important issue to all of us.

I would like to thank all those who aided in and supported my work on this project. This includes everyone in the Geology Department. Thanks for your interest and ideas contributed throughout the study. I want to extend special thanks to my project advisors, Paul Bierman, Andrea Lini and Stephen Wright, and the Chairman of my thesis defense, David Dougherty from Civil Engineering. Your reliable guidance has been truly valuable. My apologies to Andrea for all the laboratory equipment that I managed to break. Also, thanks to Rolfe Stanley, for his direction in the system dynamics modeling, which turned out to be a major part of this thesis. But I still don't know who Stella is (with apologies to Tennessee Williams).

Several people, geologists and others, helped at various times with my fieldwork and laboratory analysis. These included (in alphabetical order) David Abbott, Linda Abbott, Darlene Autery, Sarah Bentil, Maureen Carr, Peter Gillingham, Jen Levesque, Brenda Mahnken, Laura Mallard, Kim Marsella, Kathy McCosh, and David Shaw.

Thanks to Sandra Wilmot, Vermont Agency of Natural Resources, and Tim Scherbatskoy, UVM School of Natural Resources, for coordinating the sampling program in the Mount Mansfield State Forest, and for all members of the Vermont Monitoring Cooperative for their contributions and for sharing their research in the area. Thanks to the rangers on Mount Mansfield for helping me find appropriate locations for setting rain and snow collectors.

Thanks to Jamie Shanley, USGS, Ken Hardcastle, Emery and Garrett Groundwater, Inc. and many others for sharing their ideas, especially folks at the GSA and AGU meetings who attended presentations of this work and provided valuable input.

Thanks to Eric Steig and Bruce Vaughn, at the Institute for Arctic and Alpine Research (INSTAAR) for running the deuterium samples on such short notice. Thanks also to Waterloo labs for tritium measurements.

Many, many thanks to the residents of Underhill for allowing me to install rain and meltwater collectors in their backyards, or collect groundwater samples every week from their faucets. I will remember your hospitality and your dogs.

Thanks to Sevee & Maher Engineers, Inc. for not shunning me when I became a long-haired student, and for the advice you provided. But I am not cutting my hair.

Thanks to Beth Nadeau for emergency printing and software services.

Thanks to Adrian (and indirectly to Tracy and Andrea) for the song.

Thanks to Mount Mansfield for not killing me.

Thanks to my family and friends for their support.

Thanks to Kathy for her love and patience.

Funding for this project was provided by the United States Geological Survey and the University of Vermont.

It's been three weeks or more since I've seen the sun
It seems like even longer since I've talked to anyone
Do you think about me when you're all alone
Do you see my face in the clouds when you climb a mountain of your own

Everybody's a Wierdo

TABLE OF CONTENTS

LIST OF TABLES

LIST OF FIGURES

CHAPTER I

INTRODUCTION

Upland bedrock aquifers in New England represent, in some cases, the cleanest sources for drinking water supplies. This is due to limited development of the uplands, and thus a lower exposure to common pollutant sources. In addition, precipitation is typically greater at the higher elevations, providing a larger potential source for recharge to the bedrock. In terms of planning for future water supply development, knowledge of the variability of recharge mechanisms, and the time scale of groundwater flow through the aquifers, is needed. Recent work undertaken in New England that attempts to characterize groundwater flow in upland fractured bedrock aquifers includes several projects at the Mirror Lake Research Station in New Hampshire (Barton, 1993; Drenkard et al., 1993; Harte and Winter, 1993; Hsieh and Shapiro, 1993; Shapiro and Hsieh, 1993; Shapiro et al., 1993). These studies and other recent work in New England (Hardcastle et al., 1989; Mabee et al., 1990) have affirmed that the mechanisms of recharge and flow of groundwater in these aquifers can be quite complex. This is due in part to the fact that rocks do not exhibit uniform fracture networks. Therefore, methods that have been developed to evaluate water resources in unconsolidated materials (i.e., sand and gravel) are not always applicable. The rate of recharge is difficult to predict, and rates of groundwater flow through the complex hydrogeologic network created by rock fractures can vary over many orders of magnitude within a small area.

In the area chosen for this study, the upper basin of the Browns River Watershed in Northwestern Vermont, the rock type, topography, weather patterns, and vegetative

distribution produce a regime of recharge and flow mechanisms unique to New England. This study is an attempt to characterize the temporal and spatial distribution of recharge to bedrock through isotopic characterization of precipitation and groundwater. Weekly samples of rain, snow, meltwater, and groundwater were collected over an 18 month period in order to observe changes in the stable isotope composition ($\delta^{18}O$ and δD) of water over time. Radiogenic isotope measurements (^{3}H) were also made to infer residence times of water in the bedrock. This information was incorporated into a system dynamics model to simulate temporal recharge and flow processes in the basin, using the $\delta^{18}O$ well records as a calibration tool. Equations were developed to describe recharge mechanisms according to elevation and season. These equations may be used to model hydrologic systems in this and similar upland watersheds, providing a tool for planning of water supply development in these settings.

This study began in June, 1995 under a USGS Vermont Water Resources grant. Field collection of samples started in July, 1995 and continued through December, 1996. This chapter contains a detailed description of the chosen study area and a discussion of issues related to water supply management in this and other similar upland watersheds. A discussion of how results of this work may be applied is also provided.

Geographic Location and Regional Watershed

This section contains a description of the watershed chosen for this study, the upper basin of the Browns River in Northwestern Vermont (44°30' latitude and 72°50' longitude). The approximate area of the watershed chosen for this study is 10.5 km^2. The

lowest elevation within the watershed, located just east of the small town of Underhill Center, is 250 m above mean sea level (asl). The highest point in the basin is near the summit of Mount Mansfield (1339 m asl). The north-south trending ridge of the Mount Mansfield, containing the Chin, Nose, and Forehead summits, creates the eastern border of the watershed. Sunset Ridge, a ridge extending westward from the Chin, is the northern divide. Several small, unnamed tributaries drain the upper slopes of the mountain, feeding into the main branch of the Browns River (Figure 1.1). Near Underhill Center, the Browns is joined by Clay Brook and Stephensville Brook, which drain the two watersheds lying to the south, adjacent to the study basin. Downstream from Underhill Center, the Browns River flows generally west through Underhill and Jericho, intercepting several larger tributaries, including the Creek and Roaring Brook, both flowing from the north. In Jericho, the Lee River flows from the east into the Browns River. Downstream from Jericho, the Browns River turns North and drains into the Lamoille River near the town of Fairfax. The Lamoille discharges into Lake Champlain at Mallets Bay, southwest of Milton, Vermont.

The topography of the study basin is controlled largely by bedrock structure at higher elevations. More substantial sediment deposits at the lower elevations (below 350 m) control the landscape in the valley. Land use in this basin is largely residential with a few small farms, and Underhill State Park in the Mount Mansfield State Forest. Most of the watershed is forested, except for sections above treeline on the mountain ridges and summits, and some land cleared for farming and residential purposes.

Bedrock Composition and Structure

The bedrock in portions of the study area was mapped by Christman (1959) and by Christman and Secor (1961). Later mapping was begun by Thompson and Thompson (1991) and is ongoing (Thompson, 1997, pers. comm.). The entire basin lies within the mapped limits of the Underhill Formation of the Camels Hump Group (Christman, 1959). This formation consists of predominantly chlorite-quartz-muscovite to quartz-albite-muscovite phyllite and schist, with lenses of amphibolitic and feldspathic greenstone. Material was originally deposited and cemented as fine-grained graywacke, siltstone and shale in a Cambrian shelf. Minor amounts of volcanic, calcareous, and carbonaceous material are incorporated. Principal deformation and metamorphism occurred during the Taconic Orogeny in the Late Ordovician. Acadian (Middle or Late Devonian) deformation is believed to be minor in the area (Stanley and Ratcliffe, 1983; Roy and Skehan, 1993). These rocks thrust from east to west during the Taconic Orogeny and later folded into a broad anticlinal arch known as the Green Mountain Anticlinorium. Mafic lava and volcanic detritus were metamorphosed to greenstones. The bulk of the sediments, greywacke and siltstones, were metamorphosed to principally phyllite and schist. The north-south ridge of Mount Mansfield coincides very closely with the aniticlinorium axis which plunges gently to the south. Schistosity in rocks west of the ridge dips generally to the west, whereas schistosity in rocks east of the ridge dips generally to the east. The anticlinorium is slightly overturned to the west as indicated by drag folds and fracture cleavage.

The typical schist of the Underhill Formation is light to dark gray, but may appear in variations of silver-gray or greenish depending upon the amounts of mica or chlorite

present (Christman, 1959). Schistosity is well developed and folded throughout the rock. Lenses of milky quartz, derived locally during metamorphism, are aligned with the schistosity. Small scale folding is evident in these lenses. Larger concentrations of quartz occur in fractured areas and may contain small amounts of bright green chlorite. Garnet is present in much of the rock on the upper slopes and summit of Mount Mansfield, an indicator of higher grade metamorphism in the area of the anticlinorium.

The schistosity is defined by the parallel orientation of mica and chlorite, and is especially strongly displayed at outcrops high on the mountain. Lenses of the original bedding are parallel to the schistosity. The average strike of schistosity is N10°E, except along the crest of the anticlinorium where minor folds cause the schistosity planes to deviate from the general trends. Small and large scale folds also trend approximately north-south (Christman, 1969). A spaced cleavage is axial planar to the anticlinorium. Typically, this feature cross-cuts the earlier schistosity and is only faintly developed in rocks with well developed minor folds, but is observed in rocks east of the anticlinorium as a crinkle lineation on the schistosity surface. Fracture cleavage and minor drag folds along the anticlinorium are essentially parallel to the axial planes of the major folds (Christman, 1959).

The orientation of joints in the rock is of particular importance to the study of groundwater flow in the bedrock aquifer. Three predominant joint directions were identified along the north-south ridge of Mount Mansfield by Christman (1959): 1) a vertical north-south set, 2) a N30°E set dipping 75°NW, and 3) a vertical N80°E set. The north-south joints form many of the cliff faces, accentuated by the plucking action of

Pleistocene glaciers. Some joints, away from the faces, have been enlarged by downhill creep or frost action. Sheeting joints parallel to the land surface and generally parallel to the foliation in the rock, were also observed in cliff faces.

As part of this study, measurements of fracture orientations were conducted at outcrops throughout the watershed (Figure 1.2) for the purpose of supplementing Christman's measurements. The same general sets of fracture orientations observed by Christman (1959) are evident. However, no single fracture set is predominant (Figure 1.2). The variability in fracture directions suggests that there is a high potential for interconnection of fractures, and, thus, mixing of groundwater from different original recharge locations.

Surficial Deposits

Based on striae measurements in and near the study area, the most recent glacial advance moved in a general southeasterly direction (Stewart and MacClintock, 1969). Striae at the upper elevations of Mount Mansfield, as well as the presence of erratics, indicate that the Green Mountains were completely covered by the Laurentide ice sheet in the Late Pleistocene. Striae measurements in the Lamoille Valley indicate that the direction of ice movement was modified by topographical features at the lower elevations, especially during periods of retreat when ice was thinned sufficiently to be confined to valleys (Stewart, 1961).

Glaciofluvial and glaciolacustrine deposits of significant thickness are generally located in the valleys and on the lower slopes of Mount Mansfield. Only a thin till cover is

present at higher elevations (Stewart and MacClintock, 1969). Valley deposits exist as kames, kame terraces, eskers, and lacustrine sediments in the study basin and surrounding area. Terraces at 350 m asl represent former lake margin deposits during a period of high lakes dammed by retreating ice in the Champlain Valley lowlands. Based on well logs, glaciolacustrine deposits (mostly sands and silts) reach thicknesses of up to 150 m. Downgradient of the study area, thick deposits of lacustrine clay overlie the till, indicating a deep water depositional environment (Connally, 1968).

In terms of groundwater flow, recharge to bedrock at the upper elevations may be more rapid, given the shallow sediment cover, while recharge at the lower elevations must be transported vertically through what is in some locations a thick and complex arrangement of unconsolidated material, prior to reaching the bedrock fractures. Discharge of bedrock groundwater to the surficial deposits may occur at the lowest elevations in the watershed, as suggested by the presence of many springs.

Soils

Moisture conditions in topsoil influence runoff during rain or melting events in the basin. High soil saturation promotes infiltration directly to bedrock or to sediments overlying the rock. Soil types in the study area have been mapped by the USDA and SCS (1974;1981) (Figure 1.3). Soils at the upper elevations of this watershed are, in some areas, derived directly from weathering of the schist. At the topographical high points, some areas are devoid of soil cover. Bedrock outcrops (Rk in Figure 1.3) account for 11

percent of the entire basin area. At other locations lower in the basin, soils are developed in weathered till, glaciofluvial, or glaciolacustrine sediments.

Sandy to rocky loams are present at elevations above 800 m asl and lie adjacent to the outcropping bedrock on the ridges and summit of Mount Mansfield. These soils, called the Lyman-Marlow (Ly) and Marlow (Me) loams, typically of only several centimeters in thickness, and are positioned directly over bedrock or weathered rock. Where the soils are thin, saturation occurs quickly during rain storms, promoting both rapid runoff and recharge to bedrock where fractures are exposed to the soils (USDA and SCS, 1974; 1981). Below 800 m asl, a large portion of the watershed is dominated by Peru stony loam (Ps). This soil overlies till and colluvial rock deposits. Like the Lyman-Marlow and Marlow soils, the water-bearing capacity of the Peru stony loam is limited by its thickness, as it lies directly over material of somewhat low permeability, except where bedrock fractures may be exposed (USDA and SCS, 1974). The Lyman-Marlow, Marlow and Peru soils cover 79 percent of the basin area.

Below 350 m asl, soils overlie deltaic and lake margin deposits. Adams-Windsor loamy sands (Ad) occupy the tops of the terraces. Colton (Cs) and Stetson (St) loamy to gravely sands cover the slopes and much of the area near the river. These soils are quite permeable and produce little runoff under normal storm conditions. Due to the gentle slopes and productive soils, much of the residential development and pasture land is located in this part of the basin (USDA and SCS, 1974).

Vegetation and Trees

Vegetation type varies with elevation. The uppermost ridges and summits of Mount Mansfield support a rare arctic tundra plant community common only to the highest elevations in Vermont, specifically the summits of Mt. Mansfield (1339 m asl) and Camel's Hump (1244 m asl). Red spruce and balsam fir dominate the high slopes and the summits of the mountains. Due to the harsh weather conditions, both of these tree types are reduced to a low scrubby growth near the summits. American mountain ash, white birch, white ash, hemlock, mountain maple, and choke cherry are also common throughout the basin except for the ridges and summits (Burns, 1916; Connor, 1994).

Tree types less common, but distributed throughout the basin include red cedar, poplar, several types of aspen, black cherry, wild red cherry, sugar maple, white maple, and red maple. The forests also support a mixture of several types of mosses and bushy undergrowth (Connor, 1994).

Below 300 to 400 m asl, different tree types become predominant. These include white pine, which grows mostly in sandy soils overlying the glaciolacustrine deposits in the lower valley, beech, yellow birch, chestnut oak, red oak, black oak, basswood, tamarack, and black willow. Other trees less commonly found at these elevations are butternut, hickory, and american elm. More grasses are also found below 300 to 400 m asl, especially in cultivated fields.

A large percentage of the trees on the slopes and summits are the scrubby conifers, which transpire water from precipitation and soil, mostly during the warmer months of the year. Given their smaller size and sparse distribution at these elevations, water usage is

lower than that of conifers in the valley (Likens et al., 1977; Likens et al., 1985). The lower elevations of the watershed are dominated by larger coniferous and deciduous trees, which transpire greater amounts of water than the smaller upslope conifers during the warmer months of late April to early November, especially when leaves are present on the deciduous trees (Mather, 1964). The seasonal variability in water use by trees and other vegetation in the watershed has significant influence on recharge to the bedrock. The effects of these mechanisms are discussed in Chapter 3 and 4.

Water Supply Issues

Groundwater in fractured bedrock is a very important water supply in the upland regions of Vermont and other areas of New England. Due to the limited development of the uplands, water in the bedrock aquifers is generally clean and plentiful. Currently, the study basin is not an area of particularly high concern relative to water supply availability or contamination problems. However, as with many similar upland areas, development has increased rapidly in the last three decades, and continued residential as well as recreational development is predicted (Wilmot and Scherbatskoy, 1994). Therefore, supply and pollution problems common to water supply development in more settled areas may become more numerous in the future. Furthermore, although this particular basin may not be developed to the point where water supply becomes a serious issue for residents, upland recharge areas may in the future be looked upon as sources of clean drinking water for larger areas. This would greatly increase the demands on the bedrock aquifer.

Perhaps more importantly, other areas of this country and the world contain at present upland regions with much heavier water supply demands. There is a need in these areas to define groundwater recharge and flow for the purpose of protecting water supplies from depletion or pollution. This basin is suitable for the examination of the natural recharge and flow processes, since the groundwater supply is not being significantly stressed under present conditions. By observing recharge and flow mechanisms in their near-natural state, a more accurate description of the factors affecting these processes prior to modification by human activity can be determined.

All of the residents in the study basin obtain drinking water from bedrock wells or springs (Figure 1.4). Only three of the wells used in this study, GW3, GW7, and GW8, are true wells cored deep into bedrock. The depths of these wells range from 53 m to 213 m (see Chapter 3). The remaining wells, GW1, GW2, GW4, GW5, GW6, and GW7B are developed springs in the bedrock. Due to its steep slopes, this particular sub-basin contains a high percentage of springs compared to other basins in the region.

Deep wells are typically cased to bedrock and sealed. The portion of the well in bedrock is left open due to the strength of the rock material. Well bores intersect fractures yielding varying amounts of water. Reported yields of wells used in this study vary from 0.25 to 10 gallons per minute (gpm). Well drillers report finding several zones of significant yield along the length of some well bores, indicating that the rock contains relatively closely spaced sets of water-yielding fractures.

Springs are typically developed by driving a pipe into an existing, water-producing fracture exposed in outcrop, or by drilling into a highly fractured portion of the rock

where a spring is located. Some springs are also developed by installing a catch basin in overburden filling a hollow in the bedrock. The hollow catches water discharging from the nearby bedrock spring. Springs used for water supplies discharge water at fairly constant rates (1 to 5 gpm) throughout the year. The high spring, GW1, supplies water for Underhill State Park, a state-operated park in the Mount Mansfield State Forest. This spring is only used during the summer months (May to October), while other springs are used for water supply all year.

Most residents who participated in this study report no unusual problems with water supply or availability. However, one of the shallow springs, GW7B, occasionally goes dry. According to the owner, the timing of this spring becoming dry is unpredictable, as it has become dry during periods of frequent rain. This indicates that the spring does not respond quickly to rain events.

Due to the abundance of springs, and the accessibility of groundwater by drilling, all of the residences in the study basin are supplied by individual wells and springs. No public water supplies are in place. In the nearby town of Underhill Center, just downgradient from the watershed boundary, there is a water supply which serves fewer than half a dozen homes. This is a high-yielding bedrock spring which at one time served most of the town.

The Jericho-Underhill Water District services 240 residents in the towns of Underhill and Jericho. The average daily demand is 63,000 gpd (238,000 $L \cdot day^{-1}$). Originally, this water supply system used several well points, installed in various materials. In 1994, a new high-yielding well was installed in the permeable glacial outwash deposits

of the Browns River valley near Underhill. This well now serves the entire system. (Wagener, Heindel & Noyes, 1994). Residents in the area who are not served by the Water District have individual wells installed in bedrock or surficial deposits. Ninety-four percent of the residential wells in Jericho and Underhill are installed in bedrock, six percent of these being springs. The remaining wells are installed in the overburden (Autery, 1996, pers. comm.).

Regional Variability of $\delta^{18}O$ in Groundwater

As part of a regional study of groundwater chemistry by Darlene Autery (University of Vermont Geology Department), 140 wells in the Underhill and Jericho area, including the Upper Browns Basin, were sampled in May, 1996. $\delta^{18}O$ analysis was performed for all of these samples. The $\delta^{18}O$ values ranged from -13.4 ‰ to -10.5 ‰ with an average value of -11.6 ‰. No correlation was observed between $\delta^{18}O$ values and the thickness of surficial deposits, well yield, elevation, or well depth (Figures 1.5, 1.6, 1.7 and 1.8, respectively).

The research reported in this thesis was focused only on the uppermost sub-basin of the watershed, above Underhill Center. Furthermore, this study examined temporal trends as well as spatial variations in groundwater $\delta^{18}O$ composition. However, the regional sampling round served as a test for large scale spatial trends, and indicated the regional range of groundwater $\delta^{18}O$ values for comparison with those found in the thesis study area. The average annual groundwater $\delta^{18}O$ value in the uppermost basin was also

-11.6 ‰, although values varied over a smaller range than for the regional data (see Chapter 3).

Application of Results

As discussed in the introduction of this chapter, there is a need for an improved understanding of groundwater recharge and flow mechanisms in upland watersheds in order to improve predictive modeling for the purposes of water supply development, contamination remediation, and resource management. This study adds to the general understanding of such mechanisms and presents a conceptual model that describes these mechanisms, as well as their spatial and temporal variability. In addition, equations describing these processes are developed. It seems that the next feasible step is to couple these equations with a three-dimensional numerical groundwater flow model, capable of representing the physical dimensions of this or other upland aquifers. This approach would produce a useful tool for future modeling efforts.

This project has provided an improved conceptual understanding of the timing of recharge to bedrock in different areas of the watershed. These findings have important applications to management of land use in the basin. Given that the upper elevations of the watershed are significant zones of recharge to the bedrock, it is necessary to protect them indefinitely from potentially polluting activities. Furthermore, areas in the vicinity of drinking water wells and springs also receive recharge during the colder months. Activities with high pollution potential should therefore be limited or prohibited during these months. Examples of activities with potential for polluting the groundwater include salting

of roads in winter, any industrial activities using fuel or other chemicals that may be spilled, applications of pesticides or herbicides to agricultural fields or lawns or golf courses, and application of wastewater to agricultural fields or ski slopes during winter snowmaking. Of course, any of these activities should be controlled at any time of year, as some contaminants may remain in the soil long enough to be recharged, even if applied at a time of year when recharge was minimal.

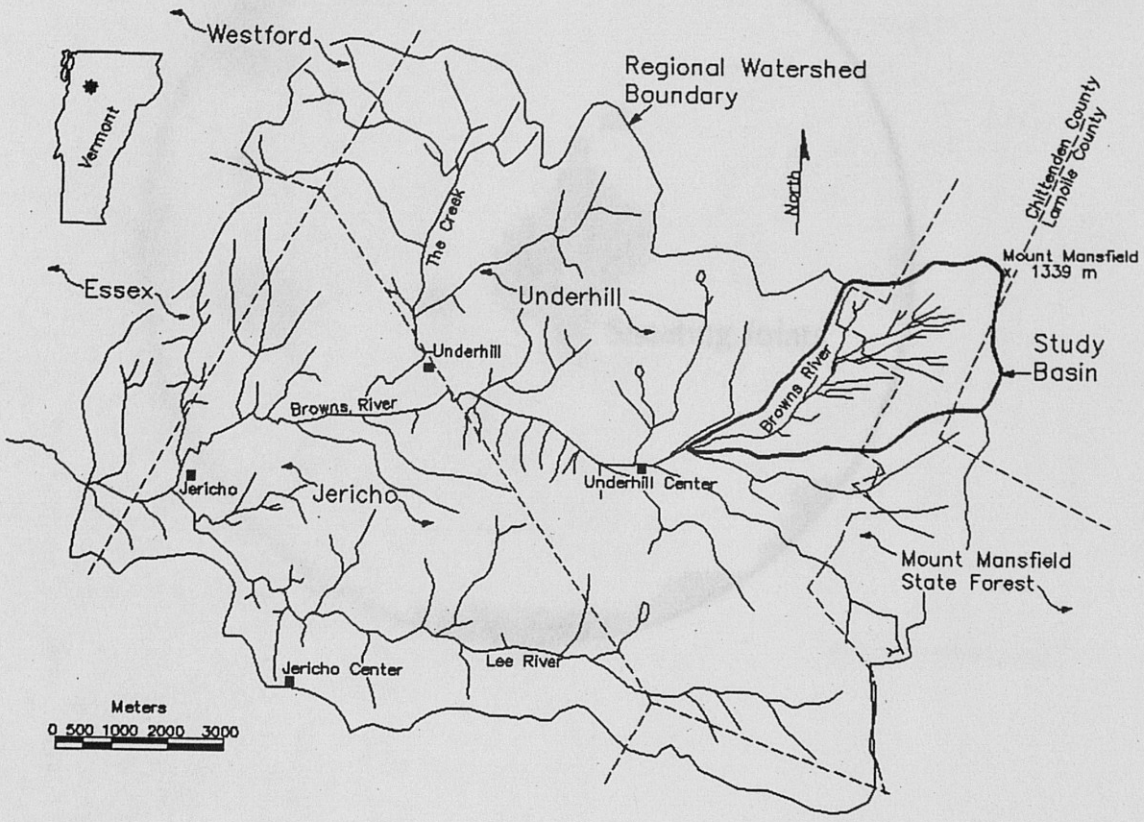

Figure 1.1

Study area and regional watershed.

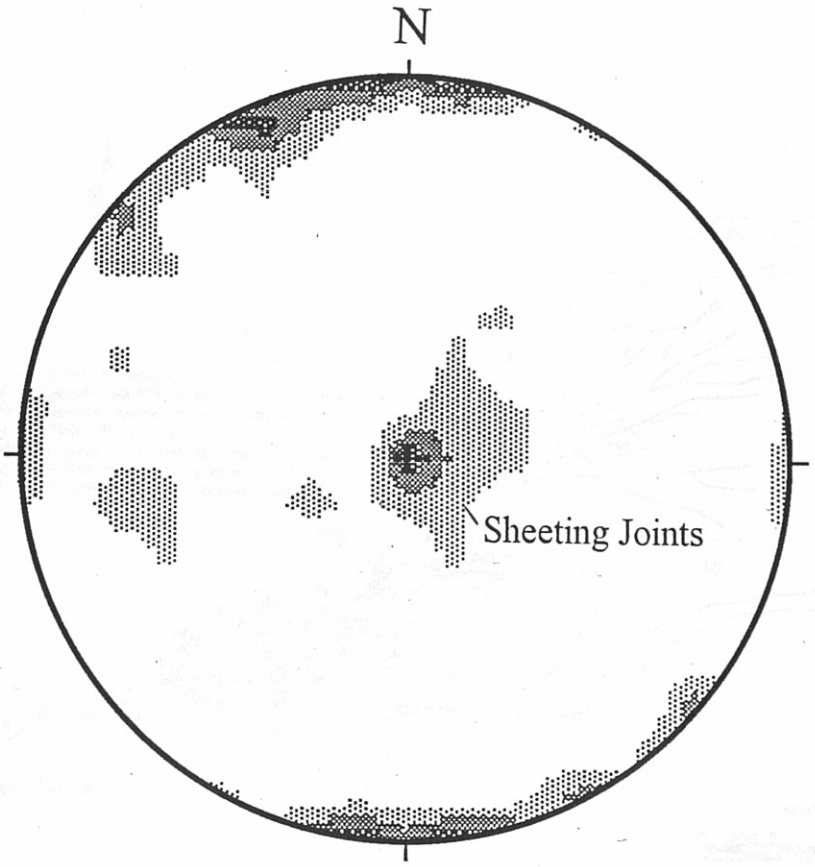

Figure 1.2

Bedrock fracture orientations. Lower hemisphere equal-area projection showing contour of poles to fracture planes (1% area plot, 5% contour interval) based on 118 field measurements at outcrop throughout the basin. Most joints are steeply dipping with the exception of several sheeting joints (n = 10) observed in cliff faces.

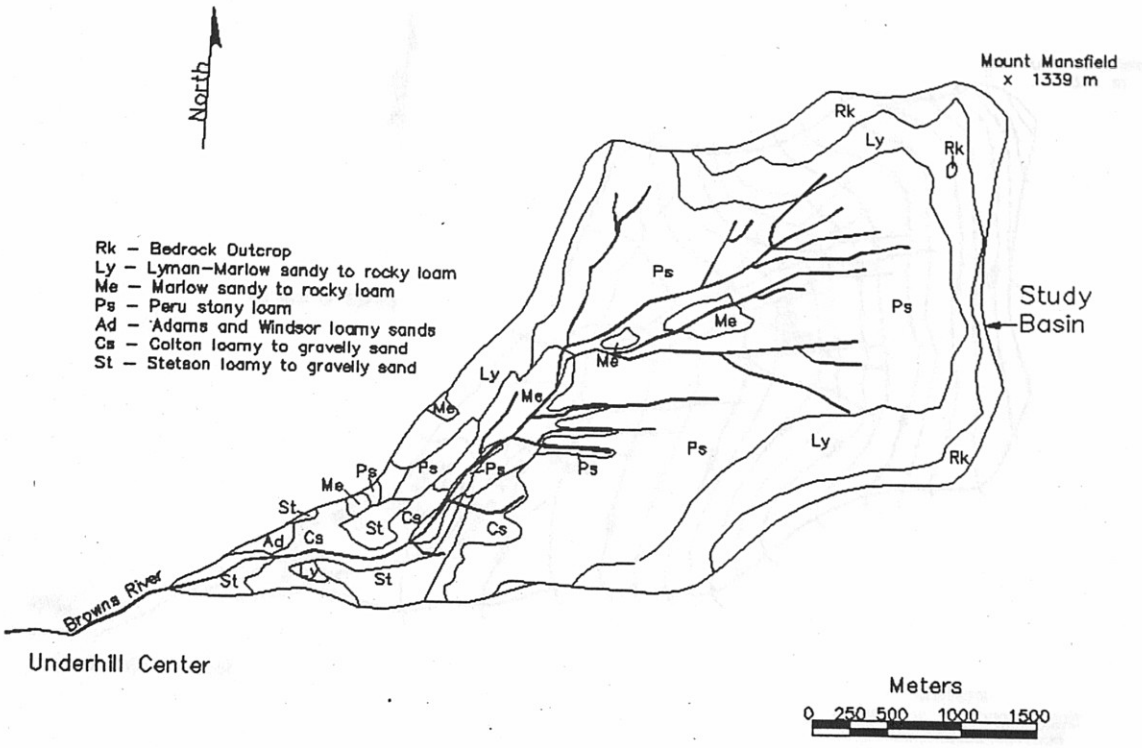

Figure 1.3

Map of soil types in the study basin. Information taken from USDA and SCS, Soil Surveys of Chittenden (1974) and Lamoille (1981) Counties, Vermont

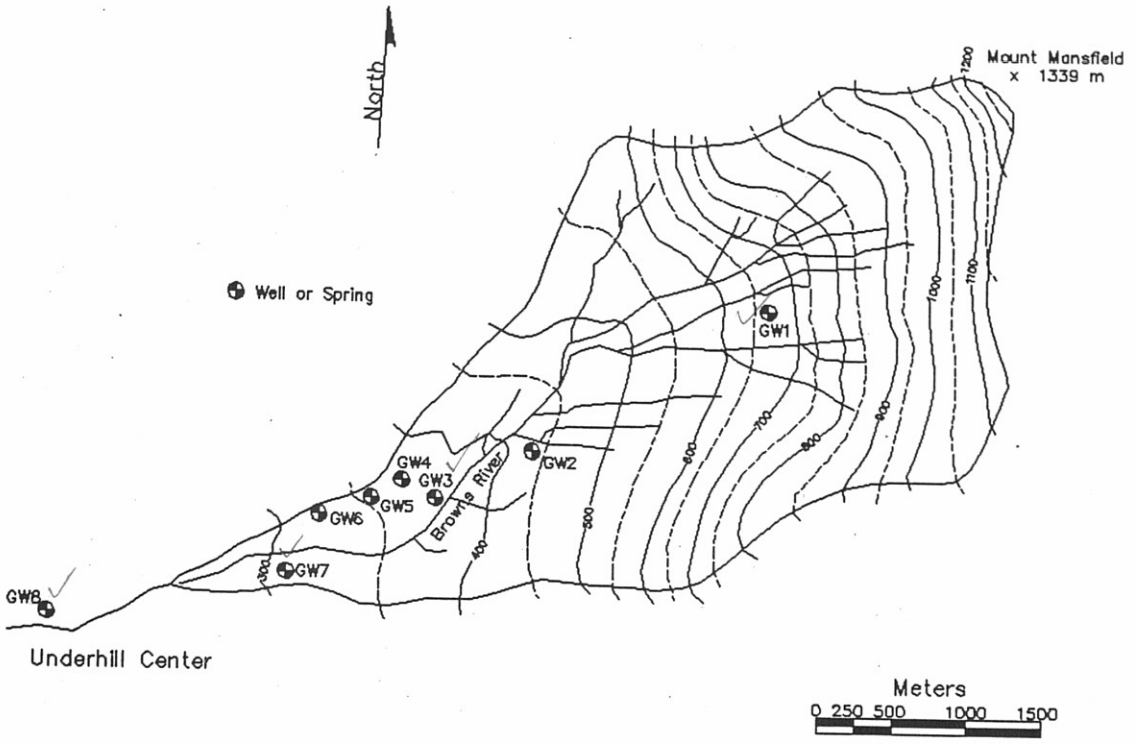

Figure 1.4

Groundwater sampling locations. GW3, GW7, and GW8 are deep bedrock wells. All others are developed bedrock springs.

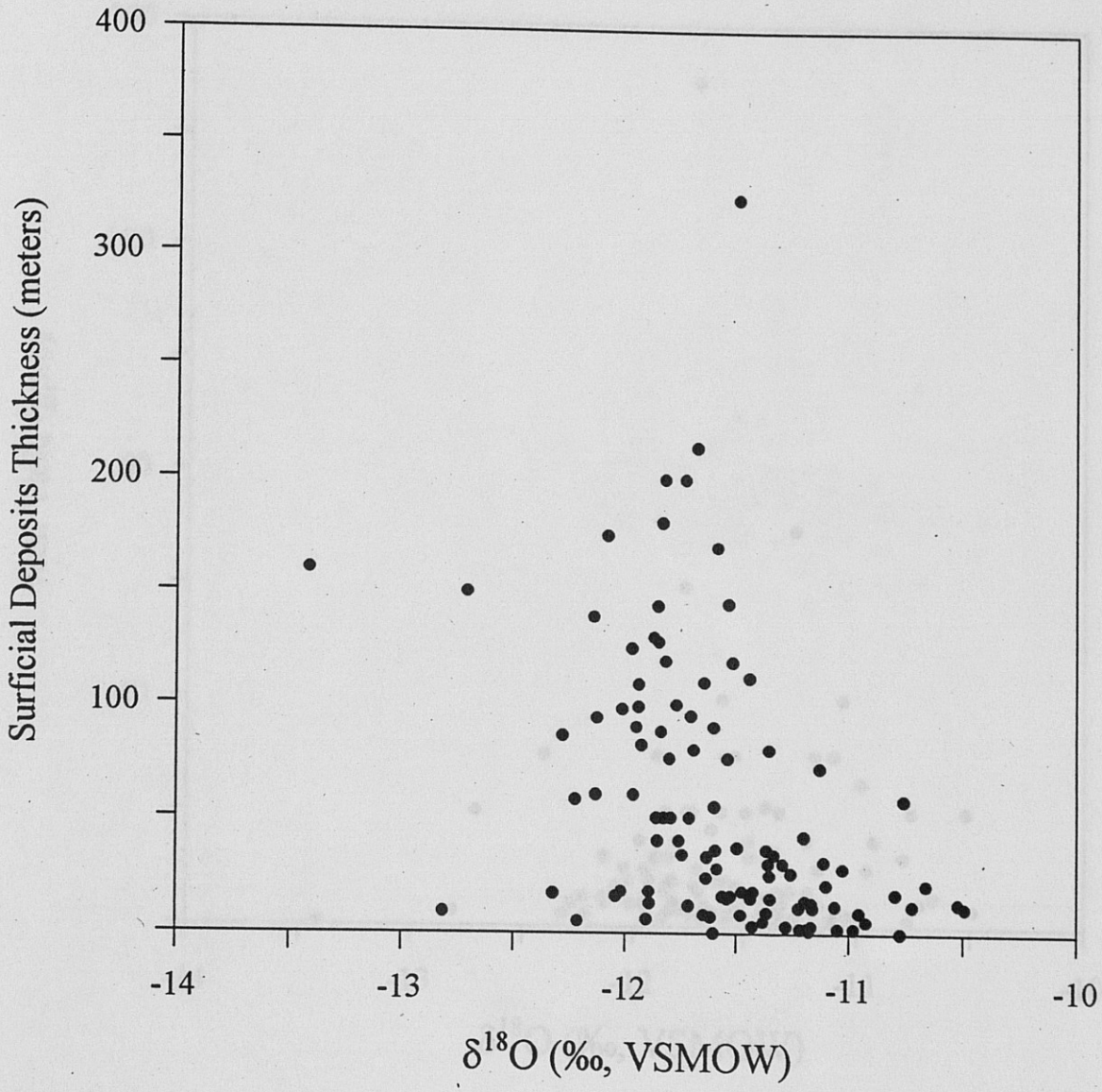

Figure 1.5

Regional variability of groundwater $\delta^{18}O$ with respect to thickness of surficial deposits. Samples were collected from 140 wells in Jericho and Underhill, VT in May, 1996 by Darlene Autery (UVM Geology Department).

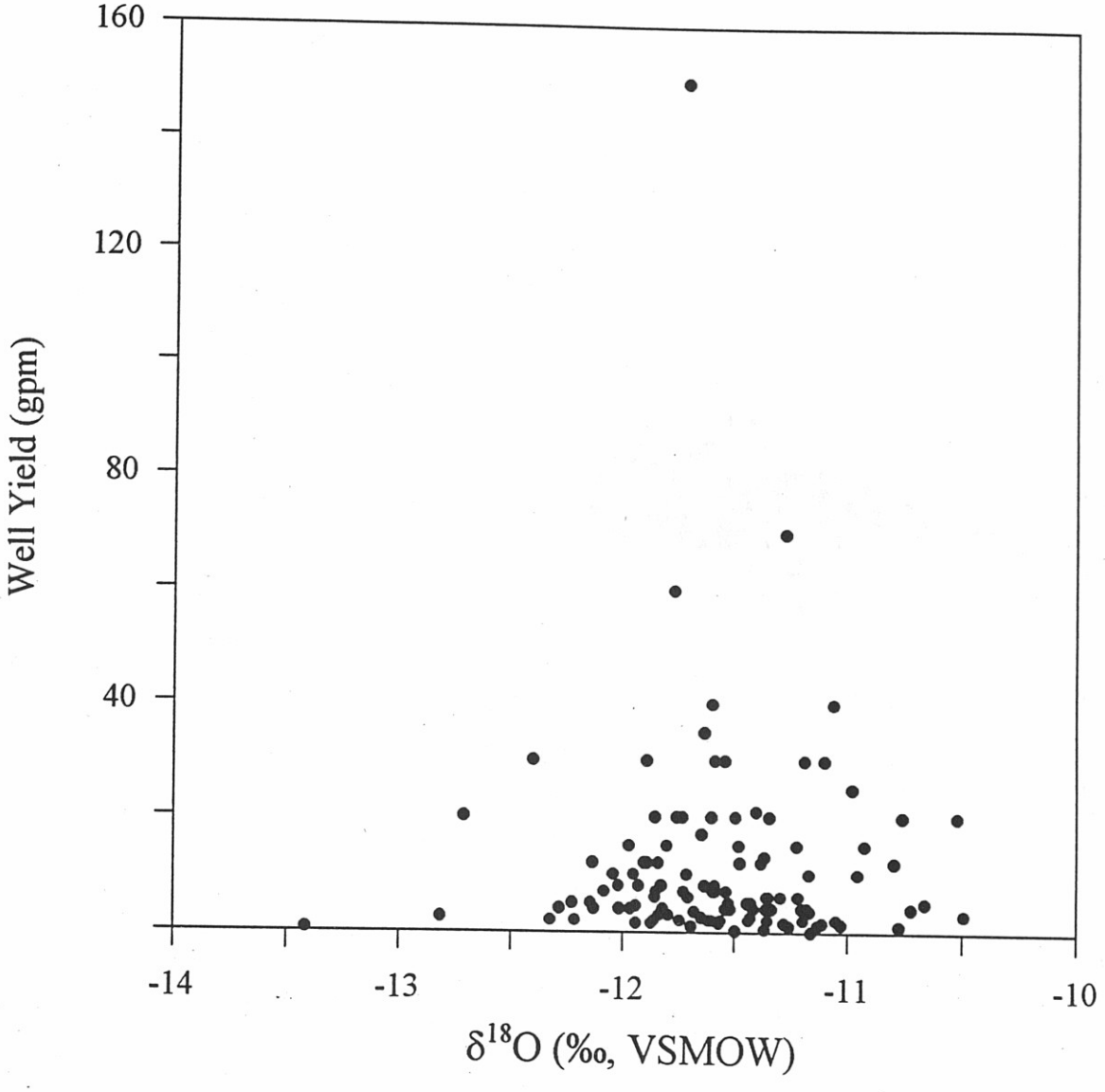

Figure 1.6

Regional variability of groundwater $\delta^{18}O$ with respect to well yield. Well yield values are as reported in drilling logs. Samples were collected from 140 wells in Jericho and Underhill, VT in May, 1996 by Darlene Autery (UVM Geology Department).

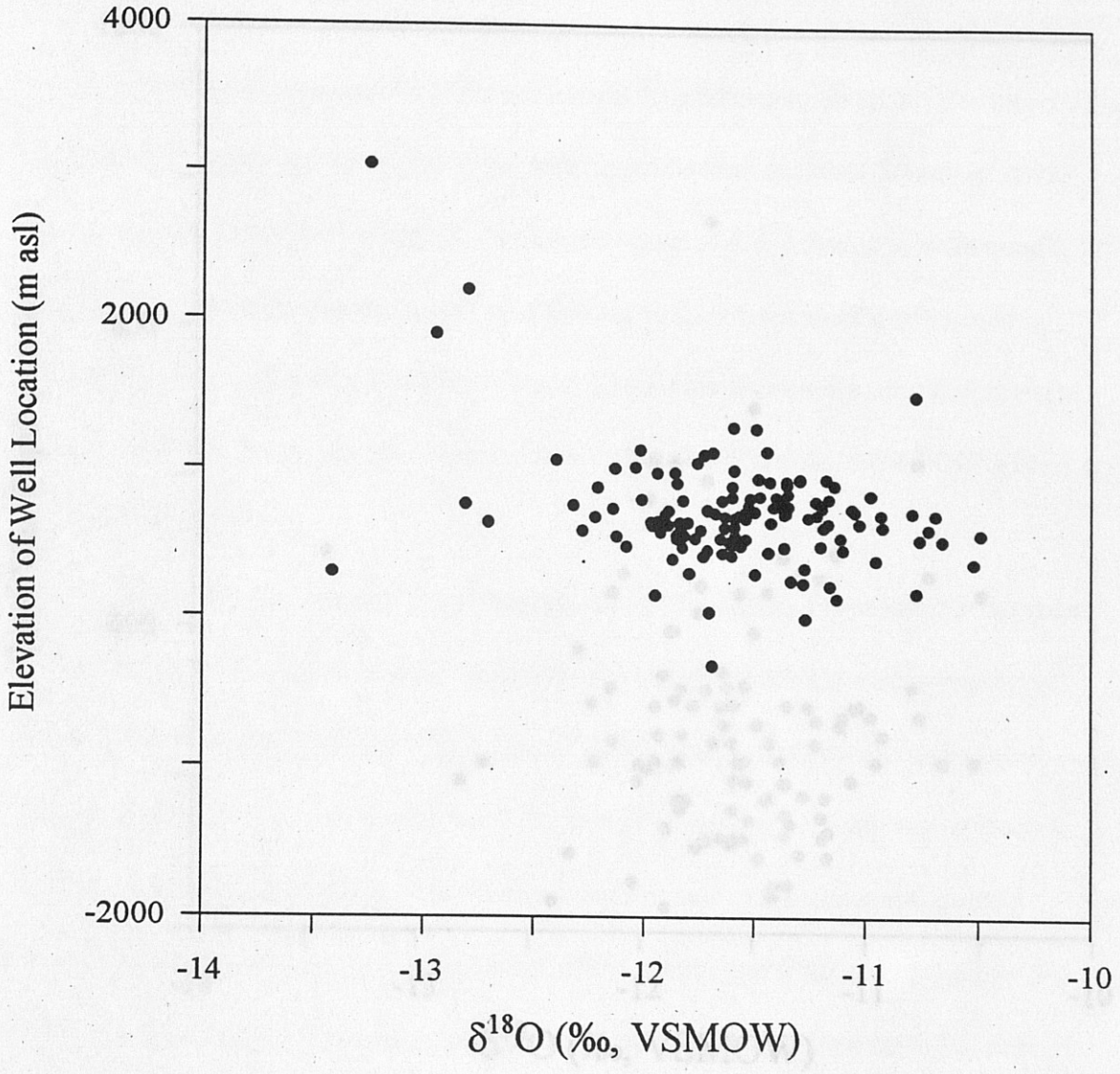

Figure 1.7

Regional variability of groundwater $\delta^{18}O$ with respect to elevation. Elevations are estimated from USGS topographical maps. Samples were collected from 140 wells in Jericho and Underhill, VT in May, 1996 by Darlene Autery (UVM Geology Department).

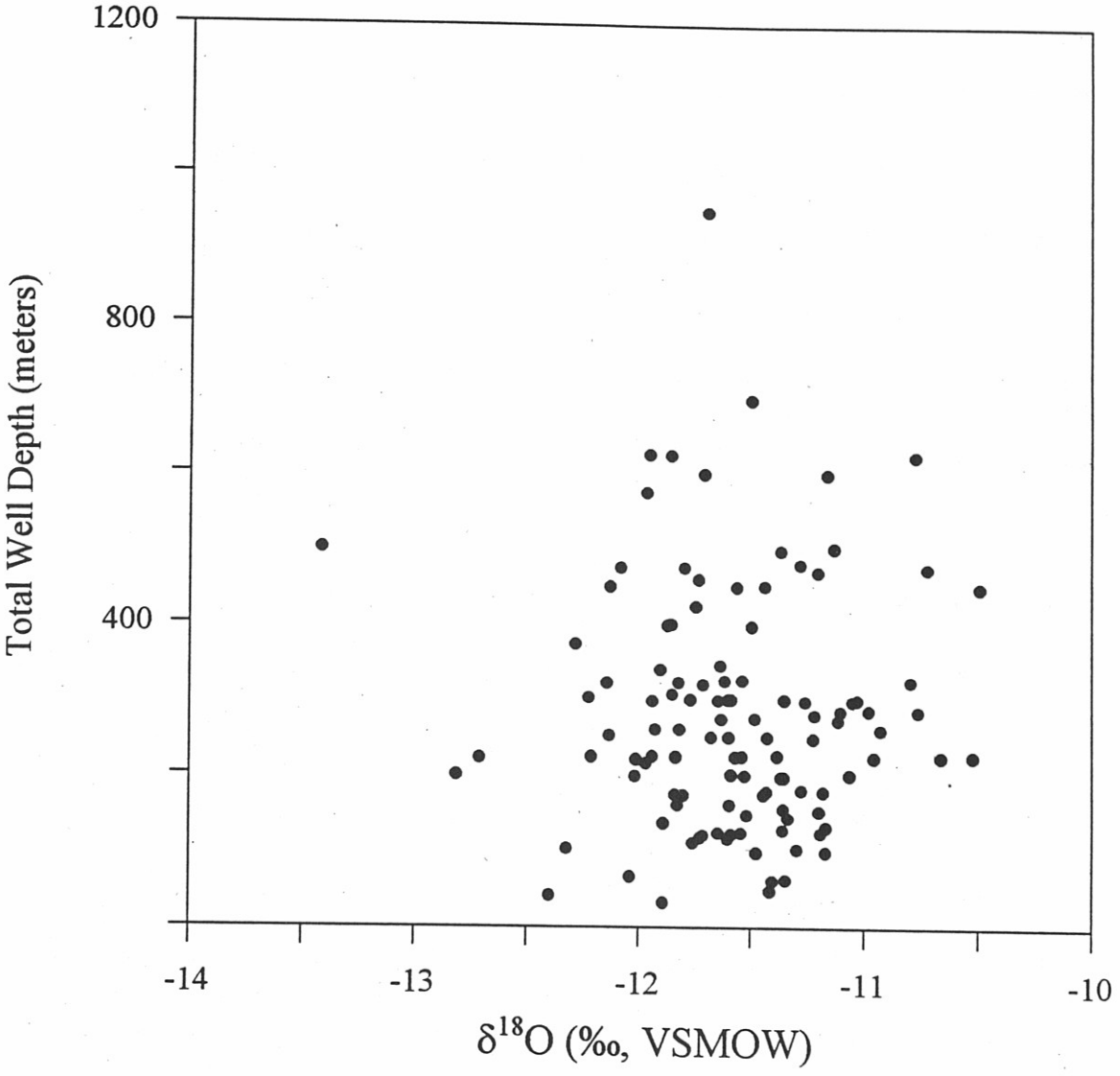

Figure 1.8

Regional variability of groundwater $\delta^{18}O$ with respect to well depth. Well depths are as reported in drilling logs. Samples were collected from 140 wells in Jericho and Underhill, VT in May, 1996 by Darlene Autery (UVM Geology Department).

CHAPTER II

COMPREHENSIVE LITERATURE REVIEW

Introduction

This chapter reviews briefly the theoretical foundations upon which this research is based. Traditional groundwater modeling techniques, as well as recent efforts to model flow in fractured rock, are reviewed. The measurement of stable isotopes is discussed, along with a description of the factors contributing to fractionation of the isotopic composition of precipitation and groundwater. Many references were used that are not cited individually in this chapter. They are included in the Comprehensive Bibliography at the end of this thesis.

This study uses many of the techniques addressed herein. However, the approach used in this study is unique, in that it combines the use of a system dynamics model of groundwater recharge and flow with temporal stable isotope records and radioactive isotope measurements generated through the sampling program. No attempt is made to represent the precise geometry of the bedrock aquifer, nor to represent the fracture network within the aquifer. Instead, a model of the spatial and temporal variability of recharge mechanisms is developed, thereby creating a useful tool for examining the interaction of several processes within the basin system. Determining the direct age of groundwater in the aquifer is complex and requires multiple approaches. However, an attempt was made to estimate groundwater ages using measurements of tritium, combined with the stable isotope data. The results of this work are discussed in Chapters 3 and 4.

Numerical Modeling of Groundwater Flow in Fractured Rock

Numerical groundwater modeling codes have been developed based on various forms of the groundwater flow equation, which is expressed in simplest terms as the Darcy flow equation (Darcy, 1856):

$$q_x = - k_x \cdot \frac{\partial h}{\partial x} ; \; V_x = q_x / n_e \qquad (2\text{-}1)$$

where

q_x = specific discharge or flow in the direction of flow (x)

k_x = hydraulic conductivity of medium

$- \frac{\partial h}{\partial x}$ = hydraulic gradient

V_x = linear velocity of groundwater flow

n_e = effective porosity of medium

This simple, one dimensional equation can be modified to account for aquifer flow in three dimensions and combined with the principal of mass conservation to obtain (Anderson and Woessner, 1992):

$$\frac{\partial}{\partial x}\left(T_x \frac{\partial h}{\partial x}\right) + \frac{\partial}{\partial y}\left(T_y \frac{\partial h}{\partial y}\right) + \frac{\partial}{\partial z}\left(T_z \frac{\partial h}{\partial z}\right) = S_s \frac{\partial h}{\partial t} - R^* \qquad (2\text{-}2)$$

where

T = transmissivity = vertically averaged hydraulic conductivity/aquifer thickness

S_s = specific storage in aquifer

R^* = sink/source term representing recharge (+) or pumping (-)

Note that recharge is incorporated as a general term representing the balance of recharge to and losses from the aquifer.

Additional equations may be developed to account for mechanical dispersion of flow, chemical diffusion, radioactive decay, or other geochemical reactions. Source terms must be added to the advection-dispersion equations to incorporate geochemical processes (Anderson and Woessner, 1992). Since this study deals predominantly with the mechanics of groundwater recharge and flow (i.e., the bulk fluid physical processes), a detailed discussion of transport and geochemical modeling is not included.

Common computer codes for flow modeling in use today can be divided into two major groups, the analytical element models and the numerical models (Anderson and Woessner, 1992). Both are based on similar governing equations. However, analytical element models (e.g., TWODAN, QUICKFLOW) solve analytically and with superposition, the flow equations between known boundary conditions, assuming conditions of homogeneous aquifer properties and one or two dimensional flow (Strack, 1987, 1988). Numerical models (e.g., MODFLOW, AQUIFEM, PLASM) may be set up to incorporate aquifer heterogeneity in two or three dimensions (Konikow and Bredehoeft, 1978; Pinder and Voss, 1979; Prickett, 1979; Townley and Wilson, 1980, 1990). Properties are most commonly input on a finite element or finite difference grid to represent the geometric distribution of materials comprising the aquifer. Additional equations are incorporated to represent the boundaries of the problem (i.e., streams or

groundwater divides) and initial conditions for the simulation. Sets of algebraic equations are developed by approximation of the partial differential equations governing flow and boundary conditions. The resultant equations are solved for fluid head values at each grid node or cell (Anderson and Woessner, 1992).

Groundwater models have been applied with some success to problems considering flow through porous media (i.e., sands and gravels). High degrees of heterogeneity in a medium complicate the flow model, adding computational requirements, as well as introducing error. Perhaps a larger problem with modeling in heterogeneous environments is the difficulty in obtaining precise measurements of aquifer properties in the detail needed to produce an accurate numerical representation of flow (Salhotra and Nichols, 1993). Flow in fractured rock aquifers is even more problematic, given the complexity of fracture networks and the difficulty in measurement of aquifer properties. Flow in rock similar to the schist in the study area tends to be controlled predominantly by fracture directions, fracture interconnectivity, and gradient. Various methods have recently been developed to improve the description of fractured rock aquifer properties though field measurements (Mabee et al., 1994; Hardcastle, 1995). These methods all incorporate some degree of uncertainty, of course, since the full complexity of the fracture network is always hidden from view.

In terms of modeling flow in these aquifers, attempts have been made to generate complex numerical representations of aquifer fracture networks (LaPointe and Hudson, 1985; Long et al., 1985; Roleau and Gale, 1985, 1987; Chiles, 1989; Dershowitz and Eistein, 1989; Cacas et al., 1990; Kulatilake and Wathugala, 1990). These models typically

combine solutions of equations for flow along a single fracture with an artificial generation of the fracture network based on stochastic principles. These efforts have met with some success. However, rigorous calculations and extensive computer time are typically required (Neuman and Roleau, 1994).

System Dynamics Modeling

System dynamics modeling can be applied to many systems in a wide range of disciplines. Computer codes developed for system dynamics simulation (e.g., STELLA and VENSIM) allow the user to develop a graphical representation of the conceptual model of a system, incorporating all significant processes working in the system. The user then enters equations to describe the actions of each model component and relationships among components.

The advantage of the system dynamics approach is that a model of almost any dynamic system can be developed according to the study being performed and the data generated by the study. A graphical user interface allow simple modification of model components and their interrelationships. System dynamics models, as used here, are especially useful in interpreting processes within complex systems for which conventional numerical modeling codes have not been developed explicitly or which require excessively detailed and unavailable information.

As with any modeling technique, in order to produce a valid, unique solution, any model must be able to solve for all unknowns, without unjustifiable assumptions being

made. In this respect, the system dynamics model may be used to guide additional data collection in order to improve the capabilities of the model.

When a model has been developed for a particular system, some factors in the model may be varied within reasonable ranges until observations in the field can be matched. Ideally, a model can be verified by an independent test. In some cases, this is accomplished by simulating a stress on the system, such as a pumping test that may be performed in the field. In the case of this study, simulated temporal changes in groundwater $\delta^{18}O$ are matched with actual measurements. When an independent test has been successfully carried out, the model may be applied for predictive purposes. Interpretations of model results should consider the limitations of the model and uncertainties inherent in any simulation of a natural system.

Measurement of Stable Isotopes

This study utilized measurements of stable isotopes of oxygen and hydrogen. The number of neutrons in an atom distinguishes the different isotopes of an element. The stable isotope measurement describes the ratio of heavy to light isotopes in a given substance. For example, oxygen exists naturally in three stable isotopic forms, ^{18}O, ^{17}O, and ^{16}O. The isotopic ratio, $^{18}O/^{16}O$ is used as a quantification of the ratio of heavy to light oxygen isotopes in a substance. The numerical designation of the isotope refers to the total number of neutrons and protons in the nucleus of the oxygen atom. The stable forms of hydrogen are ^{1}H and ^{2}H or D (deuterium). The ratio of heavy to light hydrogen atoms,

$^{2}H/^{1}H$, is also expressed as D/H. Tritium (^{3}H or T), is the unstable, radioactive form of hydrogen (Urey, 1947; Faure, 1986).

The lighter oxygen and hydrogen isotopes are far more abundant than the other stable forms. ^{16}O is estimated to account for 99.76 percent of all oxygen atoms. ^{1}H is estimated to account for 99.98 percent of all hydrogen atoms (Bigeleisen and Mayer, 1947; Broecker and Oversby, 1971). Therefore, the absolute ratio of heavy to light atoms in the measurement of a given sample is an extremely small number. Furthermore, variations in the isotopic composition of substances, the measurements on which this study is based, are typically in the parts per thousand or parts per hundred range. In order to make measurements easier to compare, it is most convenient to express these measurements relative to a standard. For the measurements in this project, the standard known as Vienna Standard Mean Ocean Water, VSMOW (Hagemann et al., 1970), was used as a reference. The actual ratio of ^{18}O to ^{16}O in this standard is 2.0052×10^{-3} and D/H is 1.5576×10^{-4} (Hagemann et al., 1970). Relative isotope values are expressed as follows:

$$\delta^{18}O = \frac{[(^{18}O/^{16}O)\text{Sample} - (^{18}O/^{16}O)\text{VSMOW}]}{(^{18}O/^{16}O)\text{VSMOW}} \times 10^{3} \qquad (2\text{-}3)$$

and

$$\delta D = \frac{[(D/H)\text{Sample} - (D/H)\text{VSMOW}]}{(D/H)\text{VSMOW}} \times 10^{3} \qquad (2\text{-}4)$$

Units for $\delta^{18}O$ and δD are parts per thousand, or per mil (‰).

The isotopic composition in water is obtained by mass spectrometric analysis of CO_2 gas that has been isotopically equilibrated with the water sample at a controlled temperature of 25°C. CO_2 is removed from the sample headspace using cryogenic separation techniques and then analyzed (Taylor, 1973; Wong et al., 1987; Socki et al., 1992). A fractionation factor, α, is used to quantify the difference in isotopic composition between a liquid and a gas in equilibrium. The value of $\delta^{18}O$ for a water sample may be calculated using the following relationship:

$$\alpha = \frac{\delta^{18}O\text{Sample} + 1000}{\delta^{18}O\text{Gas} + 1000} \qquad (2\text{-}5)$$

where

α = fractionation factor for $H_2O/CO_2 = 1.0412$ @ 25°C (O'Neil et al., 1975)

For δD determination, water is reduced to H_2 using a vacuum line and uranium furnace. The H_2 gas can be then transferred directly to measurement in the mass spectrometer (Krishnamurthy and Deniro, 1982).

Mechanisms affecting the isotopic composition of water samples are discussed below. These changes in $\delta^{18}O$ and δD, also referred to as isotopic fractionation, make isotopic measurements a useful tool in the study of hydrologic processes.

Factors Affecting Isotopic Composition of Precipitation

The mass of an atom of a given element is determined by the number of neutrons and protons in the atom. Therefore, different isotopes of an element have different masses.

The thermodynamic properties of a molecule depend on the collective mass of the atoms incorporated in the molecule. The energy of a molecule in a gas (e.g., water vapor in a cloud) depends on the interactions of electrons as well as the translational, rotational, and vibrational components of the atoms in the molecule (White, 1984; Kyser, 1987). For oxygen, vibrational energies are most important in terms of fractionation. Rotational energy is also important for the behavior of hydrogen (White, 1984; Kyser, 1987). The vibrational frequency of a water molecule is inversely proportional to the square root of its mass (Kyser, 1987). Therefore, different isotopic species have different potential energies in molecules with the same chemical formula (e.g., H_2O) (Figure 2.1) .

A water molecule composed of lighter isotopes has a higher vibrational frequency and hence a higher potential energy than a molecule containing heavier isotopes (Figure 2.1). Bonds formed by the lighter isotopes are weaker, causing the lighter molecules to be more reactive or more easily dissociated than the heavier molecules (Kyser, 1987). During a phase change of water from liquid to gas (e.g., evaporation), lighter molecules will more likely enter the gas phase than heavier molecules. Therefore, the lighter molecules will preferentially evaporate in larger numbers than molecules made up of the heavier isotopes. Conversely, when water condenses from vapor, heavier molecules will more likely form precipitation, while lighter molecules will tend to remain in the vapor phase. The heavier isotopes, ^{18}O and D, will thus be concentrated in the liquid phase, since they tend to constitute the heavier molecules. This effect is known as isotopic fractionation.

Isotopic fractionation in a system is largely temperature dependent. The fractionation factor, α, approaches unity with increasing temperature (Friedman and O'Neil, 1977; Hoefs, 1980). In other words, the difference in the behavior of water molecules of different mass lessens at higher temperature. This temperature dependence allows the interpretation of isotope fractionation in terms of environmental temperatures.

Since continental precipitation originates as evaporated ocean water, samples of continental precipitation have lower or more depleted $\delta^{18}O$ values than the VSMOW standard. In the study basin, the dependence of $\delta^{18}O$ on temperature is seen in the seasonal records of precipitation, where water is most depleted in ^{18}O during the colder winter months and least depleted in the summer. Also, mean annual $\delta^{18}O$ is lower at the upper elevations of the watershed than at lower elevations, a function of temperature gradients within the basin (Figure 2.2). This relationship between $\delta^{18}O$ and temperature has been described (on a global scale) by Dansgaard (1964) using the equation:

$$\delta^{18}O = 0.695\ T - 13.6\ ‰ \qquad (2\text{-}6)$$

where

$\delta^{18}O$ = mean annual $\delta^{18}O$ value for precipitation

T = average annual surface air temperature in °C

Other factors, such as altitude and the proximity of a location to the origin of the vapor source and the nature of the vapor source itself, also govern $\delta^{18}O$ values in

precipitation at individual locations (Yurtzen, 1975; Gat, 1981; Fritz et al., 1987; Rozanski et al., 1993). The change in $\delta^{18}O$ fractionation between liquid and vapor with the depletion (physical) of the vapor source (Figure 2.3) was described by Rayleigh in 1899 as:

$$R_v/R_o = f^{(\alpha-1)} \qquad (2\text{-}7)$$

where

$R_v = {}^{18}O/{}^{16}O$ of remaining vapor

$R_o = {}^{18}O/{}^{16}O$ of original source

f = fraction of vapor remaining

α = fractionation factor (liquid water to vapor)

This relationship has become known as the Rayleigh Distillation Model (Rayleigh, 1964).

Based on large numbers of analysis of meteoric waters (unevaporated precipitation), a linear relationship between $\delta^{18}O$ and δD has been established which is described by the equation (Faure, 1986):

$$\delta D = 8\delta^{18}O + 10 \text{ (‰)} \qquad (2\text{-}8)$$

This relationship is presented graphically as the global meteoric water line (MWL) (Figure 2.4). If water samples have been subjected to significant evaporation, the δD vs. $\delta^{18}O$ relationship no longer plots on this line. This is due to the non-equilibrium kinetic

effects that occur during evaporation into unsaturated air, causing the fractionation of hydrogen and oxygen isotopes to occur in different proportions (White, 1984). Evaporated samples typically plot to the right of the MWL, indicating greater enrichment of ^{18}O than of D. Therefore, the relationship between the δD and $\delta^{18}O$ values for a given water sample may be used as a diagnostic indicator of the sample's history. Specifically, indications of evaporative effects in rain samples may indicate that the collected water was partially evaporated before measurement (i.e., a quality control test). In groundwater samples, evaporative effects may have occurred during the recharge process. Measurements of δD and $\delta^{18}O$ in groundwater may be used to determine if recharge is subject to evaporation during the infiltration process.

Effects of Trees and Plants

Preferential removal of ^{16}O by plants during photosynthesis of CO_2 causes an addition of ^{18}O isotopes to the atmosphere. Animal respiration adds to this effect (Dole et al., 1954). Oxygen released during photosynthesis has a weighted average $\delta^{18}O$ of +0.5‰ (i.e., enriched) (Garlick, 1969). Hydrogen fractionation during photosynthesis also results in the preferential use of the light isotope (Cifuentes, 1993). Although these are important effects in the global distribution of oxygen, they have little effect on the isotopic composition of recharge to groundwater.

In this study, the most significant effect upon the groundwater isotopic signature appears to be that of water interception and uptake by trees in the basin. However, the effect on the isotopic composition of groundwater is not one of isotopic fractionation.

Instead, interception and uptake by trees and plants during the warmer months prevents a significant portion of the precipitation from infiltrating to groundwater. This results in a reduction of the influence of individual rain events on the groundwater $\delta^{18}O$ and δD signatures. Vegetative transpiration and evaporation effects, especially in the valley forests during the warm months, are capable of transferring a significant portion of precipitation back to the atmosphere, thereby removing it from the recharge flux (Saxton and McGuinness, 1982). These effects have been shown to be important in the behavior of many hydrologic systems (McGuinness and Harold, 1962; Knisel et al., 1969; Parmele, 1972; Woolhiser, 1973). In fact, several studies in the northern forests of the United States have shown that significant infiltration through soil is unlikely to occur during the summer due to high evapotranspiration (Likens et al., 1977; Dugan and Peckenpaugh, 1985; Likens et al., 1985).

Interception of falling precipitation by the leaves of trees promotes high rates of evaporation or cuticular transpiration (evaporation at the plant cuticals). Transpiration is evaporation occurring within the plant structure. When plants uptake water, evaporation occurs from the walls of the plant cells to the adjoining intercellular spaces. Water vapor then escapes through the plant stomata or lenticels. Transpiration is controlled by soil moisture and permeability, as well as air temperature and relative humidity.

Potential evapotranspiration (E_p) is used to estimate the combined use of water by trees and evaporation for a given area (Thornthwaite, 1954). This quantity is expressed as follows:

$$E_p = f(R_e, A_t)_{Sr,o,m} \quad (2\text{-}9)$$

where

R_e = available energy

A_t = ease with which water is carried from the surface by turbulent transfer

S_r = vegetation characteristics with particular reference to the surface resistance due to the stomatal characteristics of the plant leaves

o = oasis effect (ability of plants to draw water from surrounding area)

m = moisture situation (water supply available to plant)

This expression is highly dependent upon air temperatures, as well as the predominant vegetation and soils in a given location. A plot of 50 years (1910-1960) of precipitation, soil moisture and potential evapotranspiration measurements compiled for Burlington, Vermont (C.W. Thornthwaite Associates, Laboratory of Climatology, 1964) (Figure 2.5) indicates that evapotranspiration (E_p) is negligible from the months of December to March. E_p increases in late March or early April to a peak in July, decreasing again to a negligible amount in November. Although precipitation is relatively high during the warmer months, soil moisture remains much lower than during the rest of the year. This indicates that a much smaller percentage of precipitation is available for infiltration to groundwater from April to November. Since this plot was developed from data in the lowlands of the Champlain valley, a plot produced for the Mansfield basin might look slightly different. It seems reasonable to expect lower E_p rates during the warmer months,

especially at the highest elevations, given the lower temperatures and dominance of smaller, more sparsely distributed trees which use less water.

Effects of Infiltration Through Soil and Sediments

As rainwater infiltrates through soils and sediments overlying bedrock, it may encounter a number of mechanisms that have the potential to cause isotopic fractionation. In areas where climatic conditions are conducive to significant evaporation, $\delta^{18}O$ in soil water tends to be higher than that of mean annual precipitation due to preferential evaporation of light water (White, 1995). Since evaporation does not occur in the Mansfield basin during the colder months and is not high relative to more arid regions even in the summer, soil water evaporation is likely not an important mechanism for fractionation of infiltrating water in this setting.

Biologically mediated reactions in some soils may preferentially use heavy hydrogen isotopes, resulting in points which plot to the left of the MWL (White, 1995). This effect was not observed in the Mansfield basin, based on D/H measurements in groundwater.

A third effect of soils and sediments overlying bedrock is the mixing of infiltrating water from different recharge events. The path that infiltrating water takes on its way to bedrock is dependent upon the arrangement of soil grains. Soil composition also influences the rate at which water can travel. In complex depositional settings, the permeability of soils may vary significantly over small areas. Therefore, water entering the soil may not proceed at a uniform rate or along uniform paths to bedrock. This results in the mixing of

waters which originated from different rain events. Therefore, water that has a larger residence time in the soils and sediments is more likely to become isotopically mixed (McDonnell et al., 1991; Datta et al., 1996).

Effects of Melting

Snow is typically lighter in $\delta^{18}O$ than rain, given its colder formation temperature. However, isotopic fractionation may occur during the melting process from evaporation and sublimation of portions of the snow pack as well as redistribution of melting snow in the pack. Early melting tends to produce more isotopically depleted meltwater than the later stages of melting, since the loss of ^{16}O from evaporation and sublimation may increase over the time that the snow pack remains in place (Friedman, 1991). The composition of melt may vary over the melting period as these effects become more prominent (Hooper and Shoemaker, 1988; Moore, 1989; Maule and Stein, 1990). Therefore, it is most appropriate to sample meltwater (when melt is occurring) in addition to snow when constructing a record of the $\delta^{18}O$ of recharge to groundwater. Recent studies in North America have shown that meltwaters readily infiltrate in forested settings in the absence of ground frost, contributing significantly to groundwater recharge (Bottomley et al., 1986). Measurements of soil and groundwater in a study area in northeastern Vermont, indicate that melting snow and winter rains may significantly modify the isotopic composition of soils and shallow groundwater (Shanley et al., 1995). Early in the winter, this effect results in a slight lowering (~1 ‰) of $\delta^{18}O$ value for the soils and shallow groundwater, since the water in storage in the soil may have entered the

soil in the warmer months. However, as the year progresses, the direction and magnitude of each change in groundwater isotopic composition is dependent upon the $\delta^{18}O$ of individual rain or melt events (Shanley et al., 1995).

Effects of Water - Rock Interaction and Mixing

In bedrock groundwater, isotopic fractionation may occur under geothermal conditions (Taylor, 1974; Zuber et al., 1995). However, in the case of the aquifer studied in this thesis, the largest effect on the isotopic composition of groundwater flowing in the rock is caused by physical mixing of different water masses. This includes convergence of waters flowing in fractures systems from different recharge locations and possibly having different recharge times, as well as contribution through shallow fractures of local infiltration from storms during the colder months. Others have found that mixing effects have strong influence on the isotopic composition of groundwater in fractured bedrock aquifers (Nordstrom et al., 1985; Wenner et al., 1991; Garlick, 1996) .

A conceptual diagram of the mixing process in bedrock is shown in Figure 2.6. A measurement taken at a particular point in the aquifer may reflect the contributions of several sources. In a well drilled through the bedrock, the temporal $\delta^{18}O$ signature reflects changes in contribution over time from one or more deep flow zones, as well as from infiltration in the vicinity of the well from recent storm events. Since water infiltrating quickly near the well is not significantly mixed with other groundwater, it has the potential to modify the groundwater $\delta^{18}O$ signature measured in the well following storms (Turner et al., 1984; Maule and Stein, 1996).

Radiogenic Isotopes

Measurements of the abundance of ^3H (tritium) were used in this study to obtain a first approximation of the age of groundwater samples. Tritium is produced naturally by the interaction of cosmic radiation with atmospheric oxygen and nitrogen. Global variations as well as seasonal variations are caused by changes in atmospheric circulation between the troposphere and the stratosphere which is a major reservoir for tritium (Davis and Murphy, 1987). Prior to nuclear testing, tritium abundance in precipitation was 2 to 24 tritium nucleii per 10^{18} stable hydrogen nucleii, or 2 to 24 tritium units (TU) (Schlosser et al, 1988). Detonation of thermonuclear devices in the atmosphere, beginning in the early 1950s, caused an increase in the levels of ^3H in precipitation to a peak of 50 to 100 TU in the Southern Hemisphere, and 500 to 10,000 TU or more in the Northern Hemisphere in the early 1960's (Schlosser et al, 1988). This period is referred to as the "bomb peak" of atmospheric tritium levels. Tritium has a half life of 12.43 years (Unterweger et al., 1980). The amount of tritium remaining in a sample of water of a certain age at a time (t) after recharge can be modeled as follows (Schlosser et al., 1988):

$$^3H(t) = {}^3H(t_0)e^{-\lambda t} \qquad (2\text{-}10)$$

where

$^3H(t)$ = tritium concentration at time t

$^3H(t_0)$ = tritium concentration at the time of infiltration

λ= tritium decay constant = 0.0558 $year^{-1}$

Tritium concentrations in the atmosphere have undergone rapid reduction since the cessation of most above-ground nuclear testing. A temporary increase was seen in the late 1970's during the French and Chinese testing. By 1987, tritium levels in precipitation had decreased to 25 TU in central Europe (Schlosser et al, 1988) and remain 5 to 20 times lower in the Southern Hemisphere. Tritium may still be produced locally through ternary fission of uranium-235 and plutonium-239 in nuclear reactors, as well as in factories for luminous instrument dial manufacture (Davis and Murphy, 1987).

Busenberg and Plummer (1993) developed a record of volume-weighted yearly ^{3}H concentrations from 1956-1962 for the Mirror Lake Research Station in New Hampshire (Figure 2.7). This plot was generated using precipitation data and reconstructed atmospheric ^{3}H from the Mirror Lake site (Busenberg and Plummer, 1993). The "peak" in recharge ^{3}H concentrations in 1963 was 295 TU, according to this plot. Recharge ^{3}H concentrations during the last 10 years (1986-1996) have ranged between 15 and 20 TU. Given the similar setting and close proximity of the Mirror Lake site to the Mansfield basin, the ^{3}H curve shown in Figure 2.7 is assumed to be representative of ^{3}H concentrations in recharge for this study.

Numerous studies have used the bomb peak in precipitation as a marker for determining groundwater ages and travel rates (e.g., Suess, 1969; Gaspar and Oncescu, 1972; Atakan et al., 1974; Hufen et al., 1974; Vogel et al., 1974; Poland and Stewart, 1975; Hobba et al., 1979; Nordstrom et al., 1985). To use this technique effectively, the groundwater flowpath must be well understood, and an accurate record of atmospheric

tritium abundance generated for the study area. This is not possible for the Mount Mansfield basin. However, as discussed in Chapter 3, tritium abundance measurements in groundwater can lead to fairly good approximations of groundwater residence times.

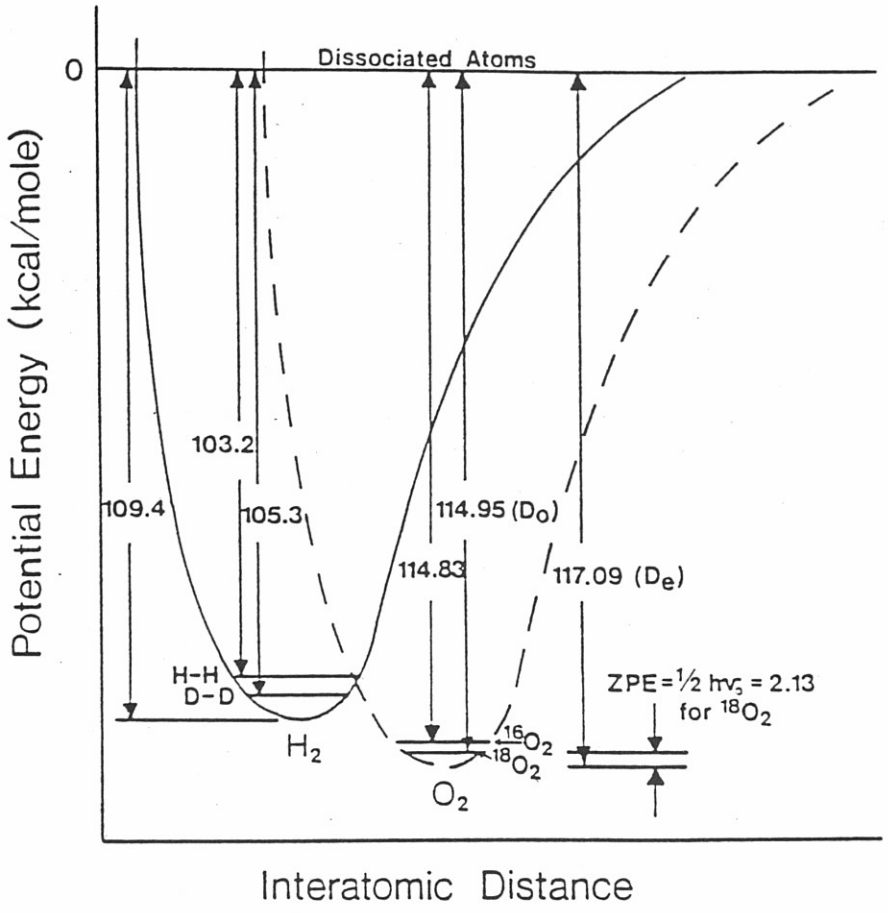

Figure 2.1

Potential energies for the different isotopic species of hydrogen and oxygen. Potential energy is related to interatomic distance of molecules. The zero-point energies of the different isotopic species of diatomic hydrogen and oxygen determine the tendency of each species to dissociate. From Kyser (1987).

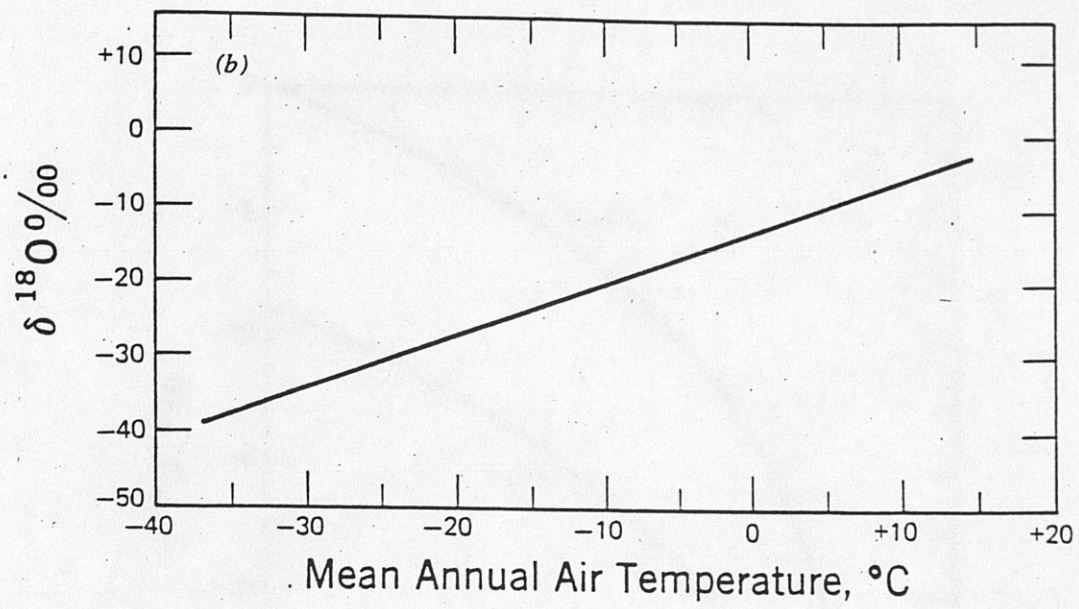

Figure 2.2

The relationship of meteoric water $\delta^{18}O$ and mean annual air temperature.
From Dansgaard (1964).

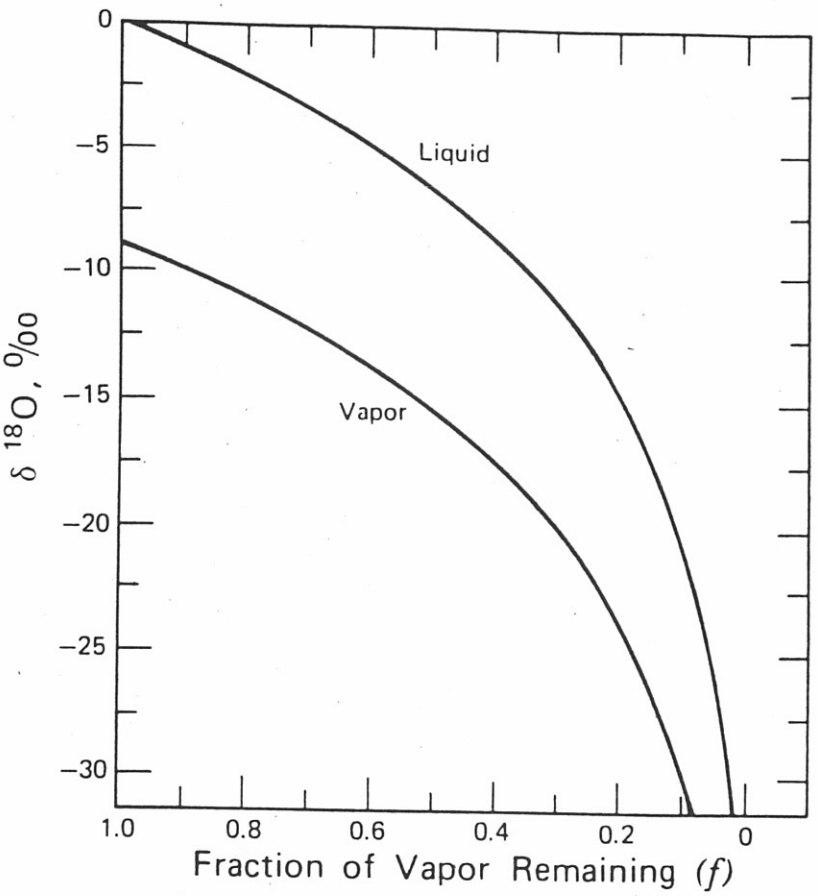

Figure 2.3

Fractionation of oxygen isotopes during condensation of water vapor (Rayleigh Distillation Model, 1899). From Rayleigh (1964).

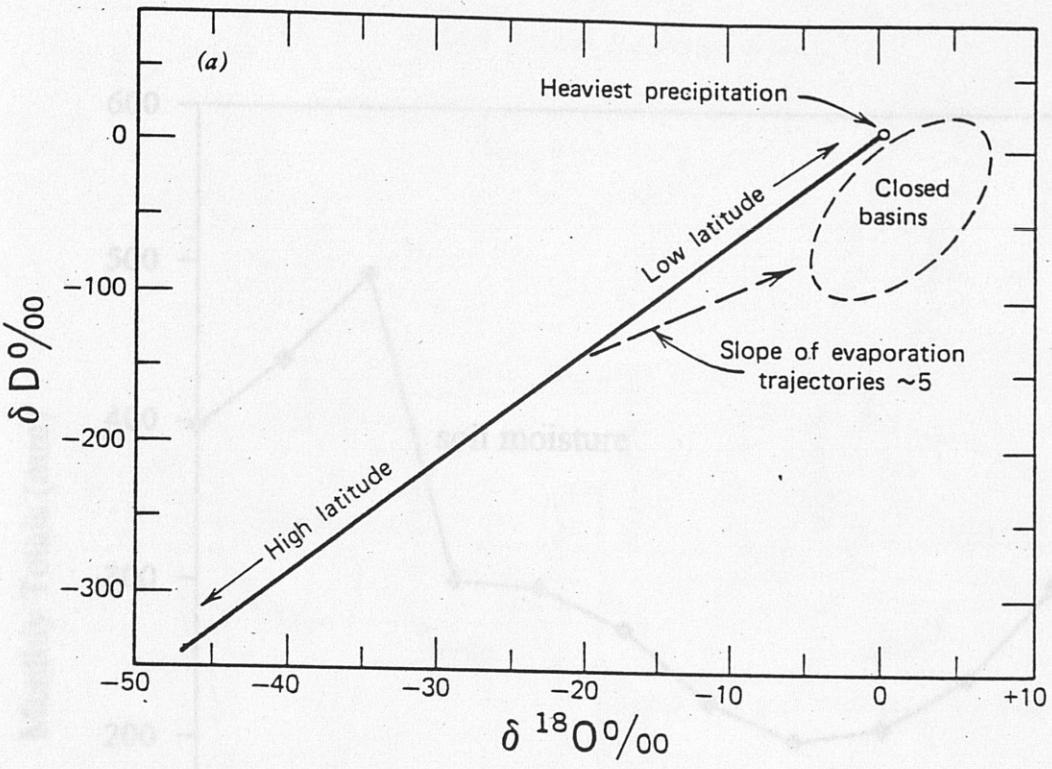

Figure 2.4

The relationship of δD and $\delta^{18}O$ in meteoric water samples. This figure was developed using measurements of samples worldwide. The linear best fit shown here is known as the meteoric water line (MWL). From Faure (1986).

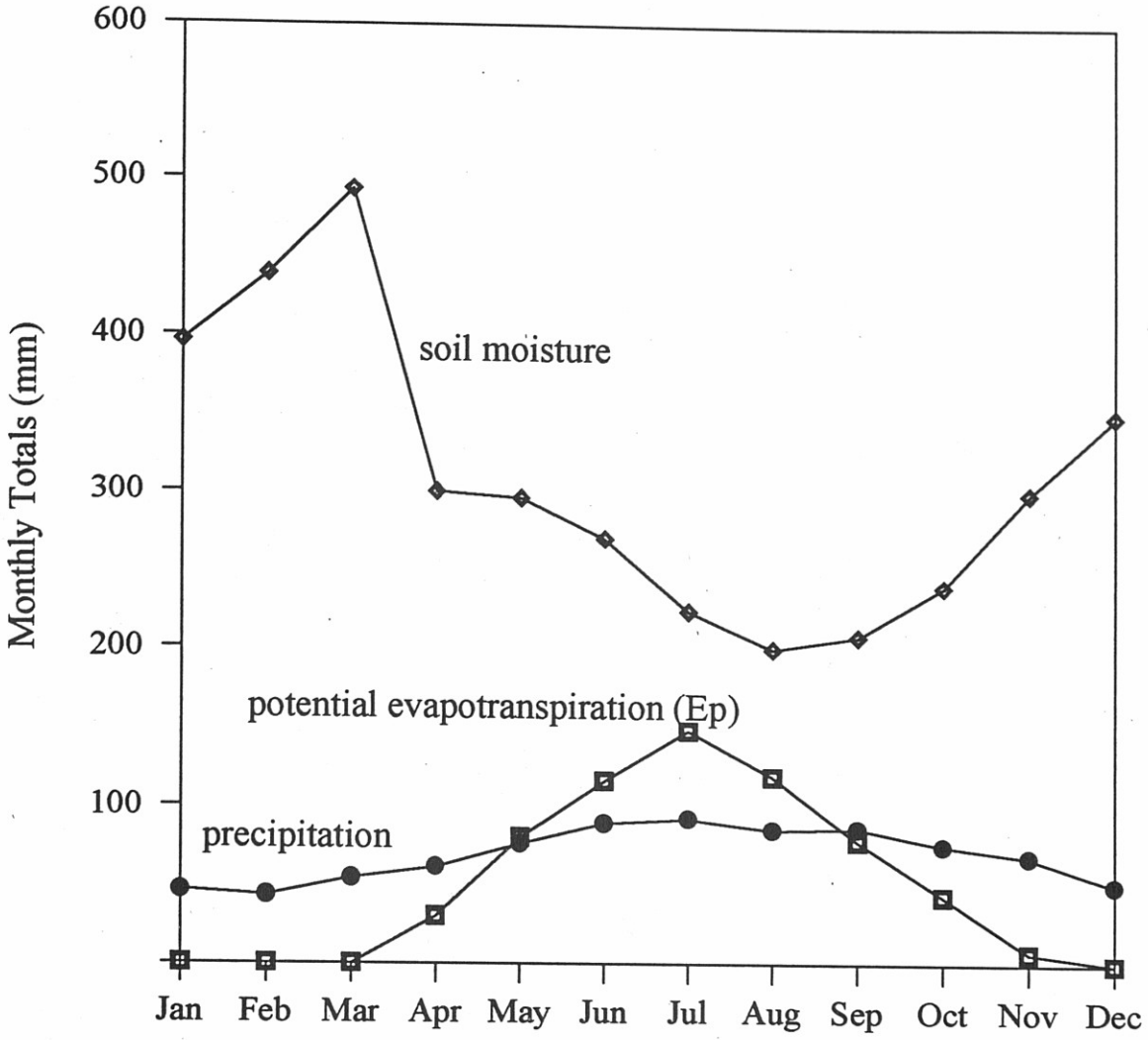

Figure 2.5

Plot of climatic data from Burlington, Vermont, 1910-1960. Produced using data from C.W. Thornthwaite Associates, Laboratory of Climatology (1964).

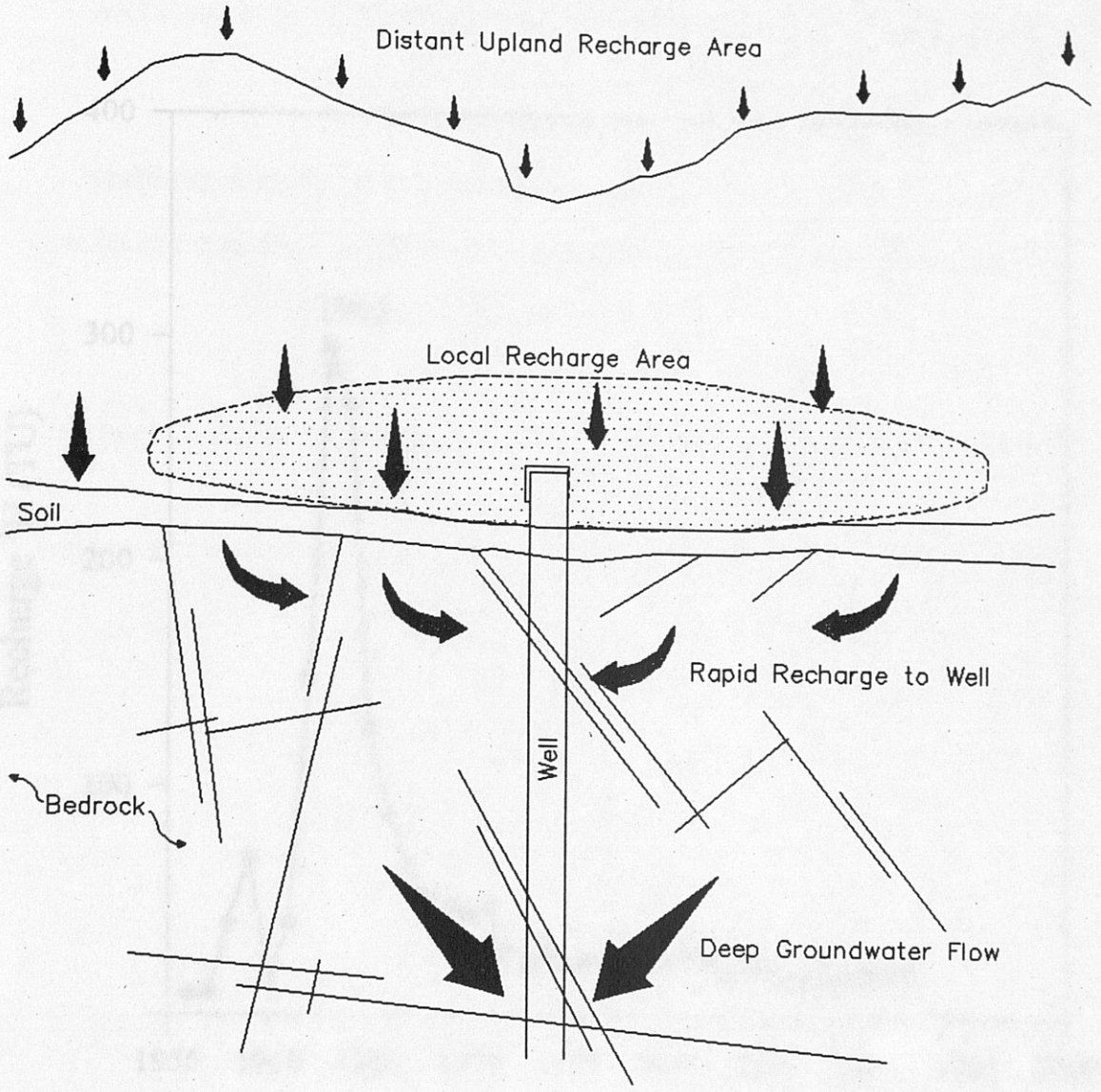

Figure 2.6

Schematic diagram of groundwater mixing. This figure illustrates the combined contribution of water to a well by shallow (local recharge) and deep (distant recharge) fractures.

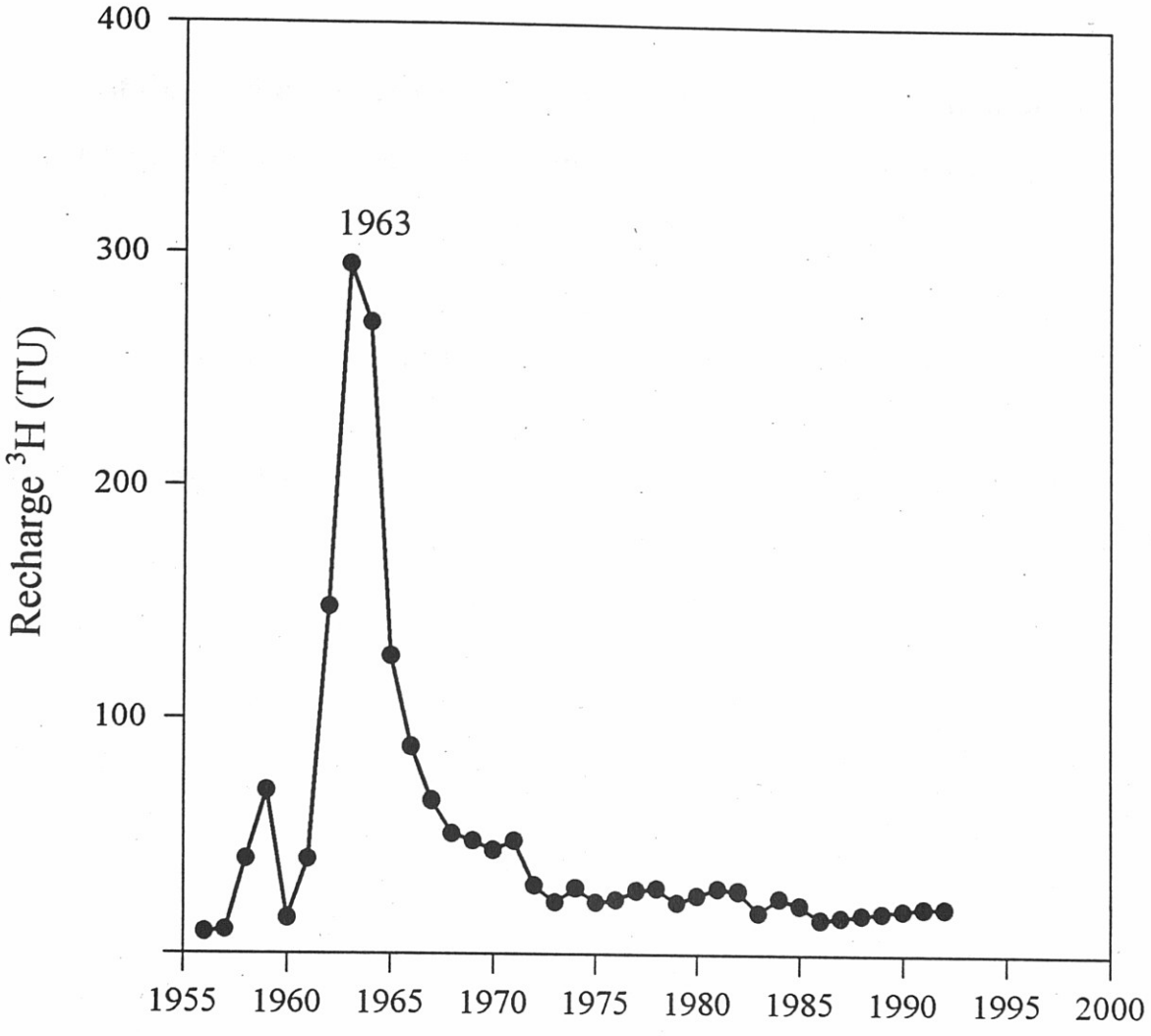

Figure 2.7

Reconstructed ^{3}H concentrations in recharge at the Mirror Lake Site. Adapted from Busenberg and Plummer (1993).

CHAPTER III

ARTICLE FOR SUBMISSION TO THE JOURNAL OF HYDROLOGY

Stable and radioactive isotope measurements describe temporal recharge and flow mechanisms in upland fractured bedrock aquifer, Vermont, USA

Michael D. Abbott, Andrea Lini, Paul R. Bierman, and Stephen F. Wright

Department of Geology, University of Vermont, Burlington, VT 05405-0122, USA

Abstract

Precipitation and groundwater samples, collected weekly over a 18 month period from a 10.5 km^2 upland watershed in northwestern Vermont, were analyzed for $\delta^{18}O$, δD, and ^3H composition. Differences in seasonal temperature and elevation are reflected in the $\delta^{18}O$ composition of precipitation, which ranges yearly over ~25 per mil (‰). Mean annual $\delta^{18}O$ of precipitation decreases by 2.5 ‰ per 1000 m of elevation gain. All precipitation and groundwater samples analyzed for both $\delta^{18}O$ and δD composition plot on or near the meteoric water line.

The $\delta^{18}O$ of groundwater collected from seven residential wells within the basin varies 2 ‰ yearly, with the exception of a spring located 300 m higher in elevation than the other wells. This spring shows a yearly variation of 4.3 ‰ ($1\sigma = 0.9$ ‰). In the warmer months (late April to early November), the $\delta^{18}O$ signature in the wells remains constant (within 0.4 ‰, $1\sigma = 0.2$ ‰), while in the colder months (late November to early April), the $\delta^{18}O$ composition varies in response to precipitation events by as much as 2 ‰, excepting the high spring, in which $\delta^{18}O$ varies throughout the year.

Flow in deep bedrock appears well mixed, exhibiting a steady isotopic composition. The $\delta^{18}O$ variation detected in wells and springs during the colder months is likely caused by a decrease in evapotranspiration near the wells, which allows influx of local recharge following precipitation events. During the warmer months, local recharge to bedrock in the valley, where most of the wells are located, appears to be greatly reduced.

Measurements of ^3H indicate that the age of groundwater at most of the sampling locations is less than 5 years. Two of the deep bedrock wells contain groundwater that may be between 21 and 34 years old, based on comparison with records of historical tritium deposition. These ages suggest travel rates of 0.2 $m \cdot day^{-1}$ to 9.6 $m \cdot day^{-1}$ for groundwater flow in the fractured bedrock.

Introduction

In New England, upland bedrock aquifers are rich sources of clean drinking water. However, groundwater recharge and flow systematics in the fractured bedrock of steep alpine environments differ significantly from other geohydrologic systems. To model groundwater flow in this type of setting, for the purpose of predicting water supply sustainability or to address contamination problems, a comprehensive understanding of recharge and flow is required. Of particular importance in the development of such a model is the location of significant recharge areas, as well as the amount and timing of recharge to bedrock (Maloszewski et al., 1982; Alley, 1984; Harte and Winter, 1993).

We used stable and radiogenic isotopic measurements in precipitation and groundwater to develop a conceptual model of groundwater recharge and flow in the upland, fractured phyllite and schist aquifer of the Browns River, northwestern Vermont (Figure 3.1). Large seasonal temperature changes (~50°C annually) and steep relief in this setting produce significant annual variations in the stable oxygen isotopic composition (-3 to -28 ‰) of precipitation. We found that some of these changes are preserved in groundwater. The temporal changes in $\delta^{18}O$ and δD can be used to estimate groundwater flow rate, and to determine the location of significant recharge areas (Love et al., 1994; Datta et al. 1996). Measurements of tritium (^3H) can be used to refine interpretations of groundwater residence time in the bedrock (Vogel et al., 1974; Allison and Hughes, 1975; Hedenquist et al., 1991). Using several isotopes as interpretive tools constrains our understanding of groundwater recharge and flow in this upland setting.

Location and Geology of the Study Area

The upland watershed (10.5 km^2) of the Browns River (44°30'N, 72°50'E) is bordered to the east by the north-south trending ridge of Mt. Mansfield, the highest of the Green Mountains (Figure 3.1). Elevations in this watershed range from 300 m asl in the town of Underhill Center, to 1330 m asl near the summit of Mt. Mansfield. The dominant tree type changes from a mix of large deciduous (oak and maple) and coniferous (fir and spruce) trees in the valley, to sparsely distributed and often scrubby fir and spruce on the mountain slopes, and finally to arctic and alpine tundra vegetation at the highest elevations on Mount Mansfield (Burns, 1916; Connor, 1994). Soils are generally thin sandy to stony loams at the upper elevations. Below 350 m asl, the topography flattens, and more sandy soils are present (USDA and SCS, 1974; 1981). The upper portion of the watershed has thin till or colluvial cover underlying soils, while at lower elevations (below 350 m asl), deposits of glaciolacustrine sediments and till may reach thickness of up to 150 m (Stewart, 1961; Connally, 1968; Stewart and MacClintock, 1969).

Urbanization in the basin is limited, consisting of 12 year-round and 3 summer residences and a recreational area (Underhill State Park) that operates only in the summer months. The small town of Underhill Center lies just downgradient from the study basin. Residents in the basin draw groundwater from drilled bedrock wells or springs for their water supply. Bedrock well yields range from less than 4 liters•min^{-1} (1 gpm) to ~ 40 liters•min^{-1} (10 gpm). This area was chosen for study because it is typical of many upland areas in New England which are facing new challenges in managing water resource development as residential populations increase.

The watershed is underlain by chlorite-quartz-muscovite phyllite and schist (Christman, 1969; Thompson and Thompson, 1991). A few lenses of amphibolitic greenstone are also found. The rock exhibits a strong bedding schistosity and folding oriented north-south along the axis of the Green Mountains (Christman, 1969). Brittle fractures exist in the form of steeply dipping joints as well as sheeting joints observed in cliff faces. Spacing of joints varies widely from 1 or 2 cm to greater than 1 m at most outcrops. Weathering along foliation surfaces is seen in outcrop on the exposed ridges above treeline, but is not evident with depth in relatively recent cuts or in less exposed areas at lower elevations. Fracture orientation measurements taken at outcrops throughout the basin indicate that there are several groupings of predominant joint directions among the steeply dipping joints, particularly north-south, N80°E, and N30°E sets (Figure 3.2). However, no orientation is predominant, suggesting that there is a high potential for interconnection of fractures. When considering the added effect of the sheeting joints and weathered foliations (at the upper elevations), it appears likely that recharging groundwater will experience mixing during transport in the bedrock. Such mixing will homogenize the isotopic signature of any groundwater with significant residence time in the bedrock aquifer.

Methodology

Samples of precipitation were collected weekly from July 1995 to December 1996 at nine locations representative of the elevation distribution in the studied basin (Figure 3.3). Several locations were also sampled downgradient from the basin. Rain samples were

collected in insulated bottles through a funnel (Figure 3.4a). Melt samples were collected in lysimeters set at the ground surface (Figure 3.4b). Snow samples were obtained by coring the weekly snowfall, then allowing the samples to melt in sealed containers. Cumulative snow pack samples were also obtained by coring at stations P6 and P8.

Nine existing residential wells were included in this study. Untreated groundwater samples were collected weekly from seven of the wells (Figure 3.3) from October, 1995 to December, 1996. Two of the wells (GW2 and GW7b) were not included in the weekly sampling program, but were sampled on several occasions during the study. Samples were collected directly from an outside or inside tap after system purging. Three of the wells, GW3, GW7, and GW8, are deep uncased bedrock wells (53, 213, and 83 meters, respectively). GW8 is located in the town of Underhill Center, downgradient from the study area. The remainder of the wells are developed bedrock springs. The high-elevation spring, GW1, is used as a water supply for Underhill State Park on Mount Mansfield. Two additional springs, GW2 and GW7b, were sampled occasionally during the study.

All collected samples (n=1021) were analyzed for $\delta^{18}O$ at the University of Vermont Environmental Stable Isotope Laboratory. Samples were equilibrated with CO_2 gas and extracted using standard cryogenic separation techniques (Taylor, 1973; Wong et al., 1987; Socki et al., 1992). Measurements were performed using a VG SIRA Series II Isotope Ratio Mass Spectrometer, and normalized to values obtained for standards. Standard deviation for the measurement of standards (n=129) relative to Vienna Standard Mean Ocean Water (VSMOW) was ± 0.12 ‰.

Seventy-five biweekly samples from groundwater sampling locations GW1, GW3, and GW5, and twenty-five biweekly samples from precipitation and meltwater collection at P6 (600 m asl.) were analyzed for δD composition. Analysis was performed at the Institute for Arctic and Alpine Research (INSTAAR), Center for Geochronology, University of Colorado using uranium furnace reduction under vacuum (Vaughn, 1994).

Samples were collected for ^{3}H analysis from all the wells and springs in June, 1996. Tritium samples were electrolytically enriched and analyzed at the University of Waterloo (Heemskerk et al., 1993).

Results of Precipitation Analysis

The $\delta^{18}O$ composition of precipitation varies in response to seasonal temperature changes and temperature gradients controlled by elevation changes within the basin. The basin experiences strong seasonal temperature variations (Figure 3.5), whereas the amount of precipitation remains fairly constant throughout the year (Figure 3.6). The $\delta^{18}O$ values measured in rain and newly fallen snow varied over a range of 25 ‰ (-3 ‰ to -28 ‰) at most locations during the sampling period (Figure 3.7). The data have a strong seasonal signal which reflects the seasonal temperature changes. A correlation (R^2 = 0.47-0.70) is observed between records of $\delta^{18}O$ in precipitation and temperature values (Figure 3.8). Records of $\delta^{18}O$ in precipitation are also well correlated (R^2 = 0.78-0.94) between sampling locations (Figure 3.9). The mean annual $\delta^{18}O$ composition of precipitation decreases with increasing elevation (-2.5 ‰ per 1000 m, R^2 = 0.96) as a result of the colder temperatures at higher elevations (Figure 3.10). Although fractionation by rainout

may occur in the case of a localized cloudburst, neither the spatial density of rain collectors nor the frequency of collection were adequate to quantify any such effects. We suspect that, in most cases, the effects of temperature and elevation override any other factors in determining the $\delta^{18}O$ composition of precipitation.

Deuterium values in precipitation maintain a linear relationship with $\delta^{18}O$ values (Figure 3.11). The equation for the best-fit line through the points representing δD vs. $\delta^{18}O$ values is:

$$\delta D = 7.7 \cdot \delta^{18}O + 11.4 \qquad (3\text{-}1)$$

All points shown in Figure 3.11 lie close to the Meteoric Water Line (MWL) (Faure, 1986). There is no indication of evaporation prior to collection of the water samples, suggesting that the rain collectors were efficient in preventing evaporation.

Results of Meltwater Analysis

The $\delta^{18}O$ composition of meltwater from the snow pack is influenced by the $\delta^{18}O$ composition of the snow pack and by mixing with rain. Plots of meltwater $\delta^{18}O$ during melting events occurring from late November to late May for four of the sampling locations, P4, P6, P7, and P8, are presented in Figure 3.12. The plots for P6 and P8 also include $\delta^{18}O$ values for weekly cumulative snow pack samples collected at those stations. Melt $\delta^{18}O$ values range from -8 to -18‰. In 11 out of 14 cases, meltwater samples have a less depleted $\delta^{18}O$ composition than the snow pack, a result of mixing with rain events

(Friedman et al., 1991; Sommerfield et al., 1991; Shanley et al., 1994; IAHS, 1995). During the period of highest melting rates, from late May to early June, the $\delta^{18}O$ value of meltwater increases sharply, reflecting the input of large amounts of spring rainfall.

Results of Groundwater Analysis

The $\delta^{18}O$ composition of groundwater varies seasonally in the wells and springs. The mean yearly variation in the $\delta^{18}O$ composition of all wells and springs is 2 ‰ (Figure 3.13), with the exception of the high-elevation spring GW1. The yearly $\delta^{18}O$ variation in GW1 is 4.3 ‰. The $\delta^{18}O$ curve for GW1 mimics the seasonal temperature curve, which is included in Figure 3.13. However, the least depleted $\delta^{18}O$ values in GW1 were recorded 2 months after peak temperature values. Similarly, the most depleted $\delta^{18}O$ values were recorded 2 months after the lowest temperatures in the winter. This may reflect the speed of groundwater infiltration and flow through the bedrock in the area recharging GW1. This spring apparently has a high percentage of contribution from recent water, perhaps infiltrating in the area close to the well or recharging higher and preserving seasonal changes (i.e., little mixing) prior to reaching GW1.

In most of the wells, with the exception of GW1, the groundwater exhibits a very constant $\delta^{18}O$ signature ($\sigma \leq 0.2$ ‰) from mid-April to mid-November, indicating thorough mixing of the groundwater. More substantial fluctuations ($1\sigma = 0.2$ to 0.5 ‰) in the $\delta^{18}O$ composition of groundwater in these wells occur during the colder months (late November to early April). The $\delta^{18}O$ values for GW1 vary over a larger range ($1\sigma = 0.9$ ‰), which remains consistent throughout the year (Figure 3.13).

The mean annual $\delta^{18}O$ values differ slightly among the wells, ranging from -12.2 ‰ (GW1) to -11.3 ‰ (GW8) (Table 3.1). No consistent relationship ($R^2 < 0.1$) between well elevation and the mean annual $\delta^{18}O$ value was observed. Furthermore, no relationships ($R^2 < 0.1$) were observed between mean annual $\delta^{18}O$ values and the physical characteristics of the well, such as well depth or yield. Unlike precipitation, the $\delta^{18}O$ values in groundwater do not correlate well with temperature changes ($R^2 < 0.1$). Groundwater $\delta^{18}O$ records are only slightly correlated between wells ($R^2 \leq 0.3$). Based on these findings, it appears that the $\delta^{18}O$ composition of groundwater in each well may respond uniquely to seasonal changes.

Deuterium values were plotted against $\delta^{18}O$ in groundwater (Figure 3.14). They plot very close to the precipitation values, indicating that groundwater has not been modified isotopically since recharge, and is probably of Holocene origin.

Results of Radiogenic Isotope Measurements

Tritium abundance measurements provide only a general estimate for the age of groundwater. Due to mixing that may occur within the bedrock system, it is likely that ^3H values represent an integration of values for several recharge times. The ^3H abundance measured in all of the springs and one of the wells (GW8) is ~15 TU ($1\sigma = 0.5$ TU) (Table 3.1). One of the deep wells, GW3, has a ^3H abundance of 26.7 ± 1.9 TU, and the deepest well, GW7, has a ^3H abundance of 6.5 ± 0.7 TU.

Recharge ^3H concentrations during the last 10 years (1986-1996) have ranged between 15 and 20 TU (Busenberg and Plummer, 1993). Therefore, the samples with ^3H

values close to 15 TU may represent recent recharge. The other samples (GW3 and GW7) must have been recharged at an earlier time. However, all samples contain water of post-1950 origin.

Discussion of Recharge

Measurements of the $\delta^{18}O$ composition of groundwater suggest that recharge to bedrock from precipitation events occurs in significant amounts only during the colder months when evapotranspiration is very low. A plot of 50 years (1910-1960) of precipitation, soil moisture, and potential evapotranspiration measurements compiled for Burlington, Vermont (C.W. Thornthwaite Associates, Laboratory of Climatology, 1964) (Figure 3.15) indicates that evapotranspiration (E_p) is negligible from the months of December to March. E_p increases in late March or early April to a peak in July, then decreases to a negligible amount in November. Although precipitation is relatively high during the warmer months, soil moisture remains much lower than during the rest of the year. This indicates that a much smaller percentage of precipitation infiltrates to groundwater from April to November, than during the remainder of the year.

We believe that the $\delta^{18}O$ signature observed in most of the wells and springs from late April to early November is governed by well mixed groundwater flow in deeper, well-connected fractures. During the colder months, infiltration near the wells enhances the effect of individual storm or melt events on the $\delta^{18}O$ composition of the sampled groundwater (Figure 3.16). During the warmer months, groundwater recharge in the valley, where most of the wells are located, is virtually shut off by vegetation. In contrast,

the watershed near GW1 has a sparse forest of smaller trees and is typically exposed to lower temperatures, allowing recharge to occur throughout the year.

The mean annual $\delta^{18}O$ value of each groundwater sampling location (Table 3.1) provides an approximation of the elevation of upland recharge to the well or spring. Based on the a best-fit linear interpretation of the relationship between mean annual $\delta^{18}O$ for precipitation and elevation (Figure 3.10), the following equation can be used to estimate recharge elevations:

$$Y = -398 \cdot X - 4003 \qquad (3\text{-}3)$$

where

Y = recharge elevation, meters asl

X = mean annual $\delta^{18}O$ in groundwater, ‰

The value for Y obtained by this calculation represents the spatially weighted mean elevation of recharge (Table 3.2). Groundwater flowing from the highest portion of the well or spring's recharge area (lowest mean $\delta^{18}O$ values) may become mixed with water recharged at lower elevations (higher mean $\delta^{18}O$ values) along the flowpath. The relative proportions of recharge contributed from different elevations within the recharge area determine the mean $\delta^{18}O$ value recorded at the well. Therefore, in order to use Y to estimate groundwater flow distances (Table 3.2), we must assume that most of the recharge contributing to the well occurs near the elevation represented by Y.

Discussion of Groundwater Age and Flow Rates

The combination of stable and radiogenic isotope measurements obtained in this study enabled us to develop an interpretation of groundwater flow rates in the study basin. The seasonal stable isotope signature of precipitation recharging bedrock is reflected in groundwater that discharges relatively quickly, as in the case of the high spring (GW1). This water appears to discharge two months after recharge to the bedrock. However, groundwater samples from most of the wells and springs did not exhibit seasonal signatures, indicating that water becomes well mixed as it travels through the bedrock.

Busenberg and Plummer (1993) developed a record of volume-weighted yearly ^{3}H concentrations from 1956-1962 for the Mirror Lake Research Station in New Hampshire (Figure 3.17). Given the similar setting and close proximity of the Mirror Lake site to the Mansfield basin, the ^{3}H curve shown in Figure 3.17 is assumed to be representative of ^{3}H concentrations in recharge for this study.

Superposed on the plot of historical tritium concentrations in recharge are three hypothetical curves: A, B, and C (Figure 3.17). These curves were generated using a tritium half-life of 12.43 years (Unterweger et al., 1980) to calculate the decay of tritium in recharge from an assumed initial concentration in precipitation (Rose, 1993):

$$T_i^* = T_i e^{-\lambda t} \qquad (3\text{-}2)$$

where

T_i^* = decay-corrected tritium concentration in groundwater at i years

T_i = initial tritium concentration at i = 0 years

λ = decay constant (0.0558/year)

t = time in years

Curve A in Figure 3.17, which represents decay to a final ^3H concentration in groundwater of 27 TU (GW3), intersects the reconstructed historical ^3H curve at 1962 and again at 1965, on either side of the 1963 "peak" of 295 TU. This indicates that a portion of the groundwater in GW3 has resided in the bedrock aquifer for a period of 31 to 34 years.

Curve B in Figure 3.17 represents decay to a final ^3H concentration of 15 TU found in wells, GW1, GW2, GW4, GW5, GW6, GW7B, and GW8. This curve intersects the historical ^3H curve at 1961, 1966, and at 1991. These samples could have been recharged between 30 and 35 years ago, or recently (within the past 5 years). Based on stable isotope data, as discussed above, it is likely that most of the water discharging in GW1 has resided only several months in the bedrock. The other springs may also contain young water. The well GW8 has a much higher yield than GW3 and GW7, indicating that it is in an area of very conductive fractures, which implies a high flux of water through the rock. Therefore, it is possible that all of the springs and the well with tritium concentrations of 15 TU contain water recharged within the last 5 years.

Curve C in Figure 3.17 represents decay to a final ^3H concentration of 7 TU (GW7). This curve intersects historical ^3H at 1959, 1961, 1973 and 1975, indicating that

the water is between 21 and 37 years old. It is also possible that the water is even older (pre-1956) and has been mixed with younger waters of higher ^{3}H concentration.

The estimated age of groundwater is assumed to be equal to the residence time of groundwater in the bedrock. Using the residence time for each of the groundwater sampling locations (Table 3.2), the flow of groundwater through the bedrock aquifer can be estimated:

$$V_x = d/r \qquad (3\text{-}4)$$

where

V_x = velocity of water through fracture network in a downgradient direction ($m \cdot day^{-1}$)

d = distance of flow from the minimum elevation of recharge to the well or spring (m)

r = estimated residence time (days)

Calculated groundwater flow rates for GW3 and GW7 range from 0.2 $m \cdot day^{-1}$ to 0.4 $m \cdot day^{-1}$. For other wells and springs, calculated flow rates range from 0.2 $m \cdot day^{-1}$ to 9.6 $m \cdot day^{-1}$ (Table 3.2). These estimates indicate that flow rates in the fractured rock may vary over more than an order of magnitude. We suspect that this is a function of the spacing and interconnectivity of the fractures along the flow paths to each well.

Summary and Conclusions

Results of this study indicate that the timing of recharge to the bedrock groundwater system is controlled largely by the effects of evaporation and plant uptake in the basin. Recharge to groundwater occurs at appreciable rates only at the higher elevations of the upland basin where evaporation and transpiration rates are low (due to harsh weather conditions), and during the colder months of the year throughout the basin.

The age of groundwater in the fractured rock varies from less than one year to over 30 years. Flow rates range from 0.2 $m \cdot day^{-1}$ to greater than 9 $m \cdot day^{-1}$, and are dependent upon the depth of flow and the density of fractures. Water moves most rapidly (up to 9 $m \cdot day^{-1}$) in the shallow bedrock.

The results of this study have implications regarding the protection of the bedrock as a groundwater source. Because recharge to bedrock occurs nearly continuously throughout the year at the upper elevations of the watershed, it is logical to protect these areas from contamination by limiting or prohibiting activities with high pollution potential. In the lower portions of the watershed, recharge occurs in significant amounts during the colder months. Therefore, activities such as salting of roads and land application of wastewater should be reduced or prohibited in any areas close to wells or springs.

Acknowledgments

Research was funded in part by the U.S. Geological Survey under a 1995 Vermont Water Resources Institute Grant and USGS Grant # HQ96GR02702-01 in 1996. A stipend for summer research was provided by the University of Vermont in 1996. We thank B. Drimmie (University of Waterloo) for tritium measurements, and E. Steig and B. Vaughn (INSTAAR) for deuterium measurements. Thanks to D. Dougherty (University of Vermont) for his review of this paper.

References Cited

Alley, W.M., 1984, On the treatment of evapotranspiration, soil moisture accounting and aquifer recharge in monthly water balance models: Water Resources Research, v. 20, p. 1137-1149.

Allison, G.B., and Hughes, M.W., 1975, The use of environmental tritium to estimate recharge to a South-Australian aquifer: Journal of Hydrology, v. 26, p. 245-254.

Bentley, H.W., 1978, Some comments on the use of chlorine-36 for dating very old groundwater, *in* Davis, S.N., ed., Workshop on dating old ground water, Union Carbide Corporation, Nuclear Division.

Burns, G.P., and Otis, C.H., 1916, The Trees of Vermont: Burlington, Vermont, Free Press Printing Company, 244 p.

Christman, R.A., 1959, Geology of the Mount Mansfield Quadrangle Vermont: Vermont Geological Survey Bulletin, p. 1-75.

Climatology, C.W.T.A.L.of., 1964, Average Climatic Water Balance Data of the Continents: Part VII United States, Publications in Climatology: Centerton, New Jersey, National Science Foundation, p. 615.

Connally, G.G., 1968, Surficial geology of the Mount Mansfield 15 minute quadrangle, Vermont: Montpelier, Vermont, Vermont Geological Society.

Connor, S., 1994, New England Natives: Cambridge Massachusetts, Harvard University Press, 274 p.

Datta, P.S., Bhattacharya, S.K., and S.K.Tyagi, 1996, 18O studies on recharge of phreatic aquifers and groundwater flow-paths of mixing in the Delhi area: Journal of Hydrology, v. 176, p. 25-36.

Dole, E.J., 1923, A study of the relative importance of air temperature and relative humidity on the transpiration behavior of coniferous evergreen trees more particularly of primus strobus [406 thesis]: Burlington, Vermont, University of Vermont.

Dugan, J.T., and Peckenpaugh, J.M., 1985, Effects of climate, vegetation and soils on consumptive water use and ground-water recharge to the central midwest regional aquifer system, mid-continent United States, USGS.

Friedman, I., Benson, C., and Gleason, J., 1991, Isotopic changes during snow metamorphism, *in* Taylor, H.P., O'Neil, J.R., and Kaplan, I.R., eds., Stable Isotope Geochemistry: A Tribute to Samuel Epstein, The Geochemical Society, p. 211-222.

Harte, P.T., and Winter, T.C., 1993, Factors affecting recharge to crystalline rock in the Mirror Lake area, Grafton County, New Hampshire, *in* Morganwalp, D.W., and Aronson, D.A., eds., U.S. Geological Survey Toxic Substances Hydrology Program Technical Meeting: Colorado Springs, Colorado, USGS.

Hedenquist, J.W., Goff, F., Phillips, F.M., Elmore, D., and Stewart, M.K., 1991, Groundwater dilution and residence times, and constraints on chloride source, in the Mokai geothermal system, New Zealand, from chemical, stable isotope, tritium, and 36Cl data: Journal of Geophysical Research, v. 95, p. 19365-19375.

Heemskerk, A.R., Johnson, J. and Drimmie, R.J., 1993, Tritium Analysis, Environmental Isotope Laboratory Technical Procedure 1.0 Rev 3.0: Waterloo Ontario, University of Waterloo, 28 p.

IAHS, 1995, Biogeochemistry of Seasonally Snow-Covered Catchments, *in* Tonnessen, K.A., Williams, M.W., and Tranter, M., eds., Assembly of the International Union of Geodesy and Geophysics, Volume 228: Boulder, Colorado, IAHS.

Likens, G.E., Borman, F.H., Eaton, J.S., and Johnson, N.M., 1977, Biogeochemistry of a forested ecosystem: New York, Springer-Verlag, 146 p.

Likens, G.E., Borman, F.H., Pierce, R.S., and Eaton, J.S., 1985, The Hubbard Brook valley, An Ecosystem Approach to Aquatic Ecology -- Mirror Lake and its Environments: New York, Springer-Verlag, p. 516.

Love, A.J., Herczeg, A.L., Leaney, F.W., Stadter, M.F., Dighton, J.C., and Armstrong, D., 1994, Groundwater residence time and palaeohydrology in the Otway Basin, South Australia: 2H. 18O and 14C data: Journal of Hydrology, v. 153, p. 157-187.

Maloszewski, P., and Zuber, A., 1982, Determining the turnover time of groundwater systems with the aid of environmental tracers: 1. Models and their applicability: Journal of Hydrology, v. 57, p. 207-231.

Rose, S., 1993, Environmental tritium systematics of baseflow in Piedmont Province watersheds, Georgia (USA): Journal of Hydrology, v. 143, p. 191-216.

Shanley, J.B., Kendall, C., Smith, T., and Wolock, D., 1994, The effect of catchment scale and land use on the relative contributions of shallow flow paths to stream discharge during snowmelt: Water Resources Research, v. preliminary submission.

Socki, R.A., Karlsson, H.R., and Gibson, E.K.J., 1992, Extraction technique for the determination of oxygen-18 in water using pre-evacuated glass vials: Analytical Chemistry, v. 64, p. 829-831.

Sommerfield, R.A., Judy, C., and Friedman, I., 1991, Isotopic changes during the formation of depth hoar in experimental snow packs, *in* Taylor, H.P., O'Neil, J.R., and Kaplan, I.R., eds., Stable Isotope Geochemistry: A Tribute to Samuel Epstein, The Geochemical Society. p. 205-210.

Stewart, D.P., 1961, The glacial geology of Vermont: Montpelier, Vermont, Development Department.

Stewart, D.P., and MacClintock, P., 1969, The Surficial Geology and Pleistocene History of Vermont, Vermont Geological Survey.

Tamers, M.A., Ronzoni, C., and Scharpenseel, H.W., 1969, Naturally occurring chlorine-36: Atompraxis, v. 15, p. 433-437.

Taylor, H.P.J., 1973, O18/O16 evidence for meteoric-hydrothermal alteration and ore deposition in the Tonopah, Comstock lode, and Goldfield mining districts, Nevada: Economic Geology, v. 68, p. 747-764.

Thompson, P., and Thompson, T., 1991, Bedrock Geology of the Camels Hump-Bolton Mountain Area, North-Central Vermont: Vermont Geological Survey Special Bulletin, p. 1-32.

Unterweger, M.P., Coursey, B.M., Schima, F.J., and Mann, W.B., 1980, Preparation and calibration of the 1978 National Bureau of Standards tritiated-water standards: International Journal of Applied Radiation Isotopes, v. 33, p. 611-614.

USDA, SCS, Station, V.A.E., and Conservation, V.A.of E., 1974, Soil Survey of Chittenden, Vermont, USDA.

USDA, SCS, Station, V.A.E., and Conservation, V.A.of E., 1981, Soil Survey of Lamoille County, Vermont, USDA.

Vaughn, B., 1994, Stable isotopes as hydrologic tracers in South Cascade Glacier [M.S. thesis], University of Colorado.

Vogel, J.C., Thilo, L., and Dijken, M.V., 1974, Determination of groundwater recharge with tritium: Journal of Hydrology, v. 23, p. 131-140.

Wong, W.W., Lee, L.L., and Klein, P.D., 1987, Deuterium and oxygen-18 measurements on microliter samples of urine, plasma, saliva and human milk: American Journal of Clinical Nutrition, v. 45, p. 905-913.

Table 3.1

Well characteristics, mean annual $\delta^{18}O$ values, and tritium abundance in groundwater.

Well	Depth (meters)	Well Elevation (meters asl)	Mean Annual $\delta^{18}O$ (‰)	^{3}H (TU)
GW1	spring	670	-12.15	15.8 (±1.3)
GW2	spring	440	n/a*	15.9 (±1.3)
GW3	53	380	-11.92	26.7 (±1.9)
GW4	spring	380	-11.35	14.6 (±1.2)
GW5	spring	360	-11.60	15.9 (±1.2)
GW6	spring	330	-11.48	15.2 (±1.2)
GW7	213	310	-11.79	6.5 (±0.7)
GW7b	spring	310	n/a	14.7 (±1.2)
GW8	83	270	-11.25	15.4 (±1.2)

* The number of $\delta^{18}O$ measurements for GW2 and GW7b were insufficient for the calculation of mean annual $\delta^{18}O$ values.

Table 3.2

Estimated recharge elevations, groundwater residence times, and groundwater flow rates at wells and springs.

Well	Estimated Mean Recharge Elevation (meters asl)	Minimum Flow Distance (meters)	Estimated Residence Time (years)	Estimated Flow Rate ($m*day^{-1}$)
GW1	830	700	0.2-5	0.4-9.6
GW2	n/a*	n/a	1-5	n/a
GW3	740	2500	31-34	0.20-0.22
GW4	520	1700	1-5	0.9-4.7
GW5	620	2400	1-5	1.3-6.6
GW6	560	2300	1-5	1.3-6.3
GW7	690	3000	21-37	0.22-0.39
GW7b	n/a	n/a	1-5	n/a
GW8	480	1800	1-5	0.8-4.9

* The number of $\delta^{18}O$ measurements for GW2 and GW7b were insufficient for the calculation of estimated recharge elevations.

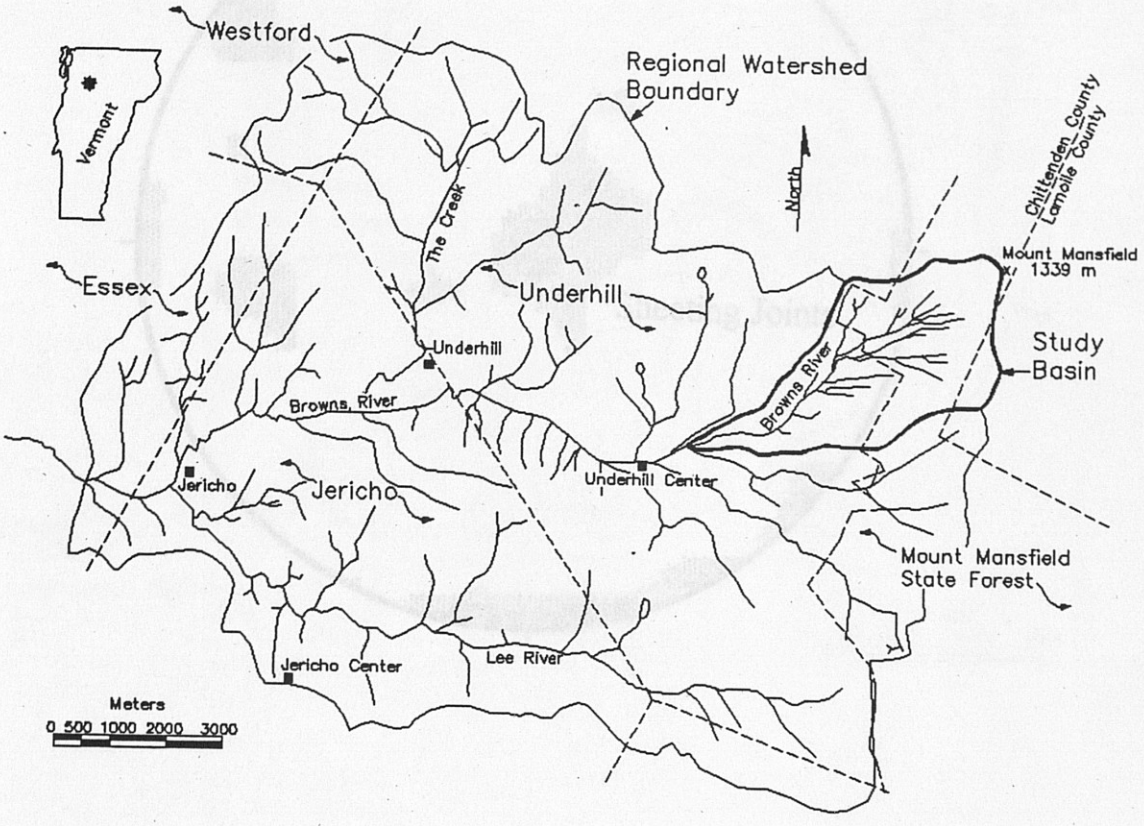

Figure 3.1

Study area and regional watershed.

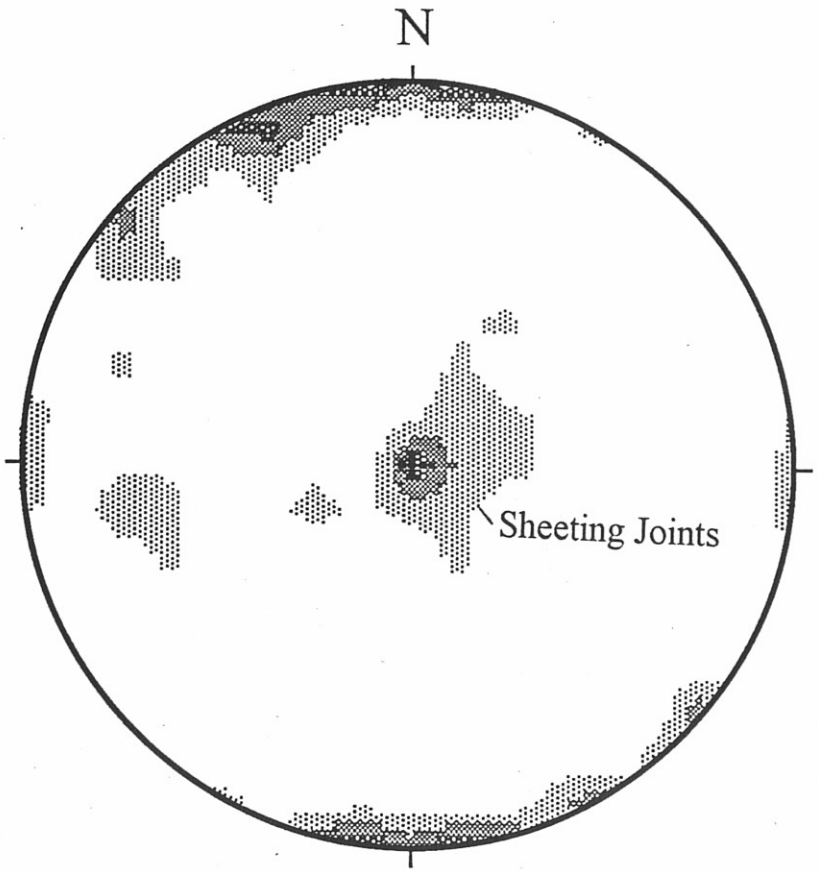

Figure 3.2

Bedrock fracture orientations. Lower hemisphere equal-area projection showing contour of poles to fracture planes (1% area plot, 5% contour interval) based on 118 field measurements at outcrop throughout the basin. Most joints are steeply dipping with the exception of several sheeting joints (n = 10) observed in cliff faces.

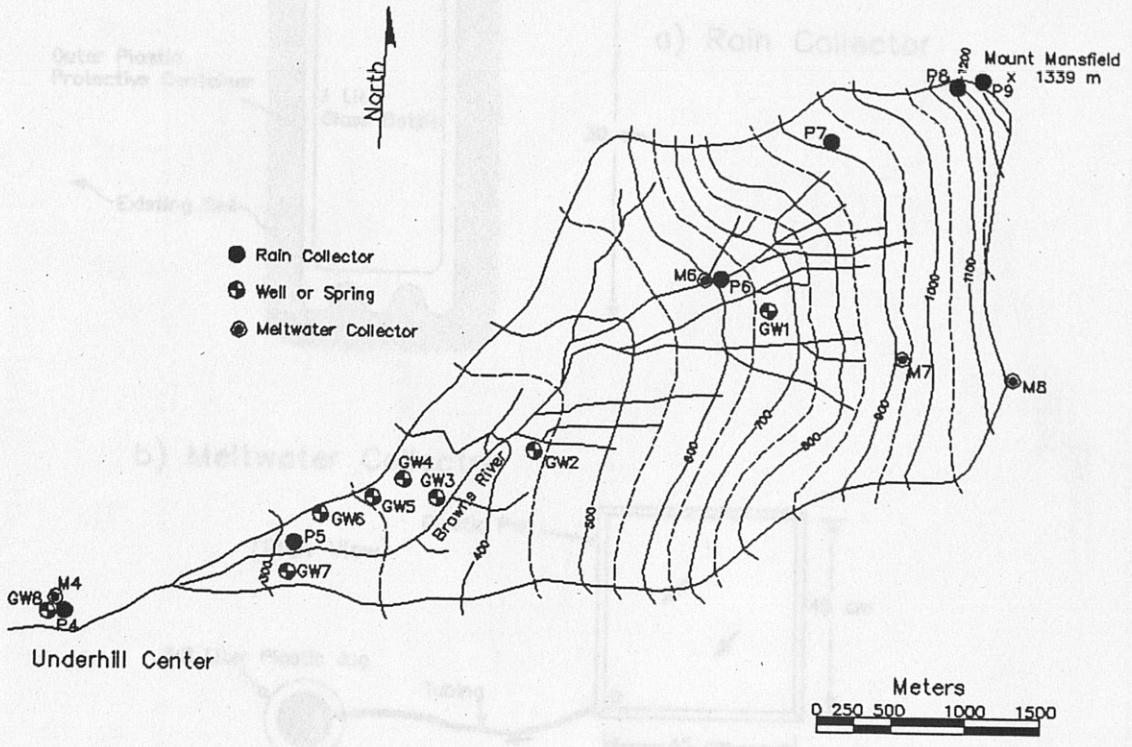

Figure 3.3

Study area and sampling locations. Groundwater samples were collected at residences. Sampling devices were installed at the locations shown for meltwater and rain collection. Countours are in meters asl.

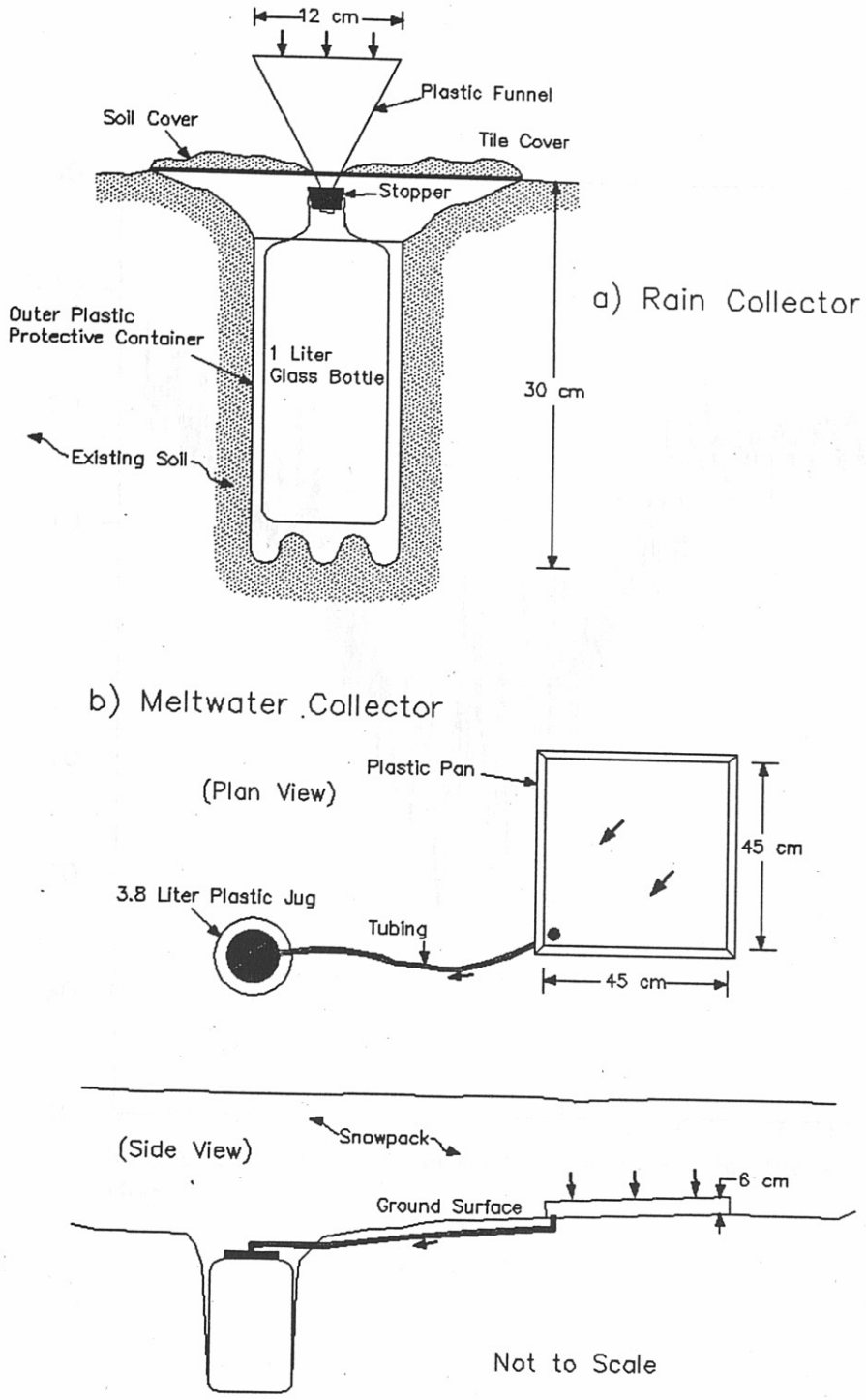

Figure 3.4

Rain and meltwater sampling devices. Rain collectors were installed in soil to prevent evaporation. Above treeline, samplers were set in insulated containers. Meltwater was collected from the buried plastic jug in order to avoid disturbing the snowpack above pan.

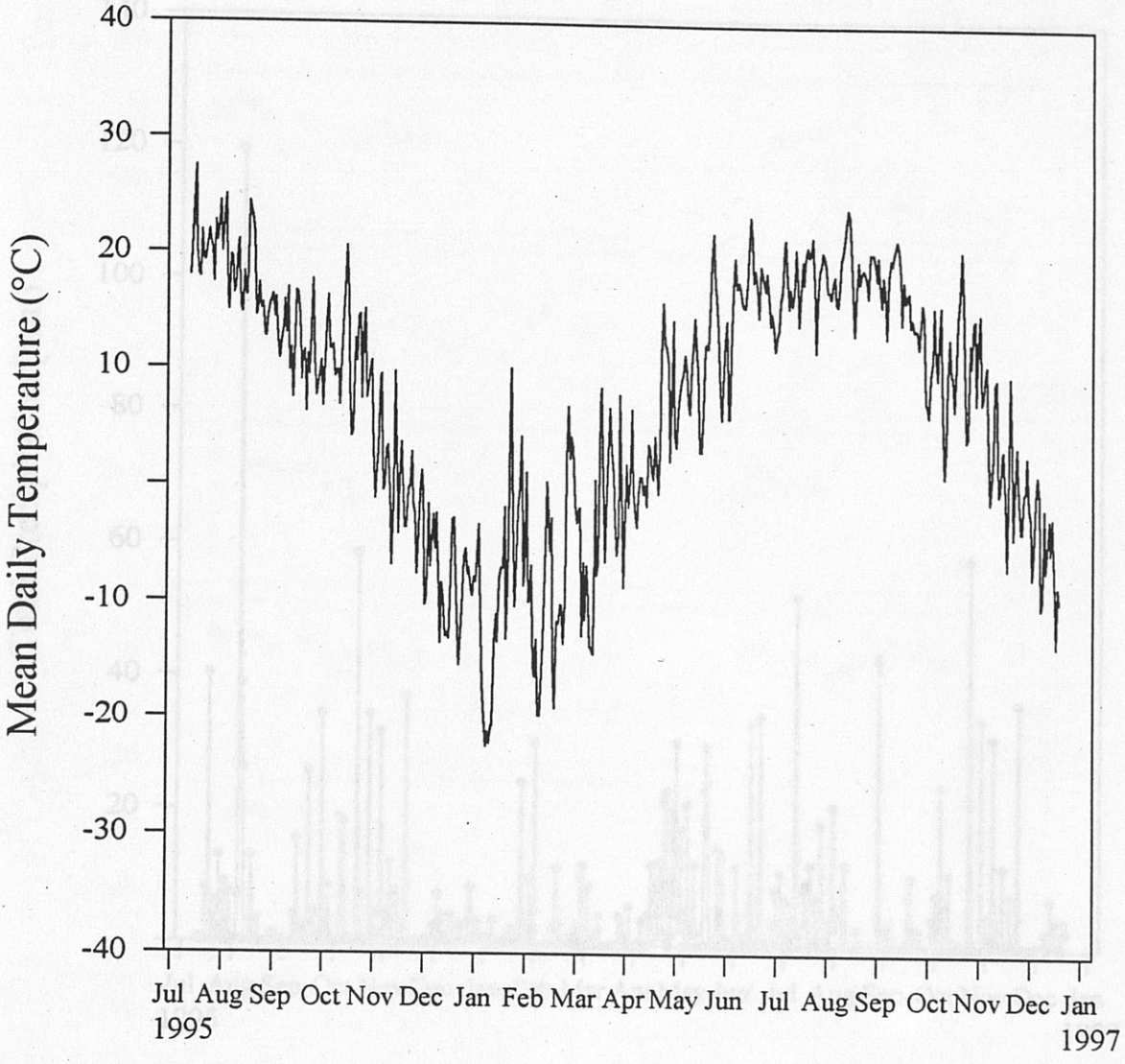

Figure 3.5

Daily temperature record. From measurements taken at Proctor Maple Research Center (600 m asl), Underhill (Cummings, 1997, pers. comm.).

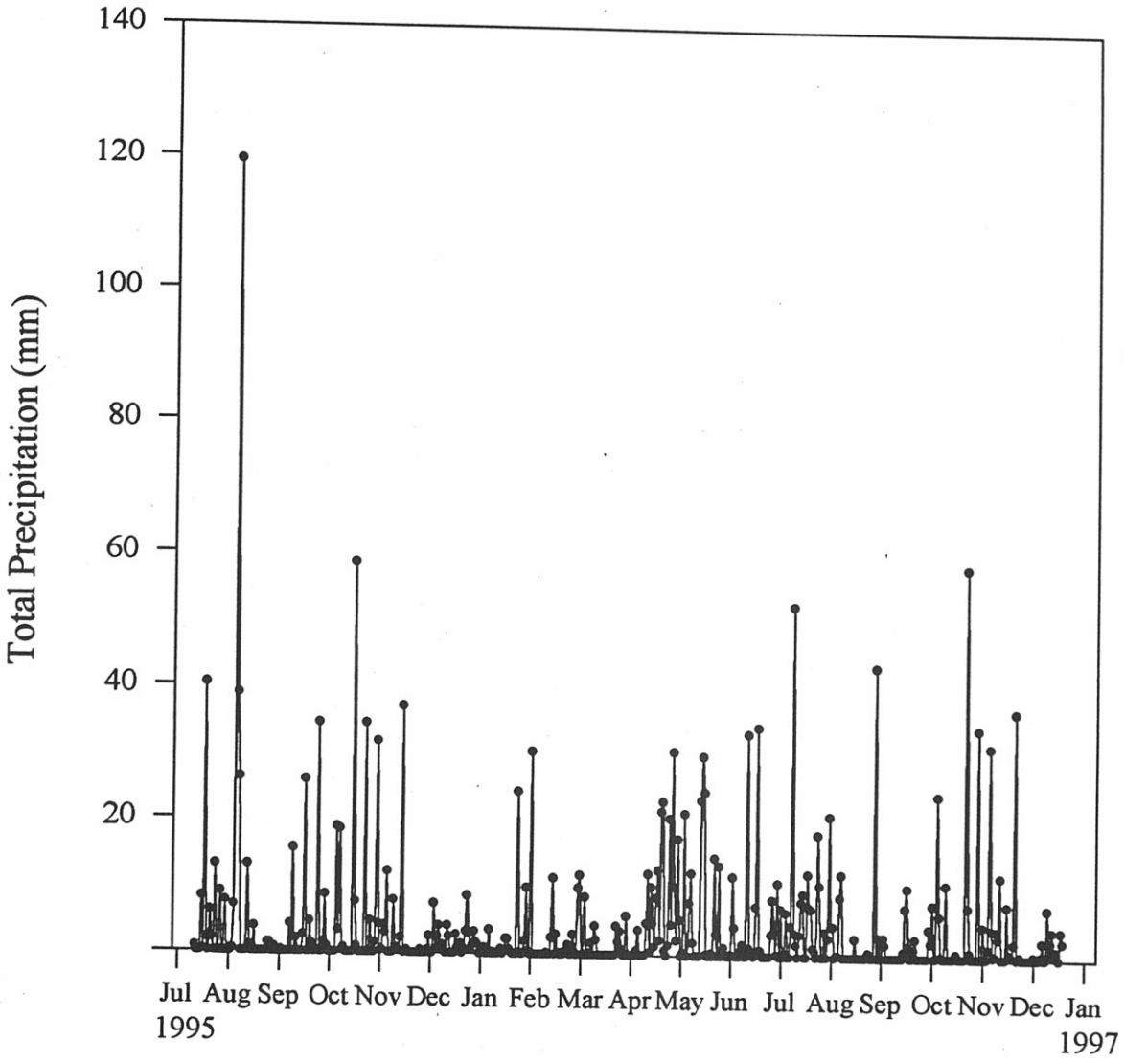

Figure 3.6

Daily precipitation record. From measurements taken at Proctor Maple Research Center (600 m asl), Underhill (Cummings, 1997, pers. comm.).

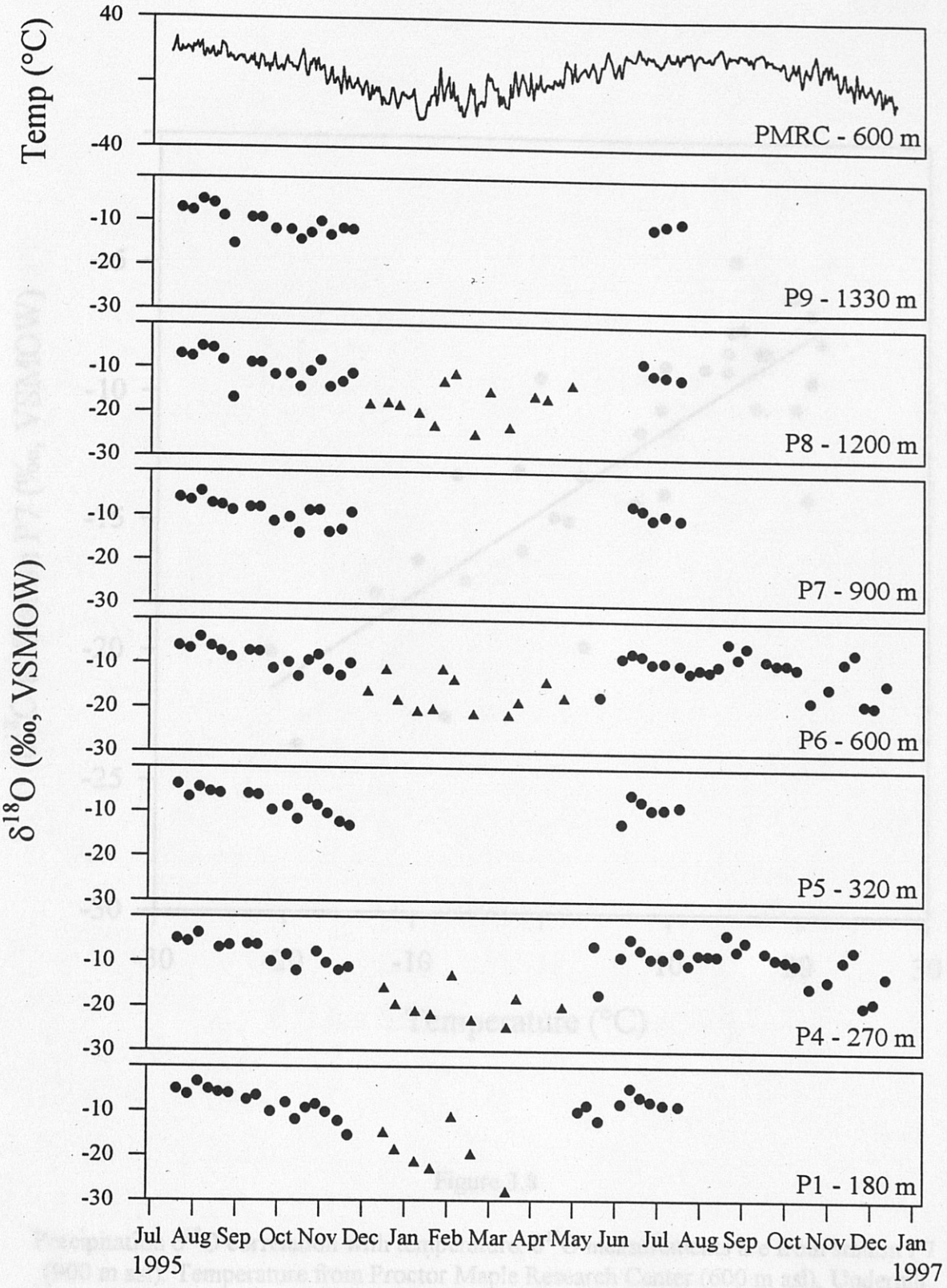

Figure 3.7

Precipitation $\delta^{18}O$ records. ● = rain samples. ▲ = snow samples. Snow samples were not collected at stations P5, P7 and P9.

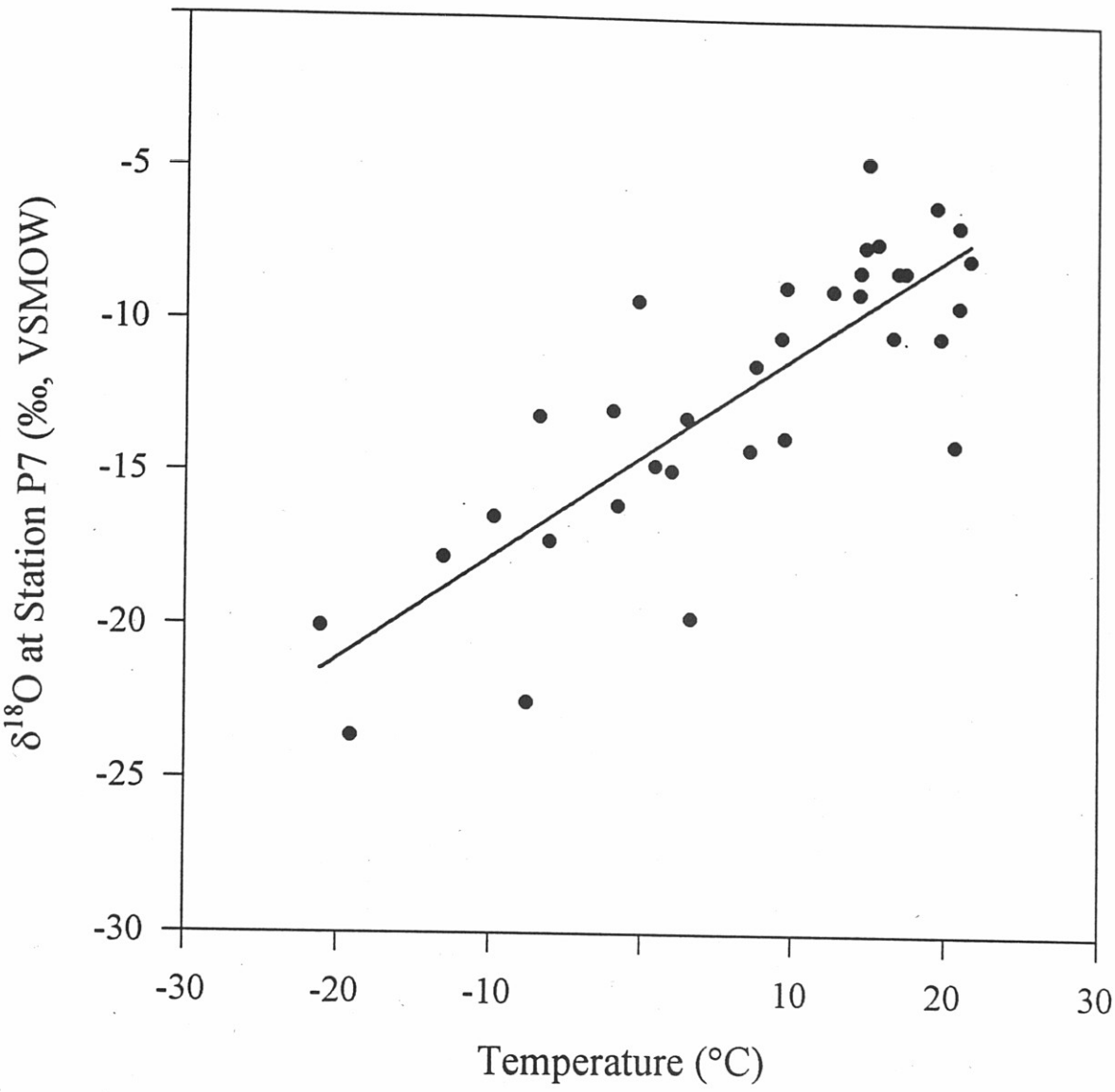

Figure 3.8

Precipitation $\delta^{18}O$ correlation with temperature. $\delta^{18}O$ measurements are from station P7 (900 m asl). Temperature from Proctor Maple Research Center (600 m asl), Underhill (Cummings, 1997, pers. comm.). Equation of linear best fit is: $Y = 0.3X - 14.4$, $R^2 = 0.68$.

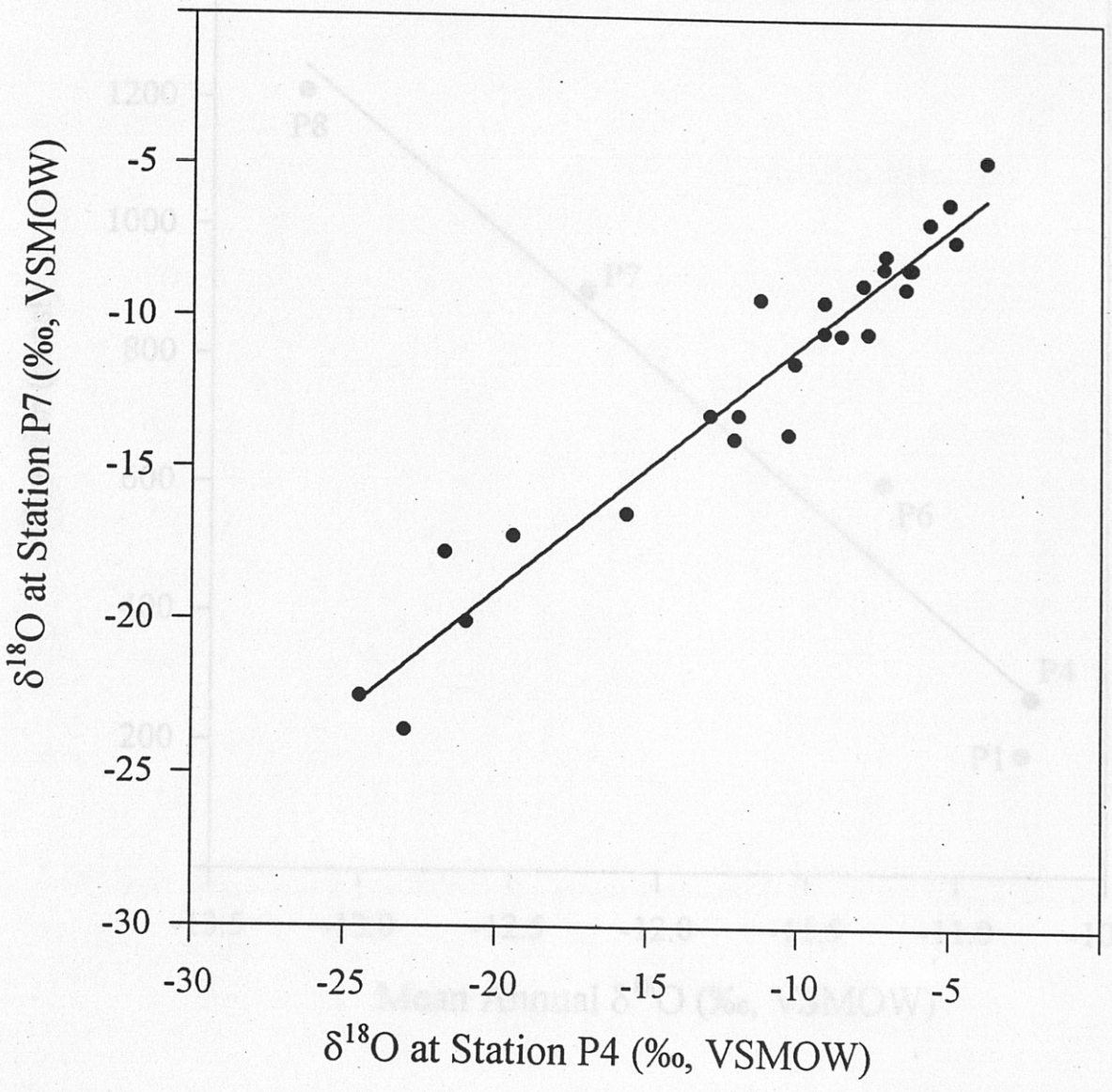

Figure 3.9

Precipitation $\delta^{18}O$ correlation between sites. $\delta^{18}O$ measurements are from stations P7 (900 m asl) and P4 (270 m asl). Equation of linear best fit is: $Y = 0.8X - 2.9$, $R^2 = 0.94$.

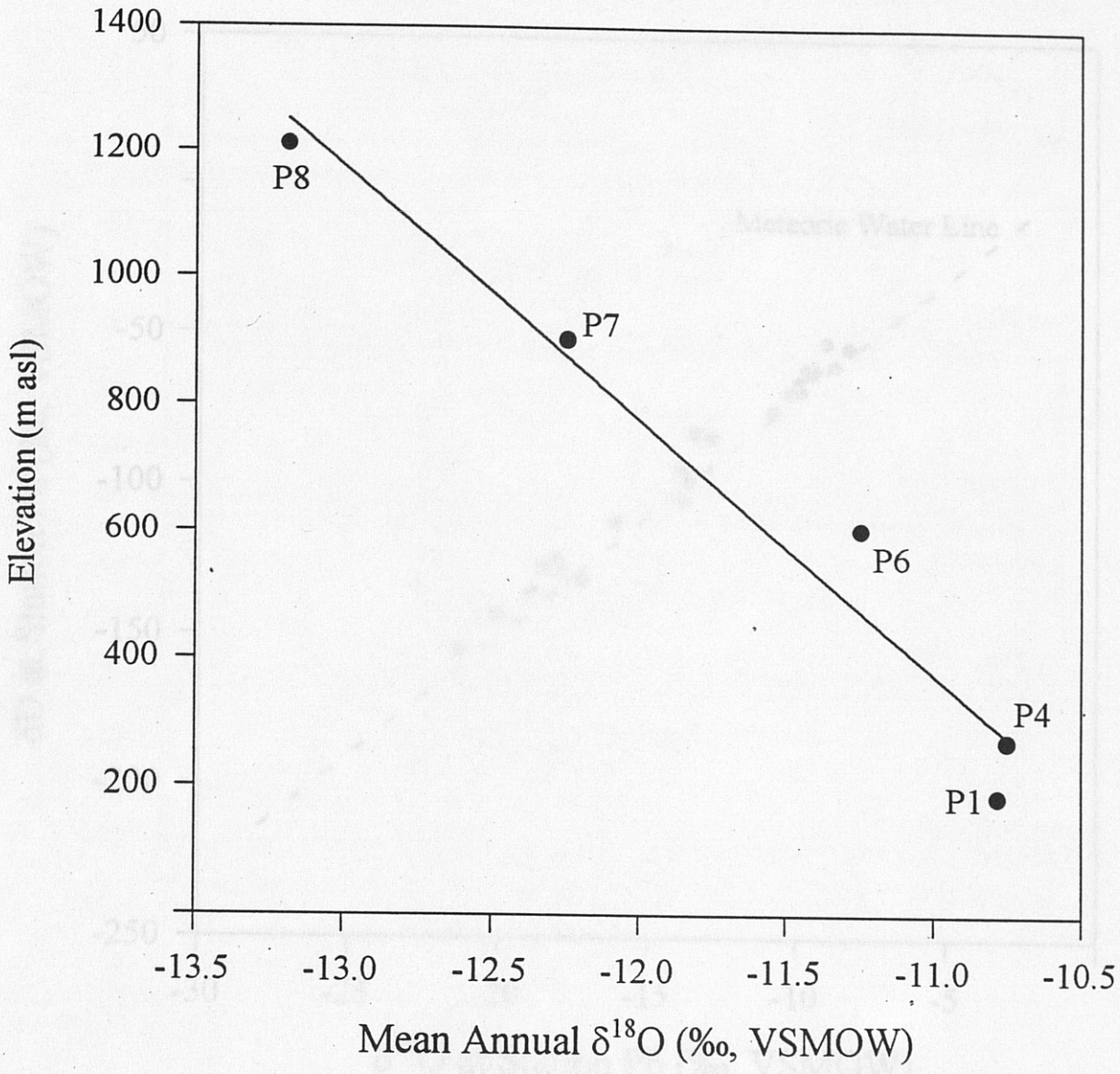

Figure 3.10

The relationship of mean annual precipitation $\delta^{18}O$ and elevation. Equation of linear best fit is: $Y = -398X - 4003$, $R^2 = 0.96$.

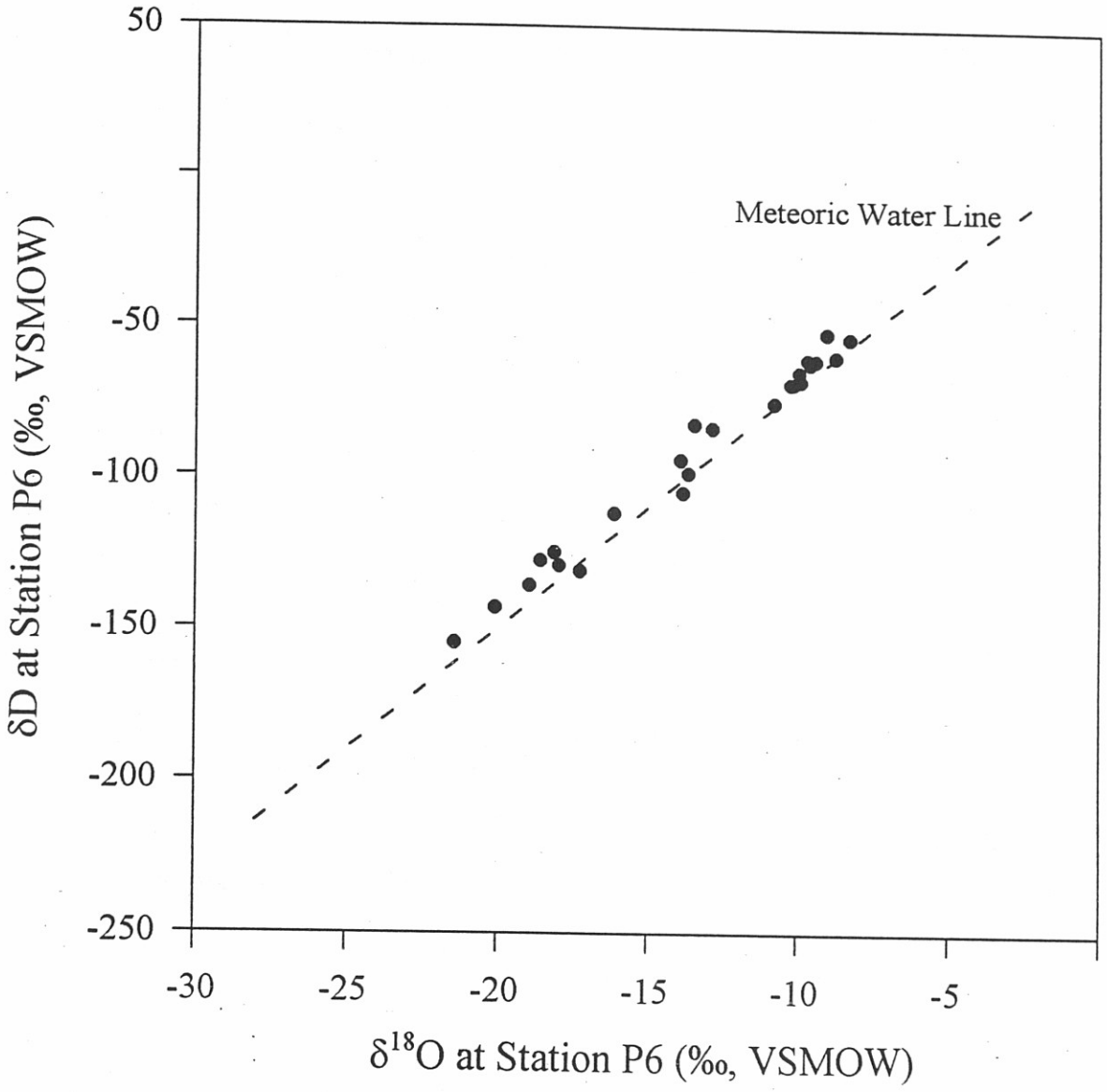

Figure 3.11

Precipitation $\delta^{18}O$ versus δD. $\delta^{18}O$ and δD measurements are from station P6 (600 m asl). Equation of Meteoric Water Line is: $\delta D = 8\delta^{18}O + 10$ (Faure, 1986).

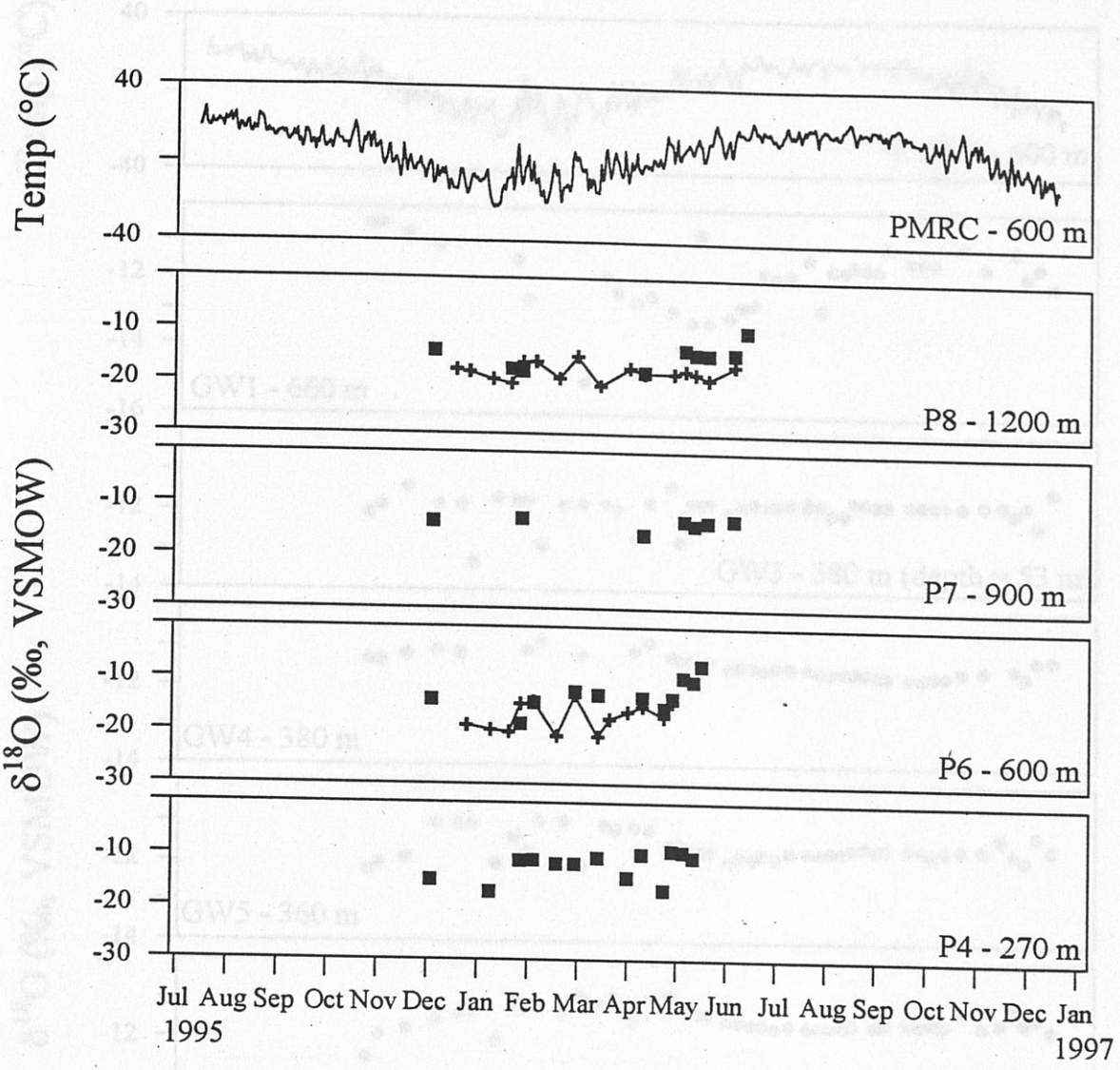

Figure 3.12

Meltwater and snowpack $\delta^{18}O$ records. ■ = meltwater samples.
✚ = cumulative snowpack samples.

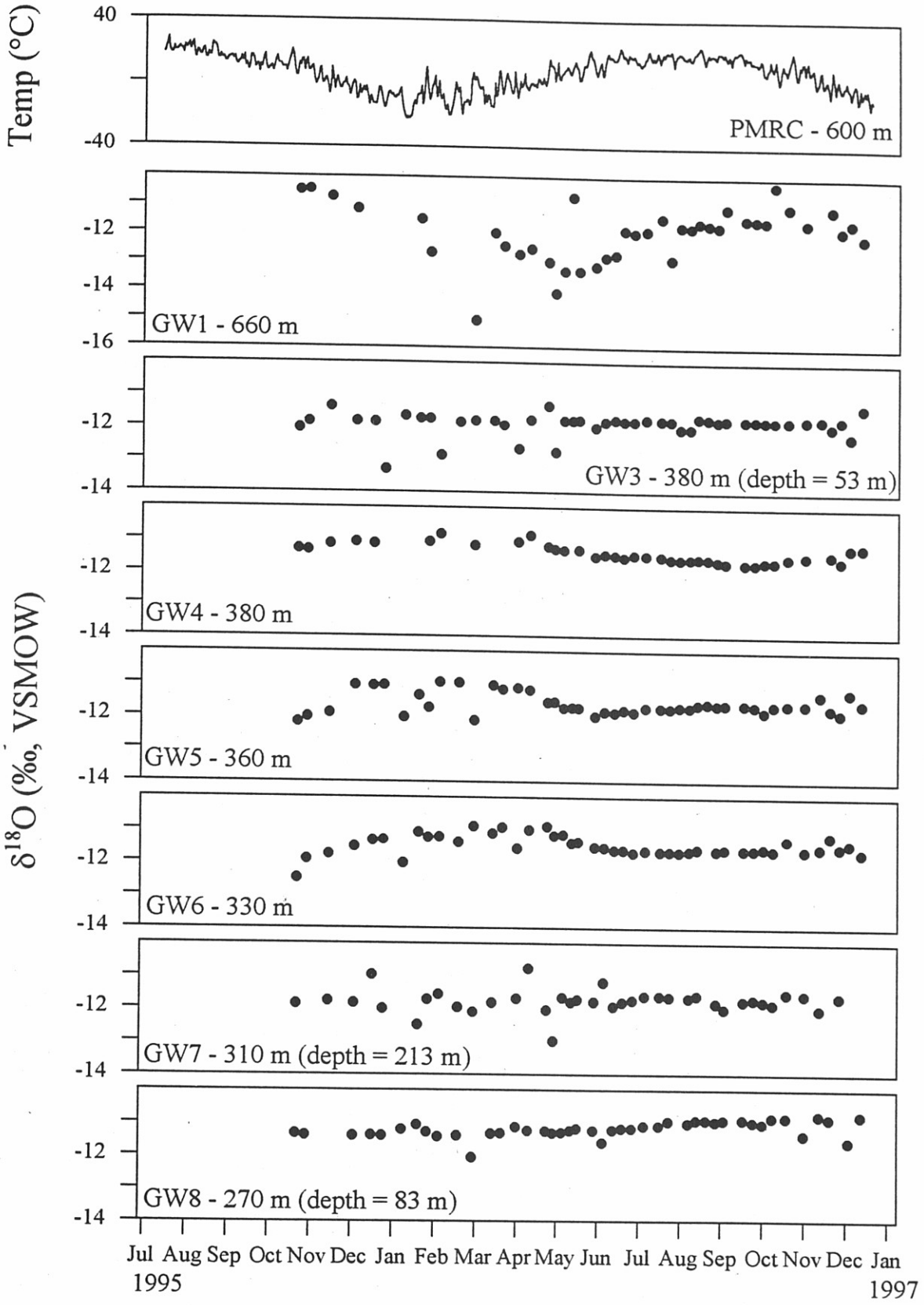

Figure 3.13

Groundwater $\delta^{18}O$ records. Complete records were not established for GW2 and GW7b.

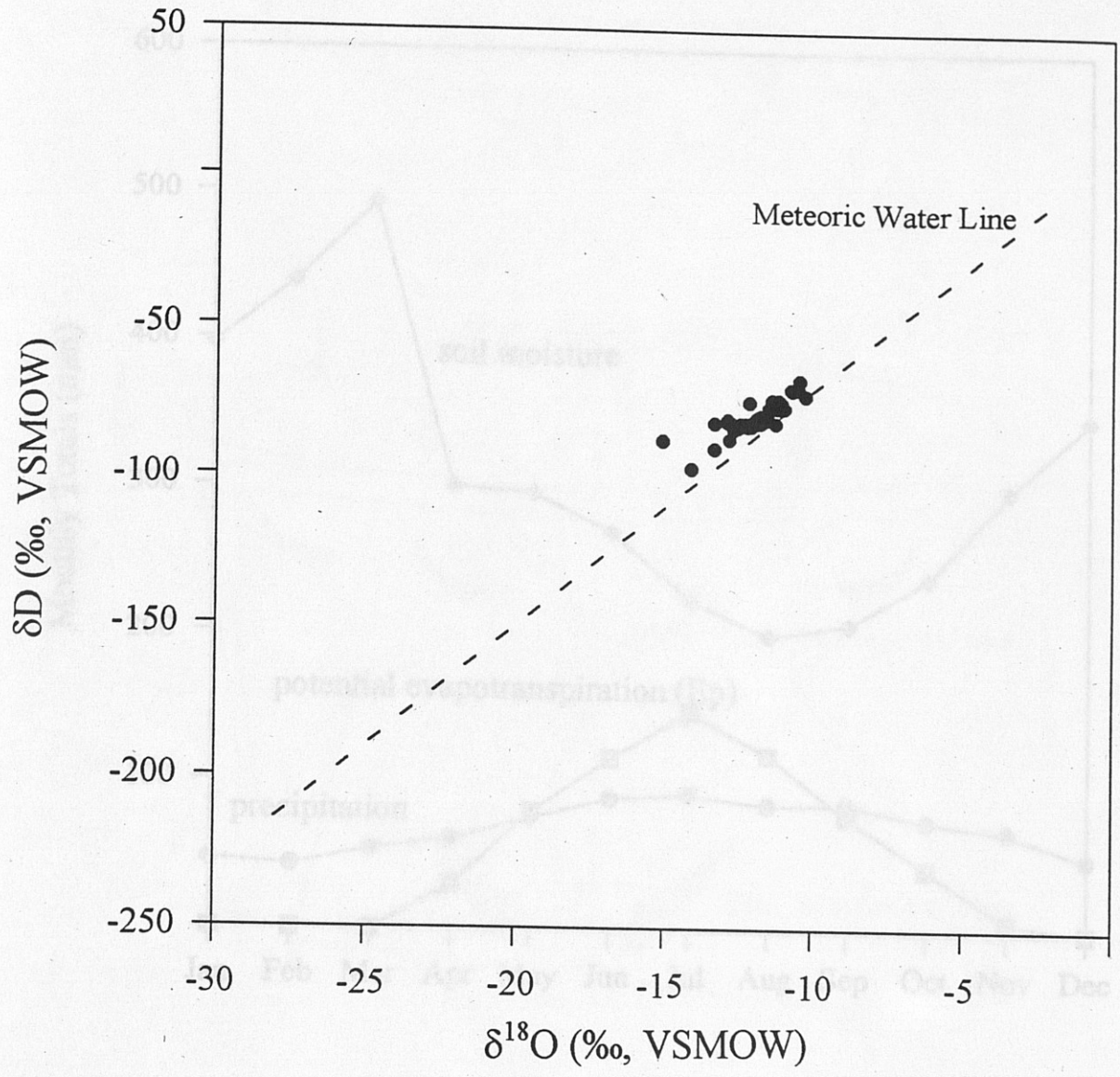

Figure 3.14

Groundwater $\delta^{18}O$ versus δD. $\delta^{18}O$ and δD measurements are from wells GW1 (660 m asl), GW3 (380 m asl), and GW5 (360 m asl).
Equation of Meteoric Water Line is: $\delta D = 8\delta^{18}O + 10$ (Faure, 1986).

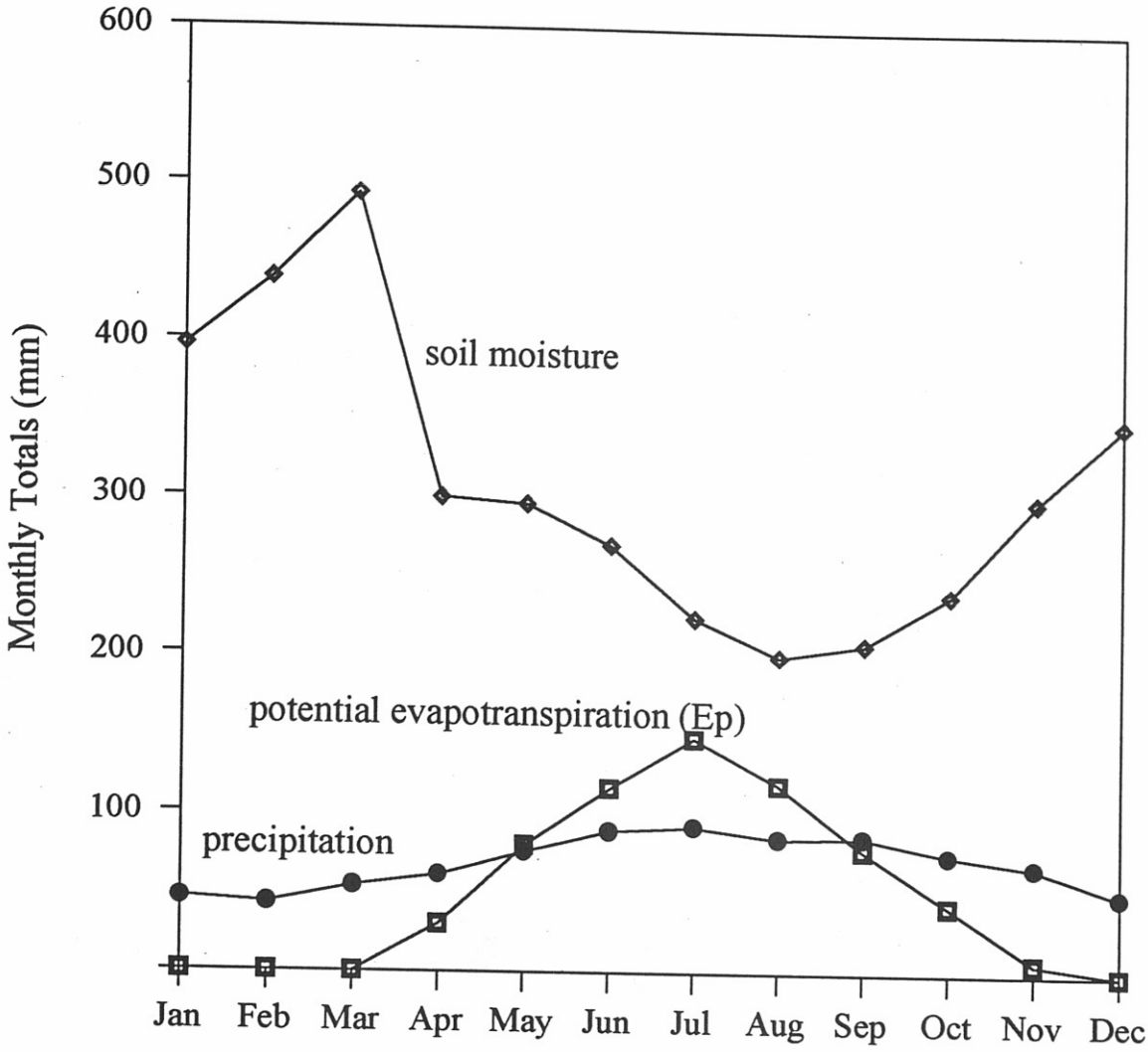

Figure 3.15

Plot of climatic data from Burlington, Vermont, 1910-1960. Produced using data from C.W. Thornthwaite Associates, Laboratory of Climatology (1964).

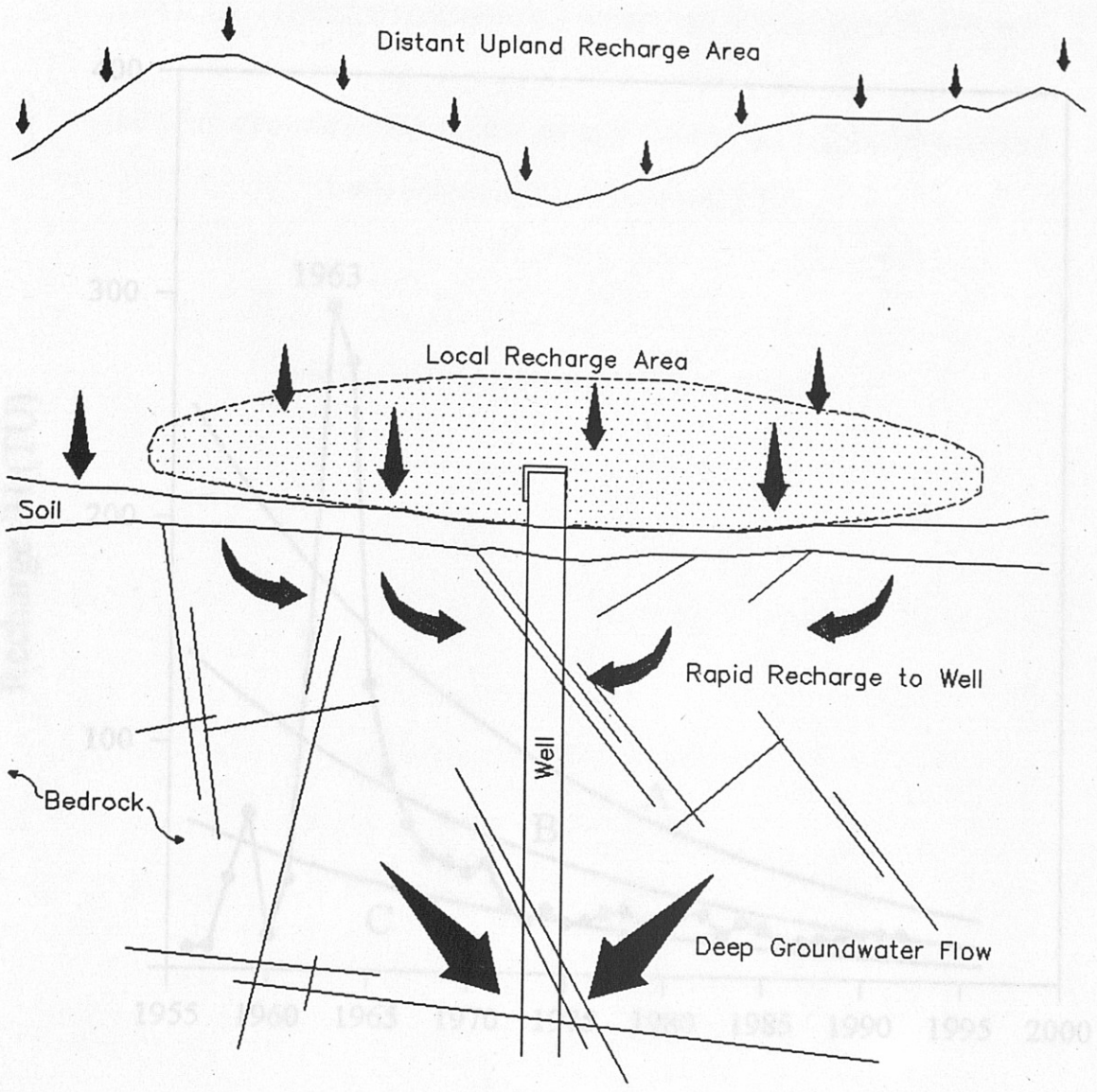

Figure 3.16

Schematic diagram of groundwater mixing. This figure illustrates the combined contribution of water to a well by shallow (local recharge) and deep (distant recharge) fractures.

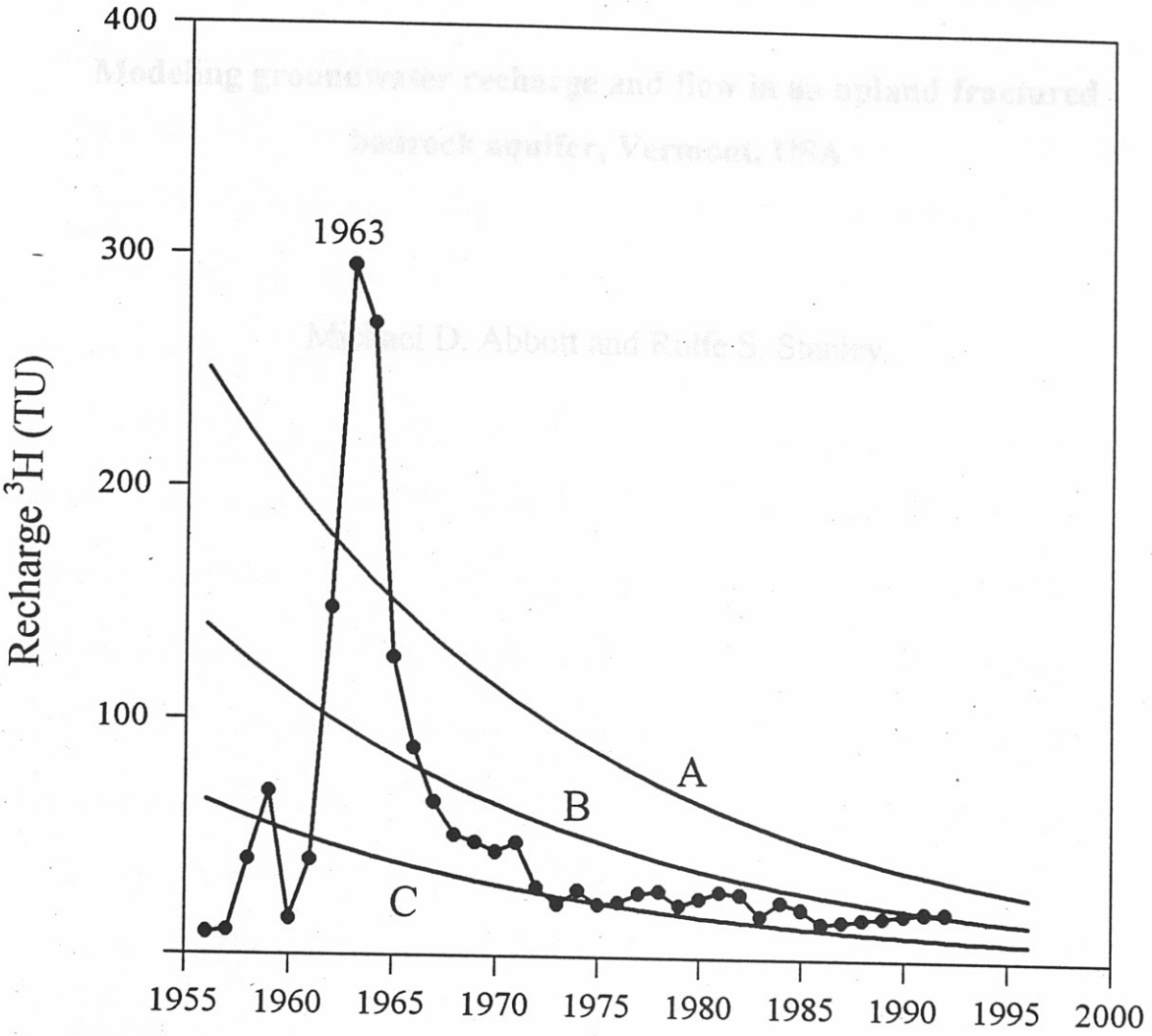

Figure 3.17

Hypothetical decay curves for ^{3}H in recharge compared to reconstructed recharge ^{3}H at the Mirror Lake Site. Historical ^{3}H curve is adapted from Busenberg and Plummer (1993).

CHAPTER IV
ARTICLE FOR SUBMISSION TO SYSTEMS DYNAMICS REVIEW

Modeling groundwater recharge and flow in an upland fractured bedrock aquifer, Vermont, USA

Michael D. Abbott and Rolfe S. Stanley

Abstract and Author Biography

We have developed a system dynamics model to simulate recharge and flow mechanisms in a fractured bedrock aquifer in northwestern Vermont. The model was constructed to aid in the interpretation of data collected as part of a stable and radiogenic isotope study of groundwater. Use of the model guided further data collection and analysis, leading to the derivation of a differential equation describing temporal and spatial changes in recharge and flow mechanisms.

Michael Abbott is a graduate student in the University of Vermont Geology Department. The modeling project is part of his Master of Science thesis research. Rolfe Stanley advised Abbott on the system dynamics modeling effort. Stanley has been a professor of Geology at the University of Vermont for 33 years. His recent research has focused on structural geology associated with the Taconian and Acadian deformation in western New England, and on the application of system dynamics modeling of geologic processes.

Address: Perkins Geology Hall, University of Vermont, Burlington, VT 05405-0122, USA

Overview

Conventional groundwater modeling incorporates aquifer geometry and hydraulic properties to simulate a flow field. Recharge is typically incorporated as a uniform value throughout the areal dimensions of the model, or varied according to changes in soil types or seasonal precipitation patterns in a transient (time dependent) model. Groundwater recharge and flow systematics in fractured bedrock in steep alpine environments may differ significantly from other geohydrologic systems. Recharge of bedrock groundwater is controlled in part by the permeability of covering soils and surficial deposits, as wells as by the transpiration effects of trees and other vegetation. These mechanisms vary seasonally and with elevation in certain environments (McGuinness and Harold, 1962; Knisel et al., 1969; Parmele, 1972; Woolhiser, 1973; Saxton and McGuinness, 1982).

In the study area (Figure 4.1), precipitation increases with elevation. The mean annual precipitation ranges from 250 cm at the highest elevations to 80 cm in the lower portions of the watershed (Wilmot and Scherbatskoy, 1994). The dominant tree type changes from a mix of large deciduous (oak and maple) and coniferous (fir and spruce) trees in the valley, to sparsely distributed and often scrubby conifers on the mountain slopes, and finally to arctic alpine tundra vegetation at the highest elevations on Mount Mansfield, the highest of the Green Mountains in Vermont (1330 meters asl) (Burns, 1916; Connor, 1994). Soils are generally thin sandy to stony loams at the upper elevations. Below 350 m asl, the topography flattens and more sandy soils are present (USDA and SCS, 1974; 1981). The upper part of the watershed has thin till or colluvial cover underlying soils, whereas at lower elevations (below 350 m asl), deposits of

glaciolacustrine sediments and till may reach thickness of up to 150 m (Stewart, 1961; Connally, 1968; Stewart and MacClintock, 1969). The large variability in soil types and dominant vegetation with elevation in this basin produces a complex collection of mechanisms affecting recharge to groundwater in the bedrock.

Groundwater flow paths are complex in fractured metamorphic rock. The bedrock in this setting consists of predominantly fine-grained phyllite and schist (Christman, 1959; Thompson and Thompson, 1991). Flow direction and rates are controlled primarily by the existing fracture network, and secondarily by the properties of the rock matrix itself. The degree of fracture interconnection controls mixing of groundwaters from different recharge locations and times. As water travels downgradient through the bedrock, it may be isolated from contribution of younger recharge at the lower elevations, or continually mixed with new water. The degree of interconnection with streams and the presence of springs may vary significantly with the bedrock type, steepness of watershed, and nature of surficial cover.

In order to understand groundwater flow in an upland fractured bedrock setting, specifically for the purpose of predicting water supply sustainability, or to address contamination problems, a comprehensive understanding of the interaction of the mechanisms controlling recharge and mixing is required.

Review of Isotopic Study

The model discussed in this paper was developed in conjunction with collection of field samples of precipitation, meltwater and groundwater for isotopic analysis. We used

the isotopic measurements to interpret the flow and recharge processes in the basin, as explained below.

Oxygen exists naturally in three stable isotopic forms, ^{18}O, ^{17}O, and ^{16}O. The numerical designation of the isotope refers to the total number of neutrons and protons in the nucleus of the oxygen atom (Urey, 1947; Faure, 1986). The isotopic ratio, $^{18}O/^{16}O$ is used as a quantification of the ratio of heavy to light oxygen isotopes in water or water vapor. This ratio is expressed relative to Vienna Standard Mean Ocean Water (VSMOW) and notated as $\delta^{18}O$.

Molecules with lighter isotopic composition have lower mass and higher vibrational energy (i.e., more rapid velocities) than do molecules with heavy isotopic composition. Lower mass and higher energy translate to higher vapor pressure (White, 1984). During the phase change of water from liquid to vapor (e.g., evaporation), lighter molecules will more likely enter the gas phase than will heavier molecules. Therefore, the lighter molecules will evaporate in larger numbers than molecules made up of the heavier isotopes. When water condenses from a vapor source, heavier molecules will more likely form precipitation, while lighter molecules will tend to remain in the vapor phase. In terms of isotopic measurements, the heavier isotope, ^{18}O, will be concentrated in the liquid phase, since they tend to constitute the heavier molecules. These effects are known as isotopic fractionation.

The degree of fractionation in a system is largely temperature dependent. As temperatures increase, the difference in the behavior of water molecules of different mass decreases. This temperature dependence (Figure 4.2) allows the interpretation of isotope

values in terms of environmental temperatures. In effect, the stable isotopic composition of water reflects the temperatures to which it has been exposed during condensation (Friedman and O'Neil, 1978; Hoefs, 1980).

Our study of this watershed using stable isotope measurements ($\delta^{18}O$) in precipitation and groundwater at several locations (Figure 4.1) has shown that differences in seasonal temperature and elevation within the watershed are reflected in the $\delta^{18}O$ composition of precipitation. Oxygen isotopic values in precipitation range over 25 per mil (‰) at most locations yearly. The average decrease in precipitation $\delta^{18}O$ with increasing elevation is 2.5 ‰ per 1000 m (Figure 4.3).

The $\delta^{18}O$ of groundwater collected from residential wells within the basin varies only 2 ‰ yearly, with the exception of a high spring (GW1) which shows a yearly variation of 4.3 ‰ (Figure 4.4). The variability of the $\delta^{18}O$ composition of groundwater changes according to the time of year. In the warmer months (late April to early November), the $\delta^{18}O$ signature remains very constant, while in the colder months (late November to early April), the $\delta^{18}O$ composition varies by as much as 2 ‰. The exception is again the high spring GW1, in which $\delta^{18}O$ varies throughout the year. The $\delta^{18}O$ composition of the water in GW1 seems reflect seasonal changes in precipitation $\delta^{18}O$, with a time lag of 2 months. This time lag may represent the residence time of groundwater traveling through the upper part of the watershed.

The variation of $\delta^{18}O$ in most wells and springs during the colder months is thought to be caused by a decrease in the vegetative uptake of water in the vicinity of the wells. Based on 50 years (1910-1960) of precipitation and soil moisture data (C.W.

Thornthwaite Associates, Laboratory of Climatology, 1964), potential evapotranspiration (E_p) is negligible from the months of December to March. E_p increases in late March or early April to a peak in July, then decreases to a negligible amount in November (Figure 4.5). Although precipitation is relatively abundant during the warmer months, soil moisture remains much lower than during the rest of the year. This indicates that a much smaller percentage of precipitation is available for groundwater recharge from April to November.

The $\delta^{18}O$ signature observed in the well represents a combination of deep and shallow groundwater contribution to the well (Figure 4.6). During the colder months, infiltration near the wells enhances the effect of individual storm or melt events on the $\delta^{18}O$ composition of the sampled groundwater. During the warmer months, groundwater recharge in the valley, where most of the wells are located, is virtually shut off by vegetative water uptake. In contrast, the watershed near GW1 has a sparse forest of smaller trees and is typically exposed to lower temperatures, because it is higher in elevation and closer to treeline. Therefore, it appears that recharge of precipitation to groundwater at lower elevations occurs at appreciable rates only during the colder months of the year when transpiration is not significant. At higher elevations, water uptake by vegetation is low throughout the year due to harsh weather conditions, allowing recharge to occur (Dugan and Peckenpaugh, 1985; Likens et al., 1985; Likens et at., 1977; Dole, 1923). In addition, the thickness of sediments underlying soil, influences the mixing of groundwater before it reaches bedrock fractures. Thus, the majority of groundwater recharge in the basin occurs at the upper elevations through thin soils. Recharge at the

lower elevations becomes significant only during the colder months. A groundwater model of this setting must incorporate variable recharge rates which are adjusted with elevation, soil and vegetation cover, and season.

Estimates of groundwater flow rates in the fractured rock were obtained using measurements of ^{3}H, a radiogenic isotope which was introduced in great quantities to the atmosphere during nuclear testing activities beginning in the 1950s. Measurements of tritium abundance in groundwater were compared with historical records of tritium abundance in precipitation for the region. The results indicate that the age of groundwater at most of the sampling locations is less than 5 years. Two of the deep bedrock wells contain groundwater that may be between 21 and 34 years old, based on comparison with historical tritium deposition. These ages suggest travel rates of 0.2 $m \cdot day^{-1}$ to 6.6 $m \cdot day^{-1}$ for groundwater flow in the fractured bedrock.

Water is transported through the bedrock along fractures that may be isolated or interconnected. As water moves downgradient, it may become mixed with groundwater from other sources (i.e., different recharge locations and times) traveling through separate but interconnecting fracture zones, or entering the bedrock from the surface through shallow fractures along the flowpath. The wells investigated in the study receive water either from single fractures or close groupings of shallow fractures in the case of springs, or from sets of shallow and deep fractures intersecting the boring of deep bedrock wells (Figure 4.6). The deepest well used in this study was 213 m.

Model Description

A model was constructed using the STELLA modeling code by High Performance Systems, Inc., (1994). This program has a graphical interface which allows the user to build models of fairly complex systems. "Stocks" in the model are used to represent components of the system where mass balances or accumulations may be assessed. "Flows" represent fluxes in the system between the stocks. "Converters" and "connectors" are used to establish relationships between components of the model. The arrow heads of connectors represent dependent variable in a particular relationship whereas the tails are attached to independent variables.

For this model, the stock representing the end result of processes incorporated in the model is a groundwater well. The temporal $\delta^{18}O$ signature in the well is dependent upon the balance of sources contributing water to the well. The other two main stocks in the model are distant infiltration (recharge of groundwater at a upland source at some distance from the well), and local infiltration (rapid recharge to the shallow fractures near the well from storm events). The model is divided into three main parts - upland recharge, local recharge, and groundwater mixing (Figures 4.7, 4.8, and 4.9 respectively).

Upland Recharge Model

The rate of recharge to bedrock at higher elevations in this watershed is dependent upon the amount of precipitation (rain and snow) and the ability of the water to make its way to bedrock fractures. Above the treeline, fractures are readily accessible.

However, due to the impermeable nature of the rock itself, precipitation may run overland for some distance and discharge to streams if fractures are not encountered.

Temperature and precipitation records for the basin were obtained during the study (Figures 4.10 and 4.11). This information is represented by converters in the form of time plots (*Precip Record*, *Temp Record*). A snow stock (*Upld Snow*) is used to represent precipitation that is temporarily held in the snow pack. The thickness of the snow pack is calculated using an assumed water equivalent of 0.2 (mm water/mm snow). Where soil or sediments are present, infiltration is controlled by the permeability of the cover, as well as the rate of evaporation and uptake by trees and other vegetation. For the upland recharge model, there is a stock representing soil saturation (*Upld Soil Sat*). This stock is fed by rain and meltwater (*Upld Rain* and *Upld Snowmelt*), and depleted by vegetative uptake and evaporation (*Upld Tree Uptake* and *Upld Evap*). The degree of soil saturation controls the percentage of water that runs off (*Upld Runoff*) for a given rain or melting event. Components which deplete the soil water are grouped in the flow *Upld Soil Losses*.

The elevation of distal recharge for a given well (*Upld Rech Elev*) can be approximated using the relationship of average annual $\delta^{18}O$ composition of rain and snow with elevation (see again Figure 4.3). The equation of the best fit line for these data is

$$Y = -398 \cdot X - 4003 \qquad (4\text{-}1)$$

where Y = elevation, meters asl, and $X = \delta^{18}O$ (‰)

Using the mean annual $\delta^{18}O$ composition of groundwater in a well (*Well Mean 18O* - must be input for each simulation) as the value of X, the elevation of recharge is calculated. For example, the estimated elevation of recharge for the high spring GW1 (mean $\delta^{18}O$ = -12.1 ‰) would be 831 m asl, 160 m higher in elevation than the spring. For well GW3 (mean $\delta^{18}O$ = -11.9 ‰), *Upld Rech Elev* would be 742 m asl, 360 m higher in elevation than the well. Calculation of recharge elevation is complicated by the mixing of water from different sources that may occur along the path of transport from a recharge zone to the well. Therefore, the elevation obtained by this calculation reflects the approximate elevation of the distal recharge area, rather than identifying the specific location of recharge. However, the estimate provides a good first approximation of recharge elevation for use in the model.

Soil and sediment porosity are estimated based on average values for these materials (Anderson and Woessner, 1992). When the elevation of recharge is known, the thickness of cover material in that area (*Upld Sed Thick*) can be estimated based on geologic mapping. Given the thin soil and cover material on the slopes of the mountain, we used a cover material thickness of 0.5 m for the upland recharge areas, which are all located above 350 m asl according to estimates made using equation 4-1.

The effect of trees and other vegetation must be also be incorporated in the model. When the elevation of recharge has been determined, the dominant types of vegetation controlling recharge (*Upld Tree Type*) can be estimated. For most of the wells, the upland recharge areas are in the largely coniferous forests on the slopes of the mountain. Portions of the recharge area for the high spring GW1 may be above treeline. The uptake of water

by trees varies according to tree type and seasonal temperatures (Dugan and Peckenpaugh, 1985; Likens et al., 1985; Likens et at., 1977; Dole, 1923). In the model, *Upld Tree Uptake* and *Upld Evap* increase dramatically in the forests during the warmer months (April to October), especially when the deciduous trees such as birch, maple and oak have their leaves. However, due to the effect of harsher weather conditions, these factors do not increase to the same extent at the higher elevations of the watershed.

Local Recharge Model

The local recharge model is similar to the upland recharge model. The same temperature and precipitation records are incorporated (*Precip Record* and *Temp Record*). The elevation of local recharge is determined by the actual elevation of the well, which must be incorporated as a constant for each simulation (*Local Elev*). This converter, combined with temperature, influences the effects of tree uptake and evaporation (*Local Tree Uptake* and *Local Evap*). Most of the wells are located at 380 m or lower in the basin, with the exception of the high spring, GW1. *Local Tree Uptake*, controlled by *Local Tree Type*, is high during the warmer months, except for at GW1 where *Local Tree Type* represents the smaller, more sparsely distributed conifers on the upper slopes of the mountain. Local recharge to groundwater in the vicinity of GW1 is less sensitive to season than at locations in the valley. *Local Evap* is also higher during the summer months at the lower wells than in the upland recharge areas. Soil and sediment thickness were determined using the information included in the installation logs for each well. For springs, a sediment thickness of 1 m was used.

Groundwater Mixing Model

Infiltrated water is carried downgradient to wells according to the simple flow equation:

$$q_x = k_x \cdot \frac{\partial h}{\partial x}; \; V_x = q_x / n_e \qquad (4\text{-}2)$$

where

q_x = specific discharge or flow

k_x = hydraulic conductivity of medium

$-\frac{\partial h}{\partial x}$ = hydraulic gradient in the direction of flow (x)

V_x = linear velocity of groundwater flow

n_e = effective porosity of medium

The gradient is assumed to be 0.12 for flow throughout the aquifer, based on topography in the upper parts of the basin, which is controlled by the slope of the upper bedrock surface. Hydraulic conductivity of aquifer fracture networks may range from 0.001 to 10 $m \cdot day^{-1}$ in fractured metamorphic rock (Anderson and Woessner, 1992). We selected an initial value of 0.1 $m \cdot day^{-1}$ for use in the model. Porosity of the fracture network (secondary porosity) is estimated at 0.005 (Anderson and Woessner, 1992). Primary porosity of the rock matrix itself is considered to be insignificant. Using the assumed hydraulic conductivity, porosity, and hydraulic gradient values discussed above,

the calculated value of Vx is estimated to be ~2 m•day^{-1}. This is within the range of probable flow rates (0.2 - 9.6 m•day^{-1}) calculated in the isotopic study.

During transport in the groundwater system, the water may be affected by local recharge or interconnection with groundwater being transported from a different source area. These factors are incorporated in the model as a "mixing" component. Both the distal and local recharge stocks feed the stock of groundwater in the well. The $\delta^{18}O$ record of a well reflects mixing of the two sources. Withdrawal of water though pumping for residential water supply may affect the balance of waters in the well. When model simulations accurately represent the groundwater system, a curve of well $\delta^{18}O$ composition versus time will match the $\delta^{18}O$ curve generated from field collection and laboratory analysis. In this case, we obtain a reasonable quantification of local and distal recharge to the groundwater system.

Simulation Results

Simulations of groundwater recharge and flow for the study area were performed for 1996, the year in which most of the field data were collected (Figures 4.12 and 4.13). Soil saturation increases with rain and melting events. Soil water losses occur in the form of evaporation and vegetative uptake under warmer temperatures. Runoff increases with the degree of soil saturation for a rain or melting event, also contributing to soil losses. In the upland recharge simulation, recharge to bedrock (*Upld Cover Transport*) is decreased by up to 50% during the summer when evapotranspiration increases. This effect is more prominent in the local recharge simulation, where *Local Cover Transport* is significantly

decreased (up to 100 %) during the warmer months. During this time, soil saturation in the local recharge model remains very low, due to summer evaporation and the consumption of water by trees.

Given the mean $\delta^{18}O$ composition measured in well GW3 (-11.9 ‰), the *Upld Recharge Elev* was set at 742 m in the model. The snow pack builds to a modeled maximum thickness of 800 mm, closely matching actual snow depths during the monitored year. In this simulation, complete melting of the snow pack occurs in late April and snow begins accumulating again in late October. The dominant tree types at this elevation are mostly scrubby conifers (Burns and Otis, 1916). Flow to bedrock (*Upld Cover Transport*) is fairly uniform throughout the simulation. However, the rate of recharge slows during the warmer months when vegetative uptake and evaporative loss is higher. Recharge also slows during brief periods of extreme cold when melting does not occur.

For local recharge, the elevation of well GW3 (380 m asl) is used to determine the effects of vegetation and evaporation, as well as sediment thickness, on recharge. The snow pack at this elevation reaches a depth of only 550 mm. Furthermore, melting occurs more rapidly here, and the snow pack is completely melted by early April, again matching field observations. *Local Evap* and *Local Tree Uptake* are minimal during the colder months, but increase to a larger extent than do *Upld Evap* and *Upland Tree Uptake* from April to November, reaching a maximum in the summer. The effect of these increases is to shut off recharge near the well. This effect is reflected in the near-zero value for *Local Cover Transport* during the warmer months.

Results of a simulation for GW3 (Figure 4.14) in the groundwater mixing portion of the model produced a record of $\delta^{18}O$ composition (*Well 18O Record*) similar to the $\delta^{18}O$ record generated during the isotopic study. The total water in the well is the sum of the *Deep Transport* and *Shallow Infiltration* components. The rate of groundwater flow controls transport of the upland recharge to the well. In the summer, the plot of total water in the well represents only Deep Transport, since shallow infiltration is decreased to the point where the only major contribution to water in the well is from the deeper flow system. This effect is also reflected in the plot of simulated $\delta^{18}O$ composition which shows significant variability throughout the year, except during the warmer months, when the $\delta^{18}O$ composition becomes constant, reflecting the $\delta^{18}O$ composition of the upland recharge source. This is a realistic representation of what we observed in our study of temporal $\delta^{18}O$ trends for well GW3.

Another simulation used the elevation of well GW1 (670 m asl) and the mean $\delta^{18}O$ composition of this groundwater (-12.2 ‰) as input for the recharge models (Figure 4.15). In this simulation, the higher value calculated for *Upld Rech Elev* produced different seasonal changes in the rate of vegetative uptake, snow accumulation, and melting than for the simulation using information from GW3. The resultant plot for *Well* is affected by contributions from *Deep Transport* and *Shallow Infiltration* throughout the simulation. In addition, the simulated range of $\delta^{18}O$ variation is greater for this well than for GW3, and mimics seasonal temperature changes as observed in the isotopic study.

We used an iterative approach in running the model. By using input from wells at two different elevations, and with different $\delta^{18}O$ compositions, we were able to work

progressively closer toward a model solution that adequately represented recharge conditions for all of the wells in our study. Upon reaching a final model solution that accurately reproduced our observations, we were able to develop series of simple equations which describe the temporal changes in bedrock recharge and flow in our watershed. These are the governing equations for the dynamic systems model. All units are in mm (water equivalent):

Recharge (ω) is a function of (rain (p), melting (m), runoff (r), evaporation (e), and vegetative uptake(u))

$$\frac{\partial \omega}{\partial t} = \frac{\partial p}{\partial t} + \frac{\partial m}{\partial t} - \frac{\partial r}{\partial t} - \frac{\partial e}{\partial t} - \frac{\partial u}{\partial t} \qquad (4\text{-}3)$$

Rain (p) at a given location is a function of (temperature (T), elevation (a), and the precipitation record for the basin (pr))

$$p = pr\,(1 + 0.02(1330 - a))\big|_{T>0}$$

Snow pack (sp) at a given location is a function of (T, a, pr)

$$sp = pr\,(1 + 0.014(1330 - a))\big|_{T\le 0}$$

Melting (m) = is a function of (T, a, sp)

$$m = 0.1\{pr\,(1 + 0.014(1330 - a))\big|_{T\le 0}\}\big|_{T>0}$$

Runoff (r) is a function of (m, pr, soil saturation (ss))

$$r = pr + m - (100\text{-}ss)$$

Evaporation (e) is a function of (T, a), estimated based on climatic data, such as presented in Figure 4.5

Predominant Tree Type (tt) is a function of f(a)

$tt = 1 \mid_{a > 350\,m}$ (scrubby growth); $tt = 2 \mid_{a \leq 350\,m}$ (mix of large trees)

Vegetative uptake (u) is a function of (T, tt), estimated based on climatic data

Conclusions

This study was an integration of field and data with system dynamics modeling. The $\delta^{18}O$ records developed through the water sampling program provided a useful means of calibrating the system dynamics model. Iterative simulations and adjustment of model components produced a realistic representation of the groundwater recharge and flow patterns, based on our current knowledge. This modeling effort guided our fieldwork and laboratory analysis, and improved our conceptual understanding of recharge and flow systems in the Mansfield basin of the Browns River, with specific reference to the effect of evapotranspiration on recharge to bedrock.

Although various modeling codes have been developed to represent flow though various mediums, fractured bedrock flow is a complex system to represent mathematically. Given the nature of the particular setting we studied, application of a traditional 3-D finite element or finite difference flow model may not have been productive. Use of the system dynamics model has allowed us to develop a better representation of the system using unique data from our site. The equations developed through this effort are representative of recharge and flow mechanisms in our study area and possible in other similar upland settings of New England.

Acknowledgments

Research was funded in part by the U.S. Geological Survey under a 1995 Vermont Water Resources Institute Grant and USGS Grant # HQ96GR02702-01 in 1996. A stipend for summer research was provided by the University of Vermont in 1996. Thanks to P. Bierman, D. Dougherty, A. Lini, and S. Wright (University of Vermont) for their reviews of this paper.

References Cited

Anderson, M.P., and Woessner, W.W., 1992, Applied Groundwater Modeling: Simulation of Advective Flow and Transport: San Diego, California, Academic Press, Inc., 381 p.

Burns, G.P., and Otis, C.H., 1916, The Trees of Vermont: Burlington, Vermont, Free Press Printing Company, 244 p.

Christman, R.A., 1959, Geology of the Mount Mansfield Quadrangle Vermont: Vermont Geological Survey Bulletin, p. 1-75.

Christman, R., and Secor, D., 1961, Geology of the Camels Hump Quadrangle Vermont: Vermont Geological Survey Bulletin, p. 1-70.

Climatology, C.W.T.A.L.of., 1964, Average Climatic Water Balance Data of the Continents: Part VII United States, Publications in Climatology: Centerton, New Jersey, National Science Foundation, p. 615.

Connally, G.G., 1968, Surficial geology of the Mount Mansfield 15 minute quadrangle, Vermont: Montpelier, Vermont, Vermont Geological Society.

Connor, S., 1994, New England Natives: Cambridge Massachusetts, Harvard University Press, 274 p.

Dole, E.J., 1923, A study of the relative importance of air temperature and relative humidity on the transpiration behavior of coniferous evergreen trees more particularly of primus strobus [406 thesis]: Burlington, Vermont, University of Vermont.

Dugan, J.T., and Peckenpaugh, J.M., 1985, Effects of climate, vegetation and soils on consumptive water use and ground-water recharge to the central midwest regional aquifer system, mid-continent United States, USGS.

Faure, G., 1986, Principles of Isotope Geology: New York, J. Wiley & Sons.

Faure, G., 1986, Principles of Isotope Geology: New York, J. Wiley & Sons.

Friedman, I., and O'Neil, J.R., 1977, Compilation of stable isotope fractionation factors of geochemical interest, *in* Fleischer, M., ed., Data of Geochemistry: USGS Professional Papers, U.S. Geological Survey, p. 440-K.

Gat, J.R., 1971, Comments on the stable isotope method in regional groundwater investigations: Water Resources Research, v. 7, p. 980-993.

High Performance Systems, I., 1994, Stella II Technical Documentation: Hanover, NH.

Hoefs, J., 1987, Stable Isotope Geochemistry (Minerals and Rocks): Berlin, Springer-Verlag.

Knisel, W.G., Baird, R.W., and Hartman, M.A., 1969, Runoff volume prediction from daily climatic data: Water Resources Research, v. 5, p. 84-94.

Likens, G.E., Borman, F.H., Eaton, J.S., and Johnson, N.M., 1977, Biogeochemistry of a forested ecosystem: New York, Springer-Verlag, 146 p.

Likens, G.E., Borman, F.H., Pierce, R.S., and Eaton, J.S., 1985, The Hubbard Brook valley, An Ecosystem Approach to Aquatic Ecology -- Mirror Lake and its Environments: New York, Springer-Verlag, p. 516.

Mather, J.R., 1972, Papers on Evapotranspiration and the Climatic Water Balance, Volume XXV: Elmer, N.J., Library of Climatology, p. 57.

McGuinness, J.L., and Harrold, L.L., 1962, Seasonal and areal effects on small-watershed streamflow: Journal of Geophysical Research, v. 67, p. 4327-4334.

Parmele, L.H., 1972, Errors in output of hydrologic models due to errors in input potential evapotranspiration: Water Resources Research, v. 8, p. 348-359.

Saxton, K.E., and McGuinness, J.L., 1982, Evapotranspiration, *in* Haan, C.T., Johnson, H.P., and D.L. Brakensiek, eds., Hydrologic Modeling of Small Watersheds, Volume 5: St. Joseph, Michigan, ASAE.

Stewart, D.P., 1961, The glacial geology of Vermont: Montpelier, Vermont, Development Department.

Stewart, D.P., and MacClintock, P., 1969, The Surficial Geology and Pleistocene History of Vermont, Vermont Geological Survey.

Urey, H., 1947, The thermodynamic properties of isotopic substances: Journal of the Chemical Society, p. 562-581.

USDA, SCS, Station, V.A.E., and Conservation, V.A.of E., 1974, Soil Survey of Chittenden, Vermont, USDA.

USDA, SCS, Station, V.A.E., and Conservation, V.A.of E., 1981, Soil Survey of Lamoille County, Vermont, USDA.

White, J.W.C., and Gedzelman, S.D., 1984, The isotopic composition of atmospheric water vapor and the concurrent meteorological conditions: Journal of Geophysical Research, v. 89, p. 4937-4939.

Wilmot, S., and Scherbatskoy, T., 1994, Vermont Monitoring Cooperative Annual Report for 1994, Volume 4, Vermont Monitoring Cooperative, p. 12.

Woolhiser, D.A., 1973, Hydrologic and watershed modeling-state of the art: Transactions of the ASAE, p. 553-559.

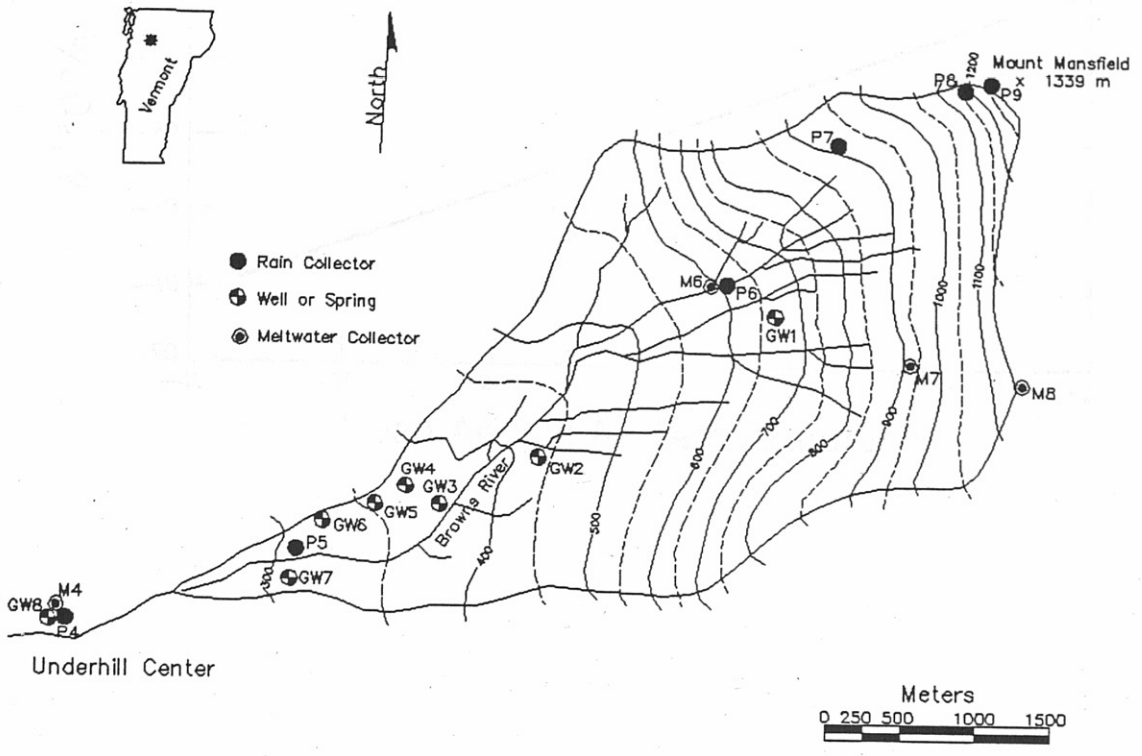

Figure 4.1

Study area and sampling locations. Groundwater samples were collected at residences. Sampling devices were installed at the locations shown for meltwater and rain collection. Contours are in meters asl.

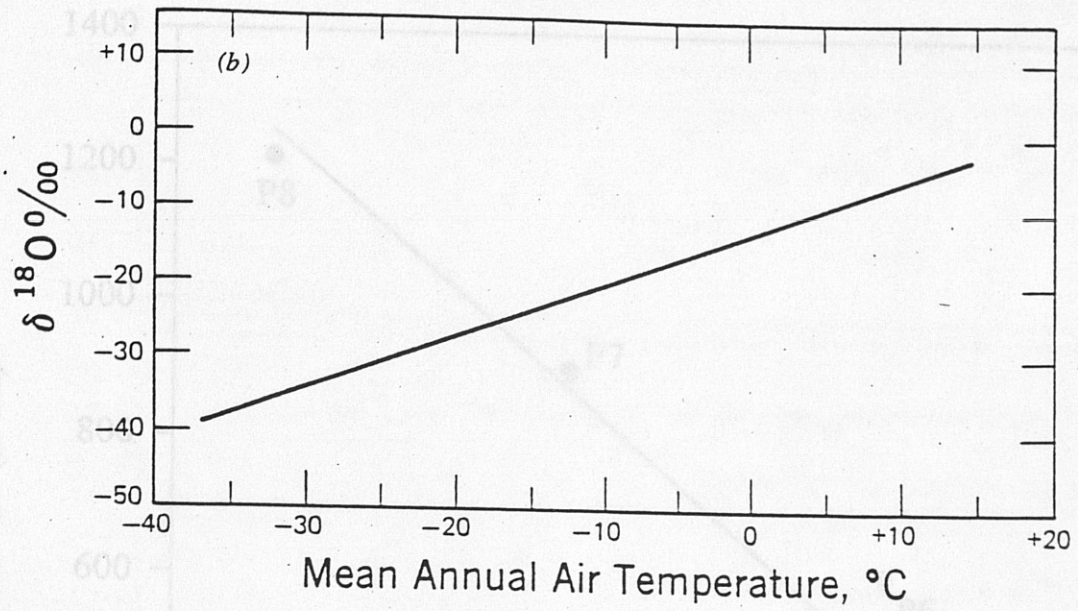

Figure 4.2

The relationship of meteoric water $\delta^{18}O$ and mean annual air temperature.
From Dansgaard (1964)

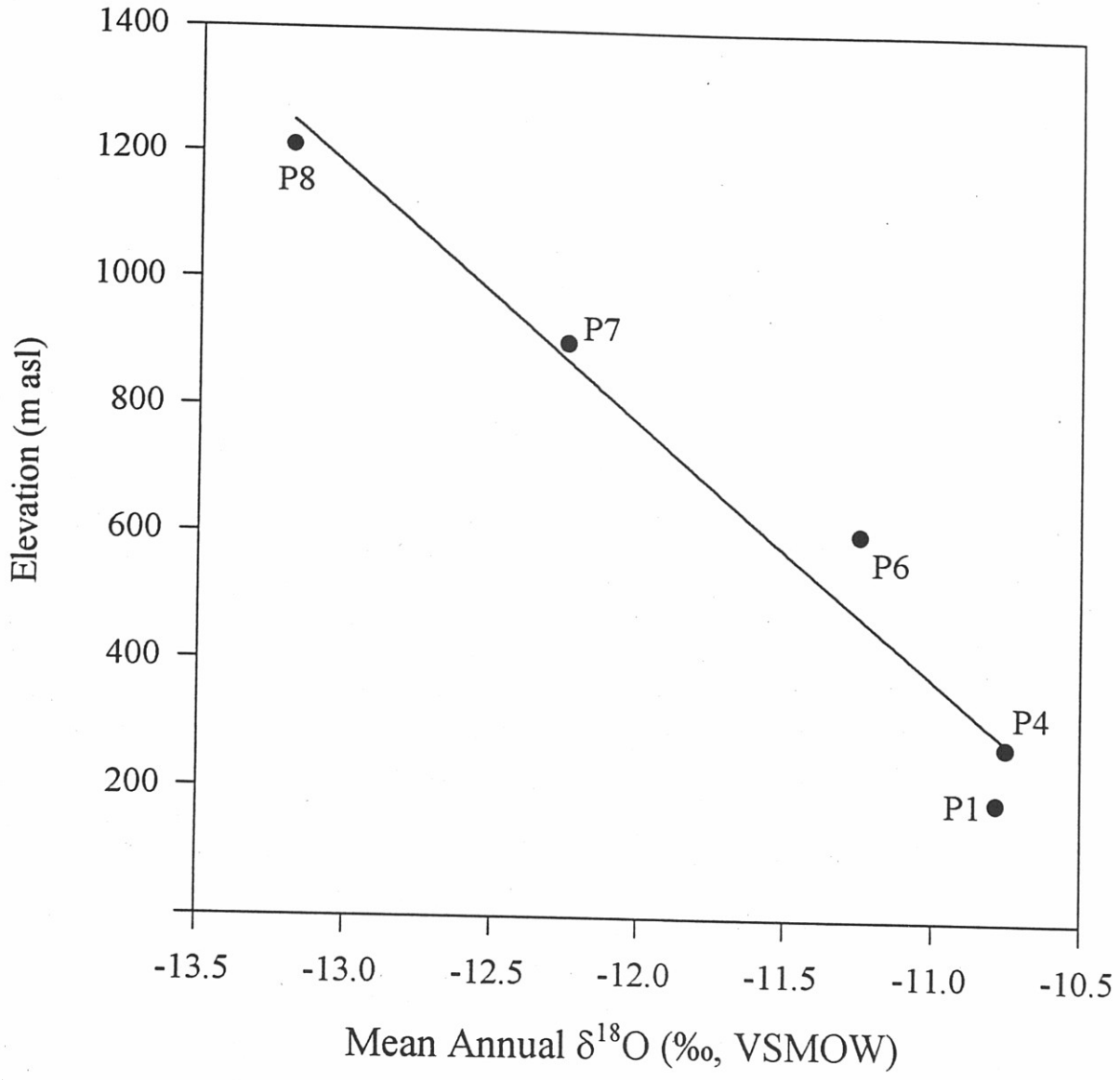

Figure 4.3

The relationship of mean annual precipitation $\delta^{18}O$ and elevation. Equation of linear best fit is: $Y = -398X - 4003$, $R^2 = 0.96$.

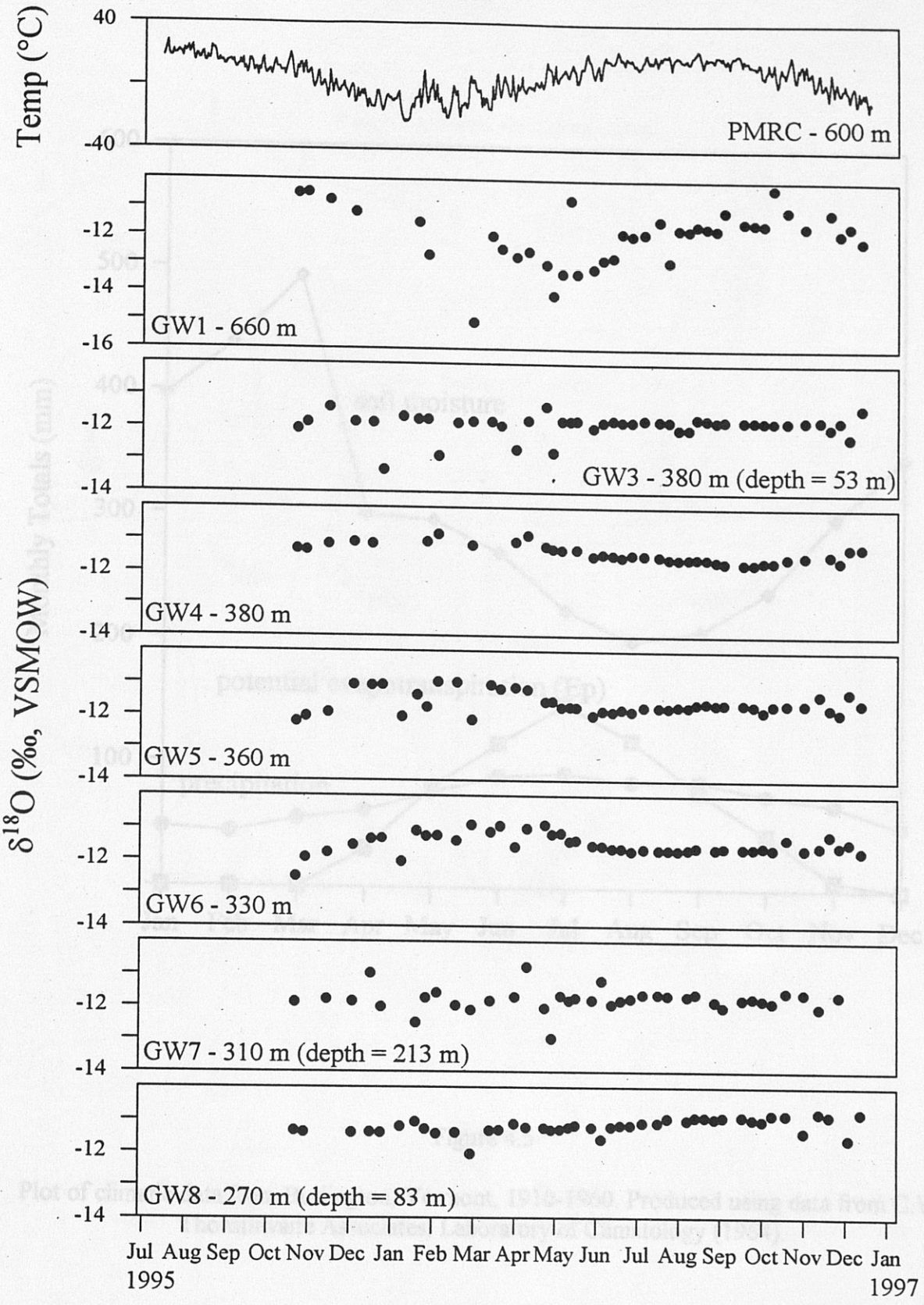

Figure 4.4

Groundwater $\delta^{18}O$ records generated through isotopic study.

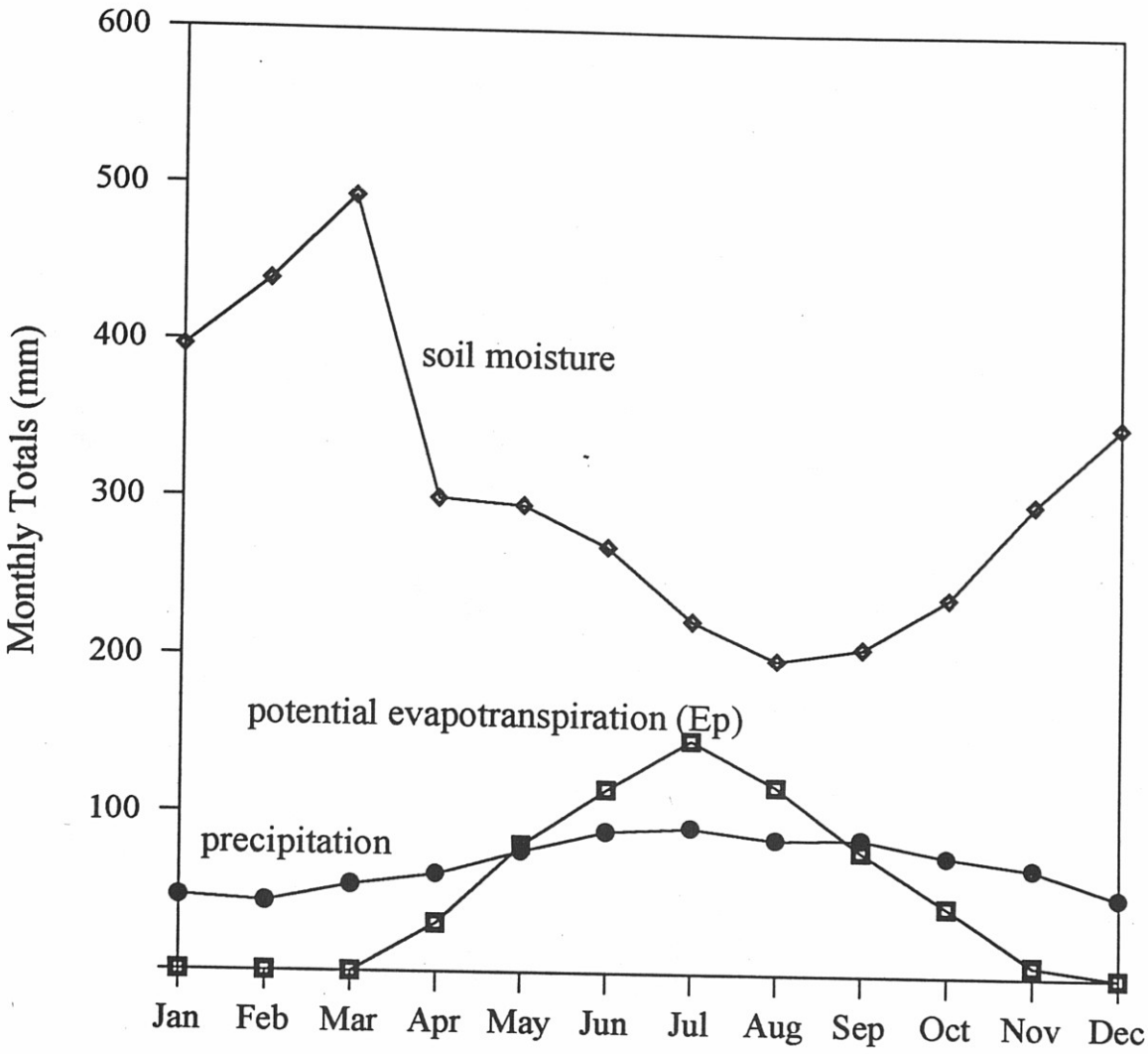

Figure 4.5

Plot of climatic data from Burlington, Vermont, 1910-1960. Produced using data from C.W. Thornthwaite Associates, Laboratory of Climatology (1964).

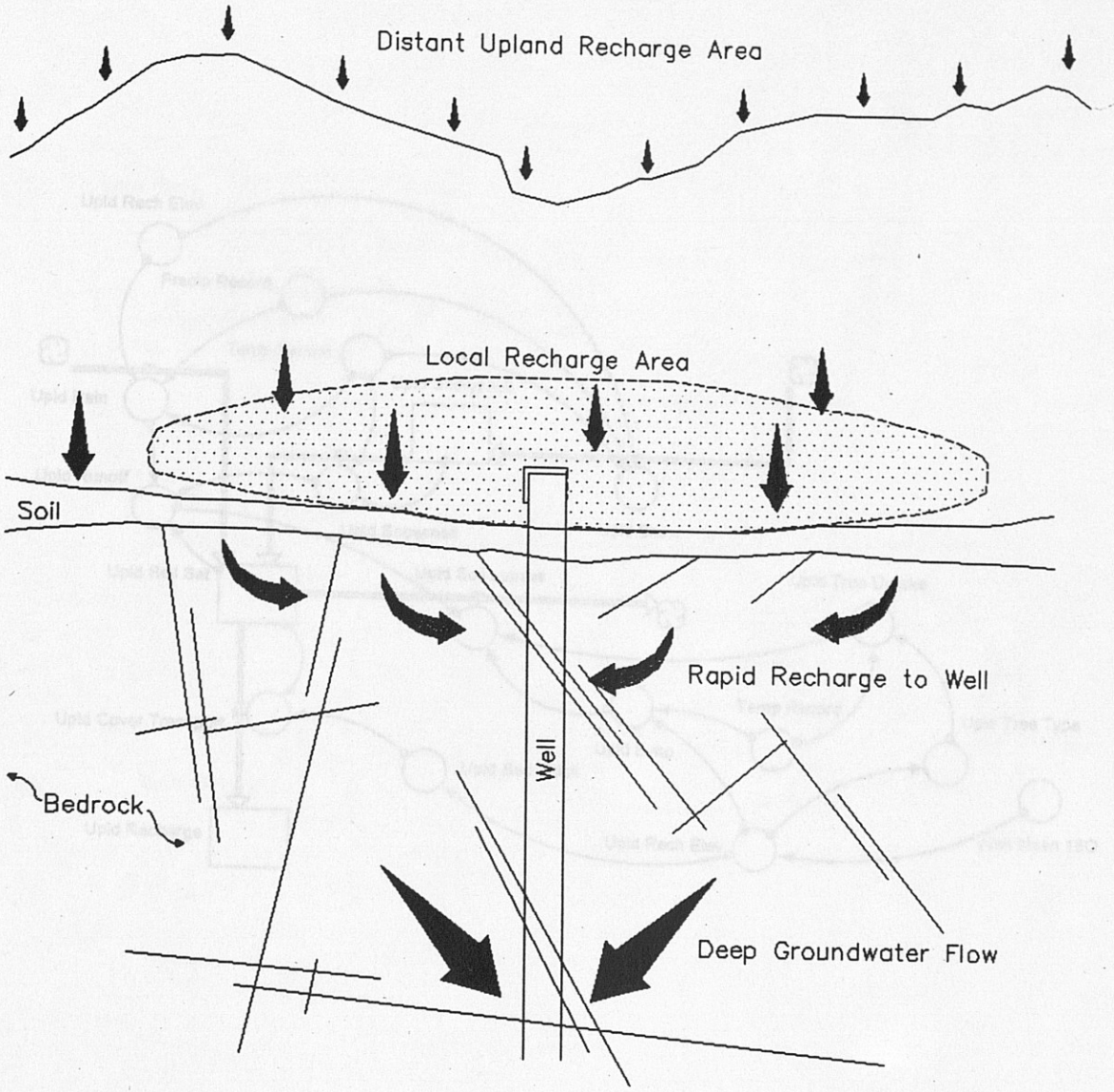

Figure 4.6

Schematic diagram of groundwater mixing. This figure illustrates the combined contribution of water to a well by shallow (local recharge) and deep (distant recharge) fractures.

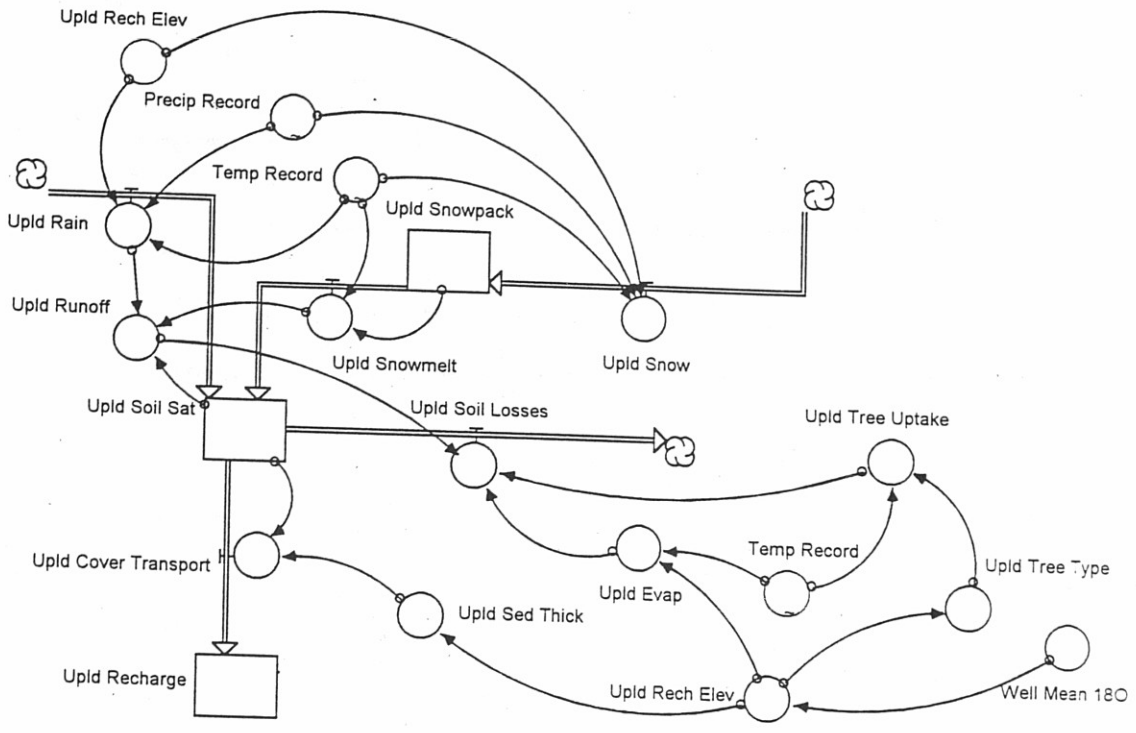

Figure 4.7

Upland recharge model diagram. Developed using STELLA 3.06 graphical interface. See text for discussion of model components.

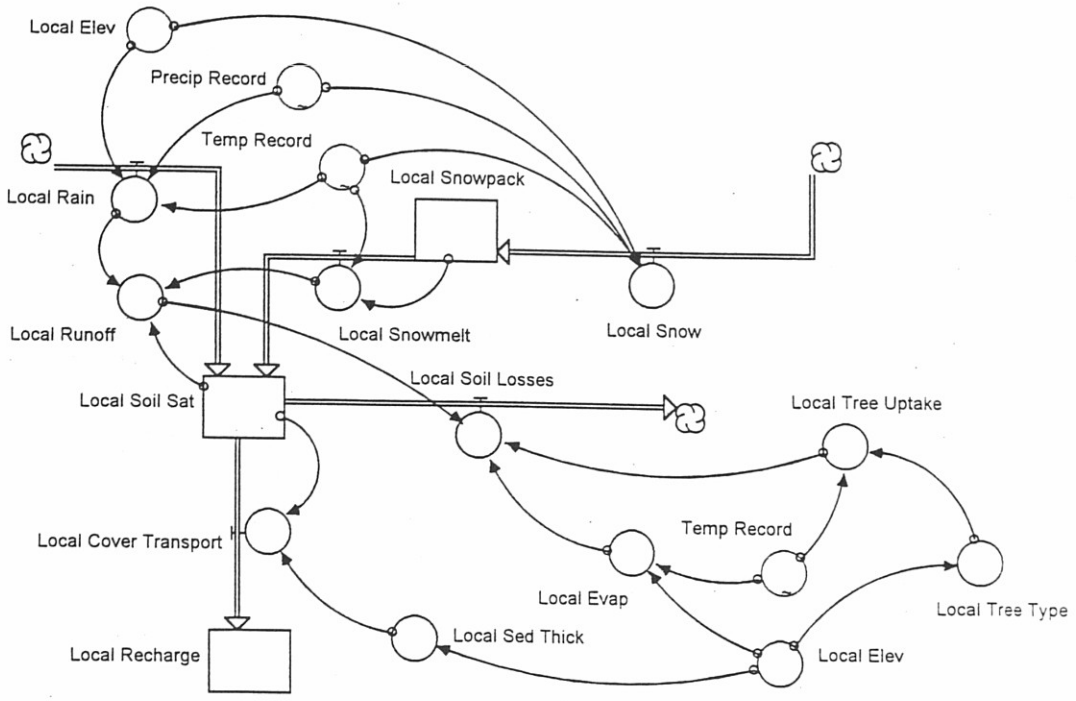

Figure 4.8

Local recharge model diagram. Developed using STELLA 3.06 graphical interface. See text for discussion of model components.

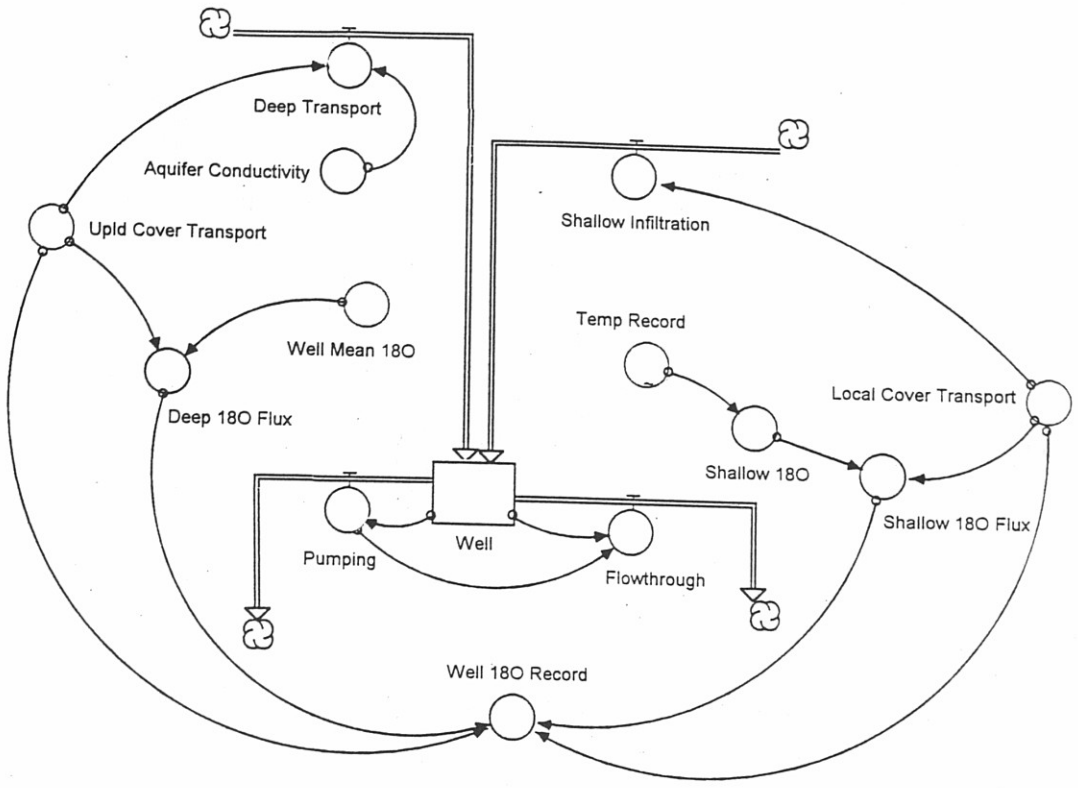

Figure 4.9

Groundwater mixing model diagram. Developed using STELLA 3.06 graphical interface. See text for discussion of model components.

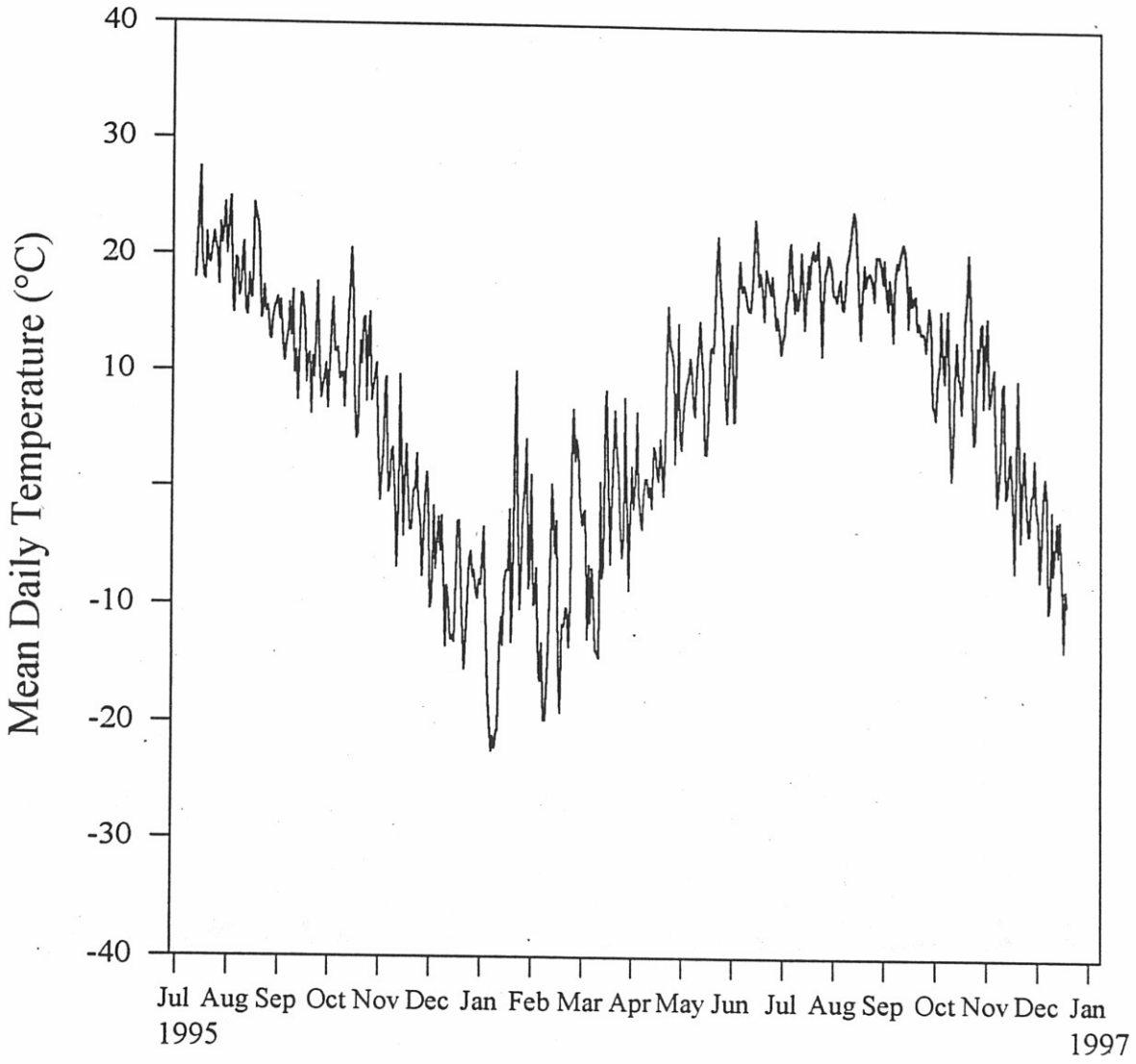

Figure 4.10

Daily temperature record. From measurements taken at Proctor Maple Research Center (600 m asl), Underhill (Cummings, 1997, pers. comm.).

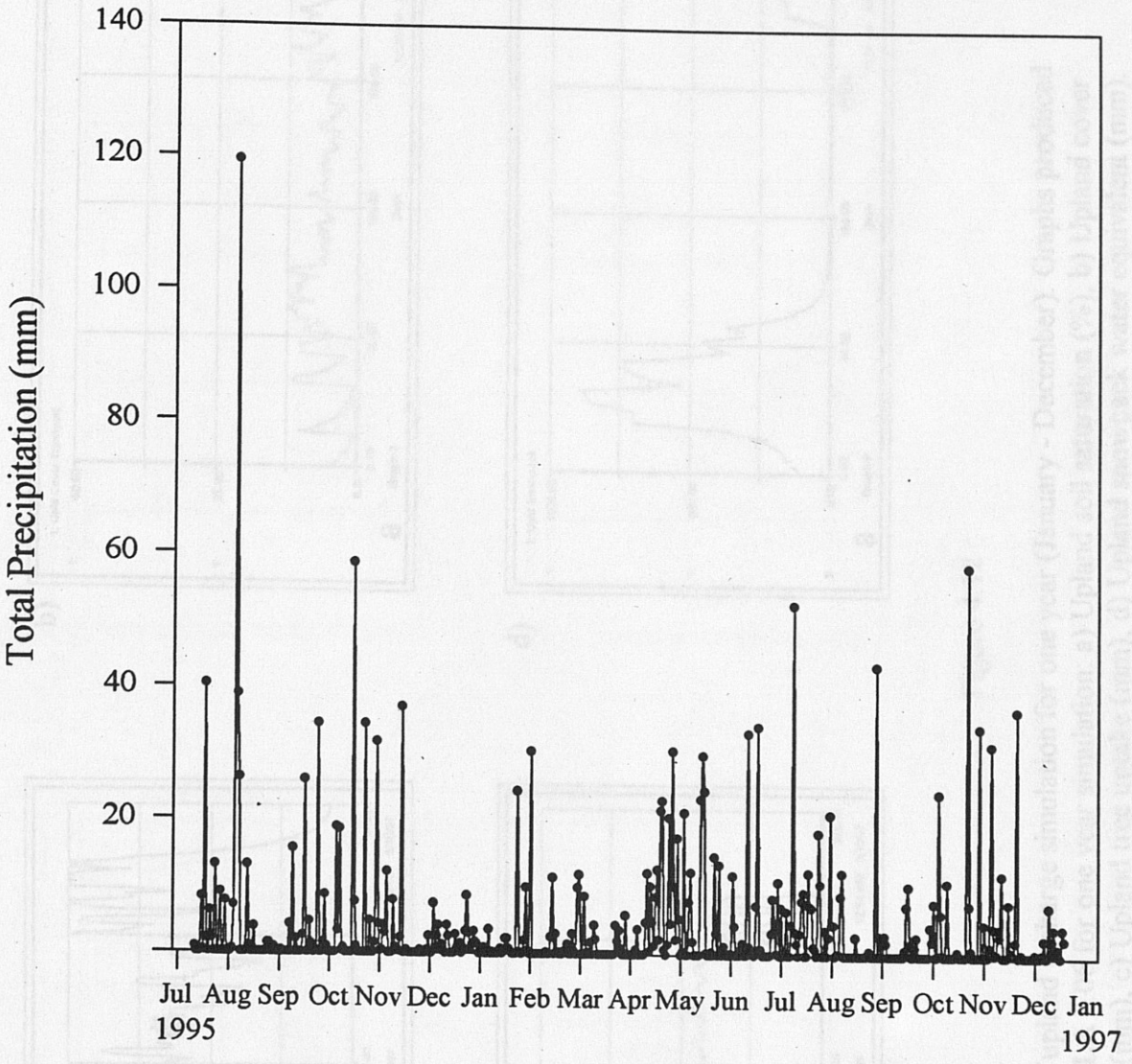

Figure 4.11

Daily precipitation record. From measurements taken at Proctor Maple Research Center (600 m asl), Underhill (Cummings, 1997, pers. comm.).

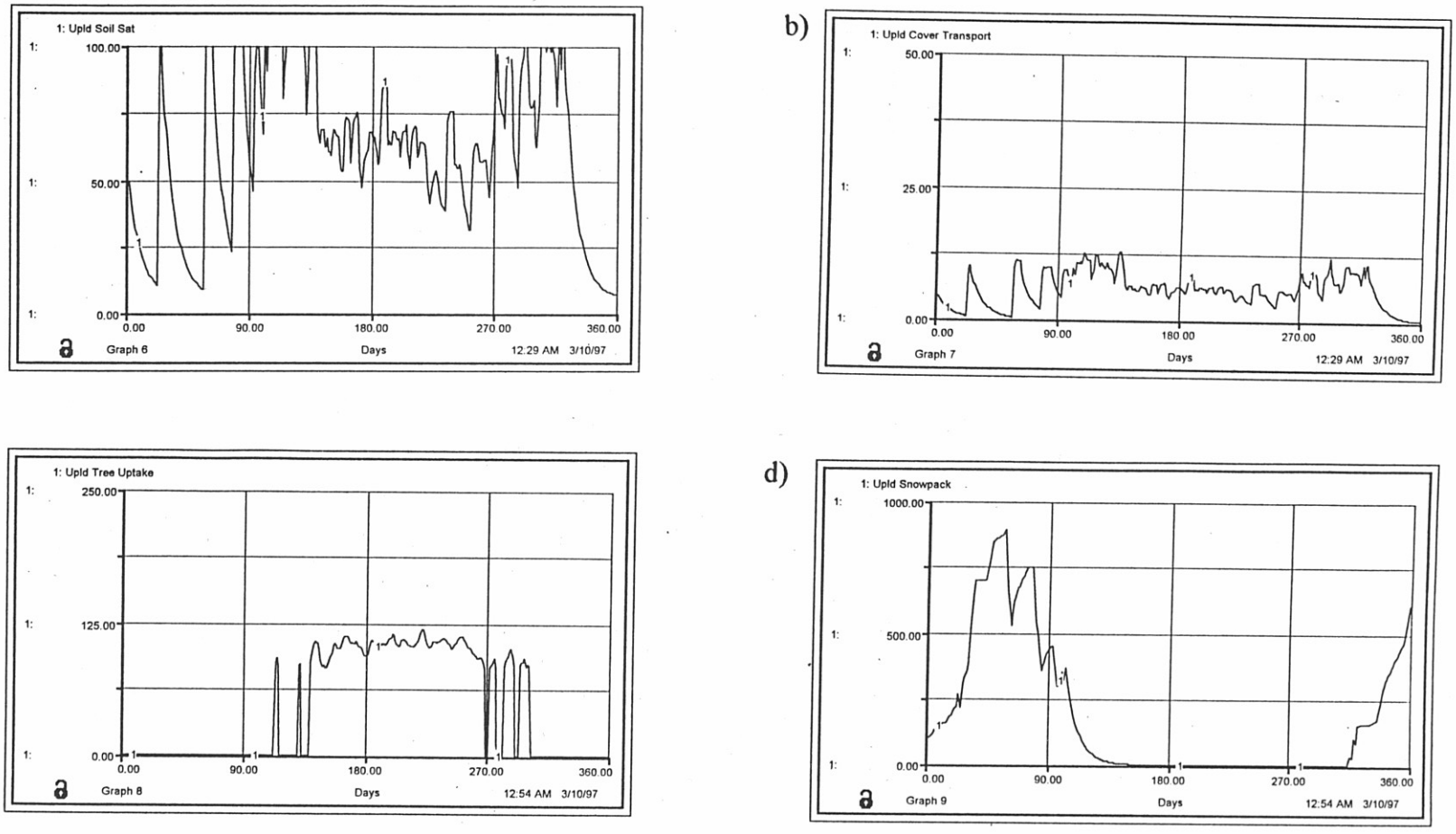

Figure 4.12

Results of upland recharge simulation for one year (January - December). Graphs produced by STELLA 3.06 for one year simulation: a) Upland soil saturation (%), b) Upland cover transport (mm), c) Upland tree uptake (mm), d) Upland snowpack water equivalent (mm).

a)

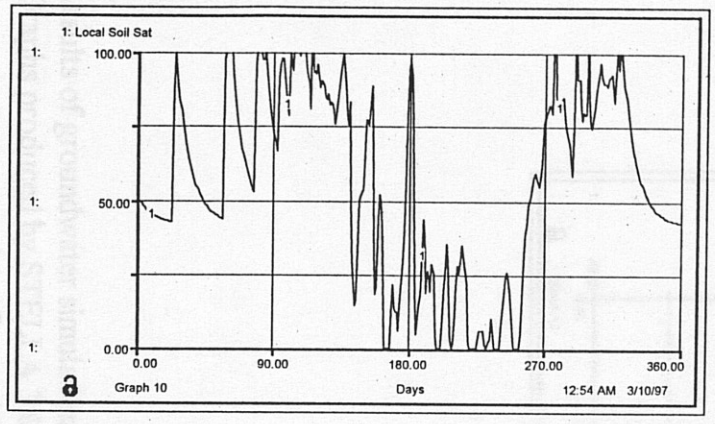

b)

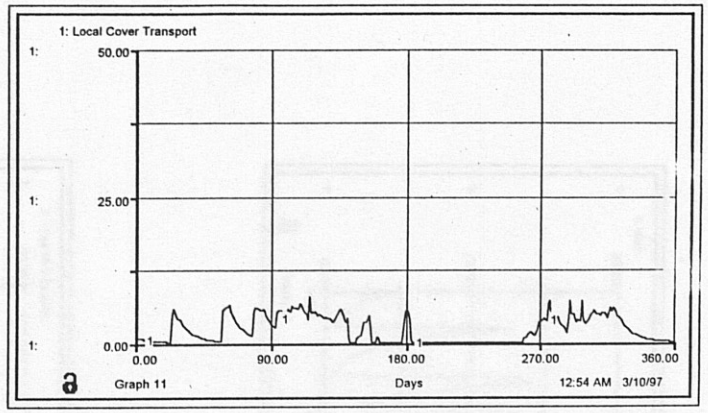

c)

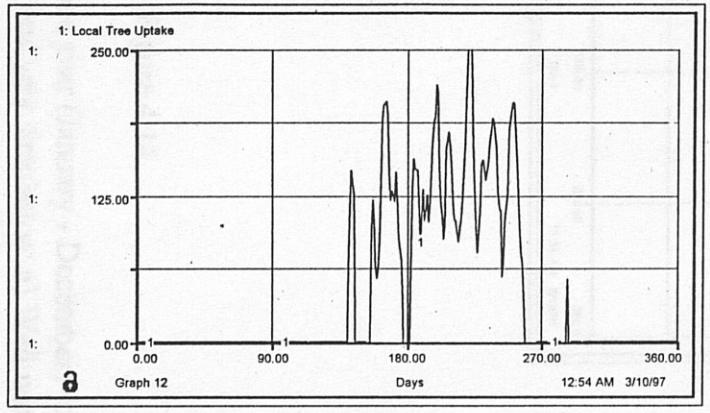

d)

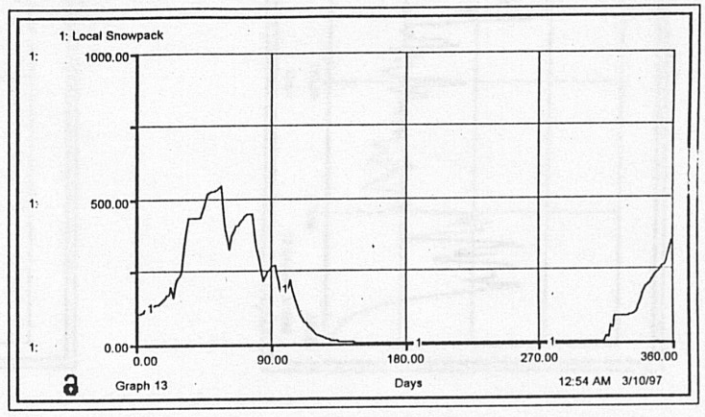

Figure 4.13

Results of local recharge simulation for one year (January - December). Graphs produced by STELLA 3.06 for one year simulation: a) Local soil saturation (%), b) Local cover transport (mm), c) Local tree uptake (mm), d) Local snowpack water equivalent (mm).

a)

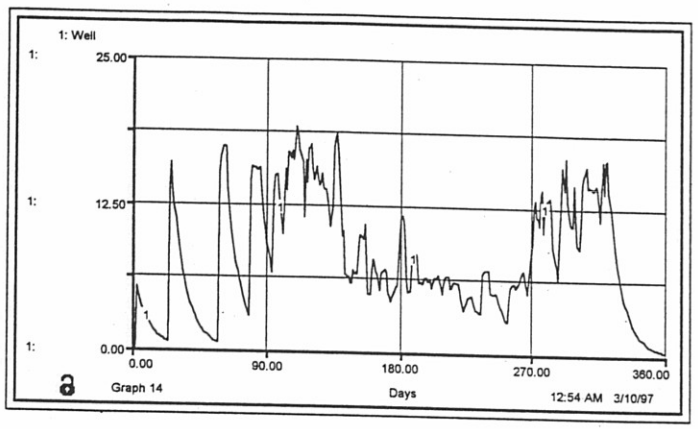

b)

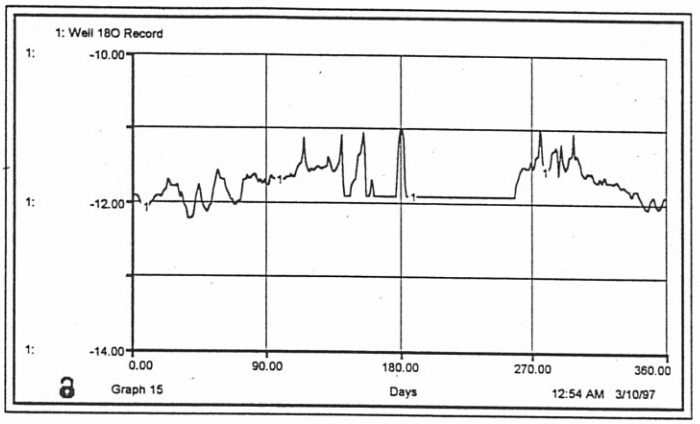

Figure 4.14

Results of groundwater simulation for one year (January - December) for valley well (GW3). Graphs produced by STELLA 3.06 for one year simulation: a) Well water flow ($m^3 \cdot day^{-1}$) = deep flow + local recharge, b) Well $\delta^{18}O$ record (‰).

a)

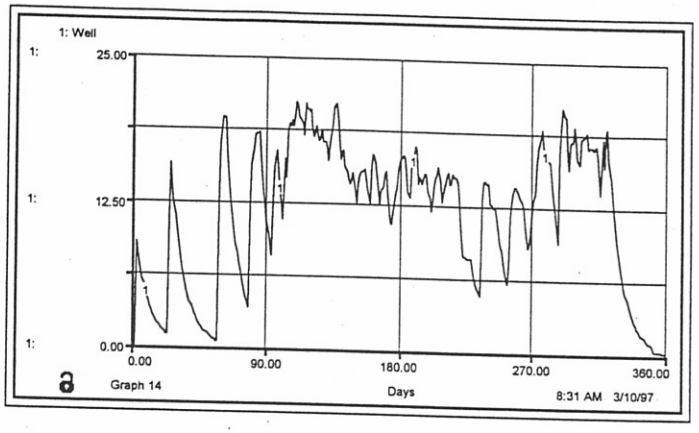

b)

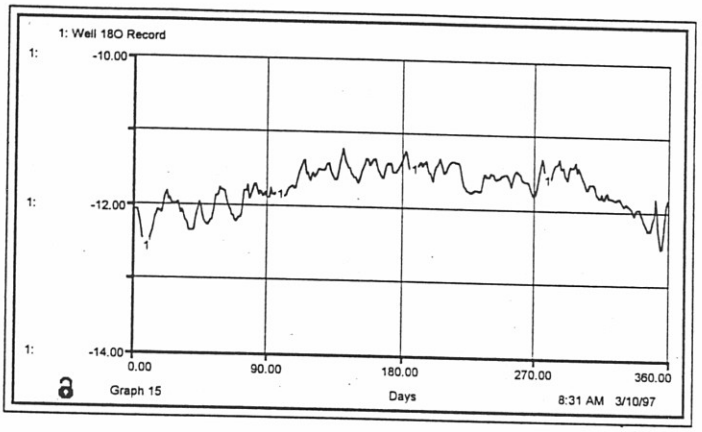

Figure 4.15

Results of groundwater simulation for one year (January - December) for upland spring (GW7). Graphs produced by STELLA 3.06 for one year simulation: a) Spring water flow ($m^3 \cdot day^{-1}$) = deep flow + local recharge, b) Spring $\delta^{18}O$ record (‰).

CHAPTER V

SUMMARY AND DISCUSSION OF FURTHER WORK

The records of $\delta^{18}O$ in precipitation and groundwater generated by this study show that trees and other vegetation have a significant control on the amount of water infiltrating through cover soils and sediments to bedrock. Deep bedrock flow, originating at upland recharge sites, appears constant and well mixed. Recharge to groundwater occurs at appreciable rates throughout the year only at the higher elevations of the upland basin where evaporation and transpiration rates are low (due to harsh weather conditions and less vegetation), and only during the colder months of the year at lower elevations.

Based on the results of stable and radiogenic measurements, the residence time of groundwater in the fractured rock appears to vary from less than one year to over 30 years. Flow rates range from 0.2 $m \cdot day^{-1}$ to greater than 9 $m \cdot day^{-1}$, and are dependent upon the depth of flow and the density of fractures. Water moves quite rapidly in the shallow bedrock and in highly fractured zones at greater depths.

Because recharge to bedrock occurs nearly continuously throughout the year at the upper elevations of the watershed, these areas warrant constant protection from contamination. This can be accomplished by limiting or prohibiting any activities with high pollution potential. In the lower portions of the watershed, recharge occurs in significant amounts during the colder months. Therefore, activities such as salting of roads and land application of wastewater should be reduced or prohibited in any areas close to wells or springs.

The modeling effort was useful in guiding fieldwork and laboratory analysis, and in developing an improved conceptual understanding of recharge and flow systems in the study basin. This study represents a potential for improvement upon conventional approaches to modeling fractured bedrock flow. The resultant model incorporates unique data from the field site to produce realistic simulations of recharge and flow mechanisms. In addition, the improved description of the nature and timing of bedrock recharge provided in this thesis should be useful in the study of other upland bedrock aquifers in New England.

Some components of this study may be continued, by the author and others, beyond the completion of the thesis. One planned objective is the measurement of ^{36}Cl abundance in some of the groundwater samples. ^{36}Cl has a half life of 3.01×10^5 years and has been used as an age determination tool for older waters (Tamers et al, 1969; Bentley, 1978). Like tritium, atmospheric ^{36}Cl abundance was greatly increased during the nuclear testing period. Within the recent time frame, ^{36}Cl acts as a conservative tracer relative to tritium. Using measurements of both ^{36}Cl and ^{3}H , a more precise age determination may be available (Allison and Hughes, 1975; Hoffman and Daniels, 1984; Davis and Murphy, 1987).

The results of this study suggest that the interpretation of groundwater recharge processes may be further refined by monitoring the hydraulic response of groundwater to precipitation events. The purpose of monitoring would be to observe correlation between variations in the isotope record and surface processes. This was not possible in the wells used for this study because they were being frequently pumped for water supply purposes.

Installation of wells for the specific purpose of monitoring in the basin, or instrumentation of springs not in use as water supplies is recommended.

COMPREHENSIVE BIBLIOGRAPHY

Alley, W.M., 1984, On the treatment of evapotranspiration, soil moisture accounting and aquifer recharge in monthly water balance models: Water Resources Research, v. 20, p. 1137-1149.

Allison, G.B., and Hughes, M.W., 1975, The use of environmental tritium to estimate recharge to a South-Australian aquifer: Journal of Hydrology, v. 26, p. 245-254.

Anderson, M.P., and Woessner, W.W., 1992, Applied Groundwater Modeling: Simulation of Advective Flow and Transport: San Diego, California, Academic Press, Inc., 381 p.

Andrews, J.N., Goldbrunner, J.E., Darling, W.G., Hooker, P.J., Wilson, G.B., Youngman, M.J., Eichinger, L., Rauert, W., and Stichler, W., 1985, A radiochemical, hydrochemical and dissolved gas study of groundwaters in the Molasse basin of Upper Austria: Earth and Planetary Science Letters, v. 73, p. 317-332.

Andrews, J.N., and Fontes, J.-C., 1993, Comment on "Chlorine 36 dating of very old groundwater: 3. Further results on the Great Artesian Basin, Australia" by T. Torgersen et al.: Water Resources Research, v. 29, p. 1871-1874.

Aravena, R., and Suzuki, O., 1990, Isotopic evolution of river water in the Northern Chile Region: Water Resources Research, v. 26, p. 2887-2895.

Atakan, Y., Roether, W., Munnich, K.O., and Matthess, G., 1974, The Sandhausen shallow-groundwater tritium experiment, Isotope Techniques in Groundwater Hydrology, Volume 1: Vienna, IAEA, p. 21-43.

Autery, D., 1996, A groundwater chemistry investigation of a typical upland Vermont watershed using bedrock residential waters supply wells [in progress thesis]: Burlington, Vermont, University of Vermont.

Barton, C.C., 1993, Characterizing bedrock fractures in outcrop for studies of ground-water hydrology: An example from Mirror Lake, Grafton County, New Hampshire, *in* Morganwalp, D.W., and Aronson, D.A., eds., U.S. Geological Survey Toxic Substances Hydrology Program Technical Meeting: Colorado Springs, Colorado, USGS.

Begemann, F., and Libby, W.F., 1957, Continental water balance, groundwater inventory and storage times, surface ocean mixing rates and world-wide water circulation patterns from cosmic-ray and bomb tritium: Geochimica et Cosmochimica Acta, v. 12, p. 277-296.

Bennet, E.R., and Linstedt, K.D., 1978, Sewage Disposal by Evapotranspiration, EPA.

Bentley, H.W., 1978, Some comments on the use of chlorine-36 for dating very old groundwater, *in* Davis, S.N., ed., Workshop on dating old ground water, Union Carbide Corporation, Nuclear Division.

Biegelson, J., and Mayer, M.G., 1947, Calculation of equilibrium constants for isotopic exchange reactions: Journal of Chemical Physics, v. 15, p. 261-267.

Blavoux, B., and Olive, P., 1981, Radiocarbon dating of groundwater of the aquifer confined in the lower Triassic sandstones of the Lorraine Region, France: Journal of Hydrology, v. 54, p. 167-183.

Bottomley, D.J., Craig, D., and Johnston, L.M., 1986, Oxygen-18 studies of snowmelt runoff in a small Precambrian shield watershed; implications for streamwater acidification in acid-sensitive terrain: Journal of Hydrology, v. 88, p. 213-234.

Broecker, W., and Oversby, V., 1971, Chemical Equilibria in the Earth: New York, McGraw-Hill.

Burns, G.P., and Otis, C.H., 1916, The Trees of Vermont: Burlington, Vermont, Free Press Printing Company, 244 p.

Busenberg, E., and Plummer, L.N., 1993, Concentrations of chlorofluorocarbons and other gases in ground water at Mirror Lake, New Hampshire, *in* Morganwalp, D.W., and Aronson, D.A., eds., U.S. Geological Survey Toxic Substances Hydrology Program Technical Meeting: Colorado Springs, Colorado, USGS.

Butte, J.M., 1994, Itsotope hydrograph separations and rapid delivery of pre-event water from drainage basins: Progress in Physical Geography, v. 18, p. 16-41.

Cacas, M.C., Ledoux, E., Marsily, G.d., Tillies, B., Barbreau, A., Durand, E., Feuga, B., and Peaudecerf, P., 1990, Modeling fracture flow with a stochastic discrete fracture network: calibration and validation; 1, The flow model: Water Resources Research, v. 26, p. 479-490.

Campana, M.E., and Simpson, E.S., 1984, Groundwater residence times and recharge rates using a discrete-state compartment model and 14C data: Journal of Hydrology, v. 72, p. 171-185.

Chiles, J.-P., 1989, Three-dimensional geometric modeling of a fracture network, *in* Buxton, B.E., ed., Geostatistical, Sensitivity, and Uncertainty Methods for Ground-Water Flow and Radionuclide Transport Modeling, Battelle Press, p. 361-385.

Christman, R.A., 1959, Geology of the Mount Mansfield Quadrangle Vermont: Vermont Geological Survey Bulletin, p. 1-75.

Christman, R., and Secor, D., 1961, Geology of the Camels Hump Quadrangle Vermont: Vermont Geological Survey Bulletin, p. 1-70.

Climatology, C.W.T.A.L.of., 1964, Average Climatic Water Balance Data of the Continents: Part VII United States, Publications in Climatology: Centerton, New Jersey, National Science Foundation, p. 615.

Coleman, M.L., Shepard, T.J., Durham, J.J., Douse, J.E., and Moore, G.J., 1982, Reduction of water with zinc for hydrogen isotope analysis: Analytical Chemistry, v. 54, p. 993-995.

Connally, G.G., 1968, Surficial geology of the Mount Mansfield 15 minute quadrangle, Vermont: Montpelier, Vermont, Vermont Geological Society.

Connor, S., 1994, New England Natives: Cambridge Massachusetts, Harvard University Press, 274 p.

Dansgaard, W., 1964, Stable isotopes in precipitation: Tellus, v. 16, p. 436-468.

Darcy, Henry, 1856, Les Fontaines publiques de la ville de Dijon: Paris, Victor Dalmont, 647 p.

Datta, P.S., Bhattacharya, S.K., and S.K.Tyagi, 1996, 18O studies on recharge of phreatic aquifers and groundwater flow-paths of mixing in the Delhi area: Journal of Hydrology, v. 176, p. 25-36.

Davis, S.N., and Murphy, E., 1987, Dating ground water and the evaluation of repositories for radioactive waste: Tucson, Arizona, University of Arizona.

Davisson, M.L., and Criss, R.E., 1993, Stable isotope imaging of a dynamic groundwater system in the southwestern Sacramento Valley, California: Journal of Hydrology, v. 144, p. 213-246.

Dershowitz, W.S., and Eistein, H.H., 1988, Characterizing rock joint geometry with joint system models: Rock Mechanics and Rock Engineering, v. 21, p. 21-51.

Dole, E.J., 1923, A study of the relative importance of air temperature and relative humidity on the transpiration behavior of coniferous evergreen trees more particularly of primus strobus [406 thesis]: Burlington, Vermont, University of Vermont.

Dole, M., Lane, G.A., Rudd, D.P., and Zaukelies, D.A., 1954, Isotopic composition of atmospheric oxygen and nitrogen: Geochimica et Cosmochimica Acta, v. 6, p. 65-78.

Drenkard, S., Torgersen, T., Weppernig, R., Farley, K., Schlosser, P., Michel, R.L., Shapiro, A.M., and Wood, W.W., 1993, Helium isotope analysis and tritium-helium

age dating in the Mirror Lake basin, Grafton County, New Hampshire, *in* Morganwalp, D.W., and Aronson, D.A., eds., U.S. Geological Survey Toxic Substances Hydrology Program Technical Meeting: Colorado Springs, Colorado, USGS.

Dugan, J.T., and Peckenpaugh, J.M., 1985, Effects of climate, vegetation and soils on consumptive water use and ground-water recharge to the central midwest regional aquifer system, mid-continent United States, USGS.

Dunkle, S.A., Plummer, L.N., Busenberg, E., Phillips, P.J., Denver, J.M., Hamilton, P.A., Michel, R.L., and Coplen, T.B., 1993, Chlorofluorocarbons (CCl3F and CCl2F2) as dating tools and hydrologic tracers in shallow groundwater of the Delmarva Peninsula, Atlantic Coastal Plain, United States: Water Resources Research, v. 29, p. 3837-3860.

Ehleringer, J.R., and Rundel, P.W., 1989, Stable Isotopes: History, Units, and Instrumentation, *in* Rundel, P.W., Ehleringer, J.R., and Nagy, K.A., eds., Stable Isotopes in Ecological Research: New York, Springer-Verlag, p. 1-15.

Ekwurzel, B., Schlosser, P., Smethie, W.M., Plummer, L.N., Busenberg, E., Michel, R.L., Weppernig, R., and Stute, M., 1994, Dating of shallow groundwater: Comparison of the transient tracers 3H/3He, chlorfluorocabons, abd 85Kr: Water Resources Research, v. 30, p. 1693-1708.

Faure, G., 1986, Principles of Isotope Geology: New York, J. Wiley & Sons.

Fontes, J., 1980, Environmental Isotopes in Groundwater Hydrology, Handbook of Environmental Isotope Hydrology, Volume 1, Elsevier Scientific Publishers, p. 25-140.

Friedman, I., 1964, The variation of the deuterium content of natural waters in the hydrologic cycle: Review of Geophysics, v. 2, p. 1-24.

Friedman, I., and O'Neil, J.R., 1977, Compilation of stable isotope fractionation factors of geochemical interest, *in* Fleischer, M., ed., Data of Geochemistry: USGS Professional Papers, U.S. Geological Survey, p. 440-K.

Friedman, I., Benson, C., and Gleason, J., 1991, Isotopic changes during snow metamorphism, *in* Taylor, H.P., O'Neil, J.R., and Kaplan, I.R., eds., Stable Isotope Geochemistry: A Tribute to Samuel Epstein, The Geochemical Society, p. 211-222.

Fritz, P., Drimmie, R.J., Frape, S.K., and O'Shea, K., 1987, Isotopic composition of precipitation and groundwater in Canada, Isotopic Techniques in Water Resources Development: Vienna, Austria, International Atomic Energy Agency, p. 539-550.

Fritz, S.J., Harvey, F.E., Drimmie, R.J., Johnston, C., and Frape, D.K., 1993, Tritium variability of repeated samplings of well waters in Southern Ontario: Mineralogical Magazine, v. 58A, p. 292-.

Garlick, G.D., 1966, Oxygen isotope fractionation in igneous rocks: Earth and Planetary Science Letters, v. 1, p. 361-368.

Gaspar, E., and Oncescu, M., 1972, Radioactive tracers in hydrology: Amsterdam, Elsevier Publishing Company, 450 p.

Gat, J.R., 1971, Comments on the stable isotope method in regional groundwater investigations: Water Resources Research, v. 7, p. 980-993.

Geyh, M.A., and Sofner, B., 1989, Groundwater analysis of environmental carbon and other isotopes from the Jakarta Basin aquifer, Indonesia: Radiocarbon, v. 31, p. 919-925.

Hage, R., Neif, G., and Roth, E., 1970, Absolute isotopic scale for deuterium analysis of natural waters: Absolute D/H ratio for SMOW: Tellus, v. 22, p. 712-715.

Halldin, S., Sangeier, B., and Partailler, J.Y., 1984, Evapotranspiration of a deciduous forest: simulation using routine meteorological data: Journal of Hydrology, v. 75, p. 323-341.

Hardcastle, K.C., Wise, D.U., and Lively, G., 1989, Interim report on the relationships between lineaments, bedrock fracture fabric and well yields in the Colchester Quadrangle, Vt., University of Massachusetts.

Hardcastle, K.C., 1995, Photolineament Factor: A new computer-aided method for remotely sensing the degree to which bedrock is fractured: Photogrammetric Engineering & Remote Sensing, v. 61, p. 739-747.

Harte, P.T., and Winter, T.C., 1993, Factors affecting recharge to crystalline rock in the Mirror Lake area, Grafton County, New Hampshire, *in* Morganwalp, D.W., and Aronson, D.A., eds., U.S. Geological Survey Toxic Substances Hydrology Program Technical Meeting: Colorado Springs, Colorado, USGS.

Healy, R.W., deVries, M.P., and Sturrak, A.M., 1989, Evapotranspiration and microclimate at a low-level radioactive waste disposal site in northwestern Illinois, USGS.

Hedenquist, J.W., Goff, F., Phillips, F.M., Elmore, D., and Stewart, M.K., 1991, Groundwater dilution and residence times, and constraints on chloride source, in the Mokai geothermal system, New Zealand, from chemical, stable isotope, tritium, and 36Cl data: Journal of Geophysical Research, v. 95, p. 19365-19375.

Heemskerk, A.R., Johnson, J. and Drimmie, R.J., 1993, Tritium Analysis, Environmental Isotope Laboratory Technical Procedure 1.0 Rev 3.0: Waterloo Ontario, University of Waterloo, 28 p.

Hobba, W.A.J., Fisher, D.W., F. J. Pearson, J., and Chemerys, J.C., 1979, Hydrology and geochemistry of thermal springs of the Appalachians, U.S. Geological Survey.

Hoefs, J., 1987, Stable Isotope Geochemistry (Minerals and Rocks): Berlin, Springer-Verlag.

Hoffman, D.C., and Daniels, W.R., 1984, Assessment of the potential for radionuclide migration from a nuclear explosion cavity, *in* Bredehoeft, J.D., and Usselman, T.M., eds., Groundwater Contamination, National Academy Press, p. 139-146.

Hooper, R.P., and Shoemaker, C.A., 1986, A comparison of chemical and isotopic hydrograph separation: Water Resources Research, v. 22, p. 1444-1454.

Hostetler, S.W., and Benson, L.V., 1994, Stable isotopes of oxygen and hydrogen in the Truckee River-Pyramid Lake surface water system: 1. A predictive model of d18O and d2H in Pyramid Lake: Limnology and Oceanography, v. 39, p. 356-364.

Hsieh, P.A., and Shapiro, A.M., 1993, Hydraulic characteristics of fractured bedrock underlying the FSE well field at the Mirror Lake site, Grafton County, New Hampshire, *in* Morganwalp, D.W., and Aronson, D.A., eds., U.S. Geological Survey Toxic Substances Hydrology Program Technical Meeting: Colorado Springs, Colorado, USGS.

Hufen, T.H., Buddemeier, R.W., and Lau, L.S., 1974, Isotopic and chemical characteristics of high-level groundwaters on Oahu, Hawaii: Water Resources Research, v. 10, p. 366-370.

Huntington, A.O., 1901, Studies of Trees in Winter: Boston, Massachusetts, Dana Estes and Company, 198 p.

Hussain, S.D., Sajjad, M.I., Ahmad, M., Tasneem, M.A., Yurtsever, Y., and Akram, W., 1991, Isotopic investigation of the interrelationship between surface water and groundwater in the mardan and chaj doab areas in Pakistan: IAEA-SM, v. 319, p. 429-444.

IAHS, 1995, Biogeochemistry of Seasonally Snow-Covered Catchments, *in* Tonnessen, K.A., Williams, M.W., and Tranter, M., eds., Assembly of the International Union of Geodesy and Geophysics, Volume 228: Boulder, Colorado, IAHS.

Isaar, A., Quijano, J.L., Gat, J.R., and Castro, M., 1984, The isotope hydrology of the groundwaters of Central Mexico: Journal of Hydrology, v. 71, p. 201-224.

Kennedy, V.C., Kendall, C., Zellweger, G.W., Wyerman, T.A., and Avanzino, R.J., 1986, Determination of the components of stormflow using water chemistry and environmental isotopes, Mattole River Basin, California: Journal of Hydrology, v. 84, p. 107-140.

Kennet-Smith, A., Cook, P.G., and Walker, G.R., 1994, Factors affecting groundwater recharge following clearing in the south western Murray Basin: Journal of Hydrology, v. 154, p. 85-105.

Knisel, W.G., Baird, R.W., and Hartman, M.A., 1969, Runoff volume prediction from daily climatic data: Water Resources Research, v. 5, p. 84-94.

Konikow, L.F., and Bredehoeft, J.D., 1978, Computer model of two-dimensional solute transport and dispersion in ground water, Techniques of Water Resources Investigations, Volume Book 7, USGS, p. 90.

Krishnamurthy, R.V., and Deniro, M.J., 1982, Sulfur interference in the determination of hydrogen concentration and stable isotopic composition in organic matter: Analytical Chemistry, v. 54, p. 153-154.

Kulatilake, P.H.S.W., and Wathugala, D.N., 1990, Stochastic three dimensional joint geometry modeling including a verification to an area in Stripa Mine, Sweden, *in* Rossmith, ed., Mechanics of Jointed and Faulted Rock, A.A. Balkema, p. 71-82.

Kyser, T.K., 1987, Equilibrium fractionation factors for stable isotopes, *in* Kyser, T.K., ed., Stable Isotope Geochemistry of Low Temperature Fluids: Saskatoon, Saskatchewan, Mineralogical Association of Canada, p. 1-84.

Lajtha, K., and Michener, R.H., 1994, Stable Isotopes in Ecology and Environmental Sciences: Oxford, Blackwell Scientific Publications.

Lapointe, P.R., and Hudson, J.A., 1985, Characterization and interpretation of rock mass joint patterns: Geological Society of America Special Paper 199, p. 1-37.

Lawrence, J.R., and White, J.C., 1991, The elusive climate signal in the isotopic composition of precipitation, *in* Taylor, H.P., O'Neil, J.R., and Kaplan, I.R., eds., Stable Isotope Geochemistry: A Tribute to Samuel Epstein, The Geochemical Society.

Leaney, F.W., and Herczeg, A.L., 1995, Regional recharge to a karst aquifer estimated from chemical and isotopic composition of diffuse and localized recharge, South Australia: Journal of Hydrology, v. 164, p. 363-387.

Likens, G.E., Borman, F.H., Eaton, J.S., and Johnson, N.M., 1977, Biogeochemistry of a forested ecosystem: New York, Springer-Verlag, 146 p.

Likens, G.E., Borman, F.H., Pierce, R.S., and Eaton, J.S., 1985, The Hubbard Brook valley, An Ecosystem Approach to Aquatic Ecology -- Mirror Lake and its Environments: New York, Springer-Verlag, p. 516.

Long, J.C.S., Gilmour, P., and Witherspoon, P.A., 1985, A model for steady fluid flow in random three-dimensional networks of disc-shaped fractures: Water Resources Research, v. 21, p. 1105-1115.

Love, A.J., Herczeg, A.L., Armstrong, D., Stadter, M.F., and Mazor, E., 1993, Groundwater flow regime within the Gabier Embayment of the Otway Basin, Australia: evidence from hydraulics and hydrochemistry: Journal of Hydrology, v. 143, p. 297-338.

Love, A.J., Herczeg, A.L., Leaney, F.W., Stadter, M.F., Lighten, J.C., and Armstrong, D., 1994, Groundwater residence time and palaeohydrology in the Otway Basin, South Australia: 2H. 18O and 14C data: Journal of Hydrology, v. 153, p. 157-187.

Mabee, S.B., Hardcastle, K.C., and Wise, D.U., 1990, Correlation of lineaments and bedrock fracture fabric: Implications for regional fractured-bedrock aquifer studies, preliminary results from Georgetown, Maine, FOCUS Conference on Eastern Regional Groundwater Issues, NWWA.

Mabee, S.B., Hardcastle, K.C., and Wise, D.U., 1994, A method of collecting and analyzing lineaments for regional-scale fractured-bedrock aquifer studies: Ground Water, v. 32, p. 884-894.

Maloszewski, P., and Zuber, A., 1982, Determining the turnover time of groundwater systems with the aid of environmental tracers: 1. Models and their applicability: Journal of Hydrology, v. 57, p. 207-231.

Maloszewski, P., and Zuber, A., 1985, On the theory of tracer experiments in fissured rocks with a porous matrix: Journal of Hydrology, v. 79, p. 333-358.

Mather, J.R., 1972, Papers on Evapotranspiration and the Climatic Water Balance, Volume XXV: Elmer, N.J., Library of Climatology, p. 57.

Maule, C.P., and Stein, J., 1990, Hydrologic flow path definition and partitioning of spring meltwater: Water Resources Research, v. 26, p. 2959-2970.

McDonnell, J.J., Stewart, M.K., and Owens, I.F., 1991, Effect of catchment-scale subsurface mixing on stream isotopic response: Water Resources Research, v. 27, p. 3065-3073.

McGuinness, J.L., and Harrold, L.L., 1962, Seasonal and areal effects on small-watershed streamflow: Journal of Geophysical Research, v. 67, p. 4327-4334.

Michel, R.L., 1992, Residence times in river basins as determined by analysis of long-term tritium records: Journal of Hydrology, v. 130, p. 367-368.

Moore, K.M., Murray, M.L., and Schoeninger, M.J., 1989, Dietary reconstruction from bones treated with preservatives: Journal of Archaeological Science, v. 16, p. 437-446.

Neuman, S., and Rouleau, A., 1994, Fractured Rocks: Characterization, Flow and Transport, Fractured Rocks: Characterization, Flow and Transport: Tucson, Arizona, Environmental Education Enterprises, p. 1542.

Nordstrom, D.K., Andrews, J.N., Carlsson, L., Fontes, J.-C., Fritz, P., Moser, H., and Olsson, T., 1985, Hydrogeological and hydrochemical investigations in boreholes: Final report of the phase I geochemical investigations of the Stripa groundwaters: Stockholm, SKB Stockholm.

O'Neil, J.R., Adami, L.H., and Eptein, S., 1975, Revised value for the 18O fractionation between CO2 and H2O at 25C: Journal of Research, USGS, v. 3, p. 623.

Ostlund, H.G., Top, Z., and Lee, V.E., 1982, Isotope dating of waters at Fram III: Geophysical Research Letters, v. 9, p. 1117-1119.

Parmele, L.H., 1972, Errors in output of hydrologic models due to errors in input potential evapotranspiration: Water Resources Research, v. 8, p. 348-359.

Penman, H.L., 1948, Natural evaporation from open water, bare soil and grasses, Proceedings of the Royal Society, Volume 193: London England, p. 120.

Pinder, G.F., and Gray, W.G., 1977, Finite Element Simulation in Surface and Subsurface Hydrology, Academic Press, 295 p.

Pinder, G.F., and Voss, C., 1979, AQUIFEM, a finite element model for aquifer evaluation (documentation): Stockholm, Sweden, Department of Water Resources Engineering, Royal Institute of Technology.

Poland, J.F., and Stewart, G.T., 1975, New tritium data on movement of groundwater in western Fresno County, California: Water Resources Research, v. 11, p. 716-724.

Prickett, T.A., 1979, Ground-water computer models- state of the art: Groundwater, v. 17, p. 167-173.

Purdy, C.B., Burr, G., Helz, G.R., and Mignerey, A.C., 1991, Dating groundwater in coastal plain aquifers in southern Maryland using DOC and DIC 14C ages: An evaluation by comparison with other dating methods: Radiocarbon, v. 33, p. 234.

Rayleigh, L.R.J.S., 1964, Scientific Papers: New York, Dover Publications.

Ronen, D., Magaritz, M., Paldor, N., and Bachmat, Y., 1986, The behavior of groundwater in the vicinity of the water table evidenced by specific discharge profiles: Water Resources Research, v. 22, p. 1217-1224.

Rose, S., 1993, Environmental tritium systematics of baseflow in Piedmont Province watersheds, Georgia (USA): Journal of Hydrology, v. 143, p. 191-216.

Rouleau, A., and Gale, J.E., 1985, Statistical characterization of the fracture system in the Stripa granite, Sweden: International Journal of Mechanics and Mining Science, v. 22, p. 353-367.

Roy, D.C., and Skehan, J.W., 1993, The Acadian Orogeny: Recent Studies in New England, Maritime Canada, and the Autochthonous Foreland: Boulder, Colorado, Geological Society of America, p. 171.

Rozanski, K., 1985, Deuterium and oxygen-18 in European groundwaters - links to atmospheric circulation in the past: Chemical Geology (Isotope Geoscience Section), v. 52, p. 349-363.

Rozanski, K., Araguas-Araguas, L., and Gonfiantini, R., 1993, Isotopic Patterns in Modern Global Precipitation, Climate Change in Continental Isotopic Records, Volume Monograph 78, American Geophysical Union, p. 1-36.

Rundel, P.W., Ehleringer, J.R., and Nagy, K.A., 1989, Stable Isotopes in Ecological Research: New York, Springer-Verlag, p. 525.

Salhotra, A., and Nichols, E., 1993, Modeling Subsurface Contaminant Transport, Modeling Subsurface Contaminant Transport: Portland, Maine, Environmental Education Enterprises, p. 571.

Saxton, K.E., and McGuinness, J.L., 1982, Evapotranspiration, *in* Haan, C.T., Johnson, H.P., and D.L. Brakensiek, eds., Hydrologic Modeling of Small Watersheds, Volume 5: St. Joseph, Michigan, ASAE.

Schlosser, P., Stute, M., Dorr, H., Sonntag, C., and Munnich, K.O., 1988, Tritium/3He dating of shallow groundwater: Earth and Planetary Science Letters, v. 89, p. 353-362.

Schlosser, P., Stute, M., Sonntag, C., and Munnich, K.O., 1989, Tritiogenic 3He in shallow groundwater: Earth and Planetary Science Letters, v. 94, p. 245-256.

Schotterer, U., Frohlich, K., Stichler, W., and Trimborn, P., 1993, Temporal variation of 18O and deuterium excess in precipitation, river and spring waters in alpine regions of Switzerland: IAEA-SM, v. 329, p. 53-64.

Shanley, J.B., Kendall, C., Smith, T., and Wolock, D., 1994, The effect of catchment scale and land use on the relative contributions of shallow flow paths to stream discharge during snowmelt: Water Resources Research, v. preliminary submission.

Shapiro, A.M., and Hsieh, P.A., 1993, Overview of research on use of hydrologic, geophysical and geochemical methods to characterize flow and chemical transport in fractured rock at the Mirror Lake site, New Hampshire, *in* Morganwalp, D.W., and Aronson, D.A., eds., U.S. Geological Survey Toxic Substances Hydrology Program Technical Meeting: Colorado Springs, Colorado, USGS.

Shapiro, A.M., Wood, W.W., Busenberg, D., Drenkard, S., Plummer, L.N., Torgersen, T., and Schlosser, P., 1993, A conceptual model for estimating regional ground-water velocity in bedrock of the Mirror Lake area, Grafton County, New Hampshire, *in* Morganwalp, D.W., and Aronson, D.A., eds., U.S. Geological Survey Toxic Substances Hydrology Program Technical Meeting: Colorado Springs, Colorado, USGS.

Socki, R.A., Karlsson, H.R., and Gibson, E.K.J., 1992, Extraction technique for the determination of oxygen-18 in water using pre-evacuated glass vials: Analytical Chemistry, v. 64, p. 829-831.

Solomon, D.K., Poreda, R.J., Schiff, S.L., and Cherry, J.A., 1992, Tritium and helium 3 as groundwater age tracers in the Borden Aquifer: Water Resources Research, v. 28, p. 741-755.

Sommerfield, R.A., Judy, C., and Friedman, I., 1991, Isotopic changes during the formation of depth hoar in experimental snowpacks, *in* Taylor, H.P., O'Neil, J.R., and Kaplan, I.R., eds., Stable Isotope Geochemistry: A Tribute to Samuel Epstein, The Geochemical Society, p. 205-210.

Spaher, N.E., 1981, Variations in climatic characteristics as related to evapotranspiration in South Park, Central Park County, Colorado.

Stanley, R.S., and Ratcliffe, N., 1983, Simplified Lithotectonic Synthesis of Pre-Silurian Rocks in Western New England, *in* Ratte, C.A., and Dorsey, R.J., eds., Vermont Geological Survey Special Bulletin, Vermont Geological Survey.

Stewart, D.P., 1961, The glacial geology of Vermont: Montpelier, Vermont, Development Department.

Stewart, D.P., and MacClintock, P., 1969, The Surficial Geology and Pleistocene History of Vermont, Vermont Geological Survey.

Strack, O.D.L., 1987, The analytic element method for regional groundwater modeling, Solving Ground Water Problems with Models: Columbus, Ohio, National Water Well Association, p. 929-941.

Strack, O.D.L., 1988, Groundwater Mechanics: Englewood Cliffs, New Jersey, Prentice-Hall, 732 p.

Suess, H.E., 1969, Tritium geophysics as an international research project: Science, v. 163, p. 1405-1410.

Tamers, M.A., Ronzoni, C., and Scharpenseel, H.W., 1969, Naturally occurring chlorine-36: Atompraxis, v. 15, p. 433-437.

Taylor, H.P.J., 1973, O18/O16 evidence for meteoric-hydrothermal alteration and ore deposition in the Tonopah, Comstock lode, and Goldfield mining districts, Nevada: Economic Geology, v. 68, p. 747-764.

Taylor, H.P.J., O'Neil, J.R., and Kaplan, I.R., 1991, Stable Isotope Geochemistry: A Tribute to Samuel Eptein, Geochemical Society Special Publication, Volume 3, Lancaster Press, p. 516.

Thompson, P., and Thompson, T., 1991, Bedrock Geology of the Camels Hump-Bolton Mountain Area, North-Central Vermont: Vermont Geological Survey Special Bulletin, p. 1-32.

Thorburn, P.J., Cowie, B.A., and Lawrence, P.A., 1991, Effect of land development on groundwater recharge determined from non-steady chloride profiles: Journal of Hydrology, v. 124, p. 43-58.

Thorburn, P.J., Halton, T.J., and Walker, G.R., 1993, Combining measurements of transpiration and stable isotopes of water to determine groundwater discharge from forests: Journal of Hydrology, v. 150, p. 563-587.

Thornthwaite, C.W., 1954, A re-examination of the concept and measurement of potential evapotranspiration: Publications in Climatology, v. 7, p. 200-217.

Tolstikhin, I., and Kamensky, I., 1969, Determination of groundwater ages by the T-3He Method: Geochemistry International, v. 6, p. 810-811.

Torgersen, T., and Ivey, G.N., 1985, Helium accumulation in groundwater II: A model for the accumulation of the crustal 4He degassing flux: Geochimica et Cosmochimica Acta, v. 49, p. 2445-2452.

Torgerson, T., Drenkard, S., Stute, M., Schlosser, P., and Shapiro, A., 1995, Mantle helium in ground waters of eastern North America: Time and space constraints on sources: Geology, v. 23, p. 675-678.

Townley, L., and Wilson, J.L., 1980, Description of and user's manual for a finite element aquifer flow model AQUIFEM-1, MIT Ralph M. Parsons Laboratory for Water Resources and hydrodynamics.

Townley, L.R., 1990, AQUIFEM-N: a multi-layered finite element aquifer flow model, user's manual and description: Perth, Australia, CSIRO Division of Water Resources.

Turner, J.V., Allison, G.B., and Holmes, J.W., 1984, The water balance of a small lake using stable isotopes and tritium: Journal of Hydrology, v. 70, p. 199-220.

Turner, J.V., Macpherson, D.K., and Stokes, R.A., 1987, The mechanisms of catchment flow processes using natural variations in deuterium and oxygen-18: Journal of Hydrology, v. 94, p. 143-162.

Unterweger, M.P., Coursey, B.M., Schima, F.J., and Mann, W.B., 1980, Preparation and calibration of the 1978 National Bureau of Standards tritiated-water standards: International Journal of Applied Radiation Isotopes, v. 33, p. 611-614.

Urey, H., 1947, The thermodynamic properties of isotopic substances: Journal of the Chemical Society, p. 562-581.

USDA, SCS, Station, V.A.E., and Conservation, V.A.of E., 1974, Soil Survey of Chittenden, Vermont, USDA.

USDA, SCS, Station, V.A.E., and Conservation, V.A.of E., 1981, Soil Survey of Lamoille County, Vermont, USDA.

Verhagen, B.T., 1991, Detailed geohydrology with environmental isotopes: a case study at Serowe, Botswana: IAEA-SM, v. 319, p. 345-362.

Vogel, J.C., Thilo, L., and Dijken, M.V., 1974, Determination of groundwater recharge with tritium: Journal of Hydrology, v. 23, p. 131-140.

Wagner, H., and Noyes, Inc., 1994, USEPA Wellhead Protection Area Demonstration Project: Jericho-Underhill Water District, Underhill, Vermont, United States Environmental Protection Agency.

Wassenaar, L., Aravena, R., Hendry, J., and Fritz, P., 1991, Radiocarbon in dissolve organic carbon, a possible groundwater dating method: case studies from western Canada: Water Resources Research, v. 27, p. 1975-1986.

Wenner, D.B., Ketcham, P.D., and Dowd, J.F., 1991, Stable isotopic composition of waters in a small Piedmont watershed, *in* Taylor, H.P., O'Neil, J.R., and Kaplan, I.R., eds., Stable Isotope Geochemistry: A Tribute to Samuel Epstein, The Geochemical Society, p. 195-203.

White, J.W.C., and Gedzelman, S.D., 1984, The isotopic composition of atmospheric water vapor and the concurrent meteorological conditions: Journal of Geophysical Research, v. 89, p. 4937-4939.

Wilmot, S., and Scherbatskoy, T., 1994, Vermont Monitoring Cooperative Annual Report for 1994, Volume 4, Vermont Monitoring Cooperative, p. 12.

Wong, W.W., Lee, L.L., and Klein, P.D., 1987, Deuterium and oxygen-18 measurements on microliter samples of urine, plasma, saliva and human milk: American Journal of Clinical Nutrition, v. 45, p. 905-913.

Woolhiser, D.A., 1973, Hydrologic and watershed modeling-state of the art: Transactions of the ASAE, p. 553-559.

Zuber, A., Weise, S.M., Osenbruck, K., Grabczak, J., and Ciezkowski, W., 1995, Age and recharge area of thermal waters in Ladek Spa (Sudeten, Poland) deduced from environmental isotope and noble gas data: Journal of Hydrology, v. 167, p. 327-349.

APPENDIX A - DATA RECORD

All results of $\delta^{18}O$, δD (in ‰), and ^{3}H (in TU) analysis are included in spreadsheet form. Also included are data obtained from measurement of bedrock fracture orientations.

Delta O-18 in
Precipitation and Meltwater

Round	Date	P1	C1	P2	P3	P4	M4	C4
		Rain	Snow	Rain	Snow	Rain	Melt	Snow
1	7/19/95	-5.113		-5.036	-4.852	-5.025		
2	7/27/95	-6.295		-6.162	-6.145	-5.655		
3	8/3/95	-3.503		-3.933	-5.28	-3.793		
4	8/11/95	-5.14		-3.615	-4.484			
5	8/18/95	-5.871		-6.186	-6.636	-7.094		
6	8/25/95	-6.106		-6.359	-6.733	-6.442		
7	9/7/95	-7.513			-7.401	-6.244		
8	9/14/95	-6.561		-6.086	-6.77	-6.335		
9	9/24/95	-10.229		-10.669	-10.807	-10.089		
10	10/5/95	-8.222		-8.147	-8.23	-8.556		
11	10/12/95	-11.963		-11.963	-12.293	-12.089		
12	10/19/95	-9.373		-10.295	-10.054			
13	10/26/95	-8.601		-6.924	-7.975	-7.826		
14	11/2/95	-10.337		-10.384	-10.703	-10.291		
15	11/11/95	-12.334		-12.881		-11.95		
16	11/18/95	-15.494				-11.244		
17	11/30/95						-14.83	
18	12/13/95		-14.751					-15.685
19	12/21/95		-18.631					-19.467
20	1/4/96		-21.324				-17.048	-21
21	1/15/96		-22.825					-21.696
22	1/22/96						-11.128	
23	1/30/96		-11.221				-10.992	-12.901
24	2/13/96		-19.554				-11.684	-23.002
25	2/24/96						-11.717	
26	3/9/96		-28.046				-10.552	-24.479
27	3/16/96							-18.051
28	3/27/96						-14.315	
29	4/5/96						-9.843	
30	4/18/96						-16.608	-19.947
31	4/23/96						-9.168	
32	4/30/96	-10.047					-9.34	
33	5/6/96	-8.747					-10.38	
34	5/11/96					-6.332		
35	5/14/96	-12.187				-17.299		
36	5/23/96							
37	5/30/96	-8.29		-10.845	-12.748	-8.809		
38	6/6/96	-4.8		-6.308	-4.201	-4.814		
39	6/13/96	-6.742		-7.07	-6.748	-7.164		
40	6/20/96	-7.855		-8.482	-8.929	-9.115		
41	6/29/96	-8.568		-8.418	-9.31	-9.109		
42	7/10/96	-8.824		-8.069	-10.411	-7.67		
43	7/17/96					-10.426		
44	7/24/96					-8.242		
45	7/31/96					-8.396		
46	8/6/96					-8.449		
47	8/13/96					-3.651		

Delta O-18 in
Precipitation and Meltwater

Round	Date	P1	C1	P2	P3	P4	M4	C4
		Rain	Snow	Rain	Snow	Rain	Melt	Snow
48	8/20/96					-7.312		
49	8/26/96					-5.312		
50	9/9/96					-7.642		
51	9/16/96					-9.079		
52	9/23/96					-9.485		
53	9/30/96					-10.192		
54	10/10/96					-15.436		
55	10/23/96					-13.94		
56	11/3/96					-9.413		
57	11/10/96					-7.212		
58	11/17/96					-19.637		
59	11/24/96					-18.661		
60	12/2/96					-13.048		

Delta O-18 in
Precipitation and Meltwater

Round	Date	P6	M6	C6	CC6	P7	M7	C7
		Rain	Melt	Snow	Pack	Rain	Melt	Snow
1	7/19/95	-6.171						
2	7/27/95	-6.769				-6.043		
3	8/3/95	-4.215				-6.711		
4	8/11/95	-6.243				-4.647		
5	8/18/95	-7.376				-7.405		
6	8/25/95	-8.618				-7.794		
7	9/7/95	-7.295				-8.874		
8	9/14/95	-7.391				-8.231		
9	9/24/95	-11.251				-8.231		
10	10/5/95	-9.78				-11.382		
11	10/12/95	-13.038				-10.434		
12	10/19/95	-9.384				-13.937		
13	10/26/95	-8.114				-8.948		
14	11/2/95	-11.537				-8.784		
15	11/11/95	-12.813				-13.752		
16	11/18/95	-9.946				-13.146		
17	11/30/95		-14.014	-16.116		-9.302		
18	12/13/95			-11.249			-13.435	-16.054
19	12/21/95			-18.129	-18.874			-16.453
20	1/4/96			-20.631	-19.677			-17.222
21	1/15/96			-20.091	-20.115			-20.04
22	1/22/96		-18.486	-11.108	-14.785		-12.871	-17.767
23	1/30/96		-14.495	-13.415	-14.311			-12.93
24	2/13/96			-21.162	-20.818			-13.157
25	2/24/96		-12.432		-13.043			-23.581
26	3/9/96		-12.935	-21.415	-20.835			-19.682
27	3/16/96			-18.43	-17.535			-22.472
28	3/27/96				-16.169			
29	4/5/96		-13.409	-13.8	-15.085		-15.843	-14.892
30	4/18/96		-15.518	-17.383	-17.104			-14.73
31	4/23/96		-13.613		-14.269			
32	4/30/96		-9.538				-13.034	-14.175
33	5/6/96		-10.23				-13.89	
34	5/11/96		-7.226					
35	5/14/96	-17.272					-13.273	
36	5/23/96							
37	5/30/96	-8.386					-12.887	
38	6/6/96	-7.277				-7.288		
39	6/13/96	-7.822				-8.221		
40	6/20/96	-9.664				-10.347		
41	6/29/96	-9.412				-9.356		
42	7/10/96	-9.874				-10.372		
43	7/17/96	-11.561						
44	7/24/96	-10.76						
45	7/31/96	-11.222						
46	8/6/96	-9.937						
47	8/13/96	-4.752						

Delta O-18 in
Precipitation and Meltwater

Round	Date	P6	M6	C6	CC6	P7	M7	C7
		Rain	Melt	Snow	Snowpac	Rain	Melt	Snow
48	8/20/96	-8.255						
49	8/26/96	-5.739						
50	9/9/96	-8.715						
51	9/16/96	-9.547						
52	9/23/96	-9.552						
53	9/30/96	-10.446						
54	10/10/96	-17.954						
55	10/23/96	-14.784						
56	11/3/96	-9.026						
57	11/10/96	-6.952						
58	11/17/96	-18.582						
59	11/24/96	-18.943						
60	12/2/96	-13.888						

Delta O-18 in
Precipitation and Meltwater

Round	Date	P8	M8	C8	CC8	P9
		Rain	Melt	Snow	Pack	Rain
1	7/19/95	-7.082				-7.081
2	7/27/95	-7.462				-7.449
3	8/3/95	-5.296				-5.045
4	8/11/95	-5.591				-5.849
5	8/18/95	-8.337				-8.762
6	8/25/95	-16.955				-15.156
7	9/7/95	-8.947				-9.196
8	9/14/95	-8.917				-9.196
9	9/24/95	-11.591				-11.805
10	10/5/95	-11.413				-11.925
11	10/12/95	-14.313				-14.123
12	10/19/95	-10.796				-12.551
13	10/26/95	-8.262				-9.945
14	11/2/95	-14.399				-13.071
15	11/11/95	-13.117				-11.572
16	11/18/95	-11.306				-11.792
17	11/30/95		-14.059	-17.971		
18	12/13/95			-17.629	-17.628	
19	12/21/95			-18.251	-18.051	
20	1/4/96			-19.904	-19.46	
21	1/15/96		-17.454	-22.905	-20.23	
22	1/22/96		-17.871	-12.691	-16.188	
23	1/30/96			-11.024	-16.037	
24	2/13/96			-24.767	-19.167	
25	2/24/96			-15.018	-14.985	
26	3/9/96			-23.1	-20.571	
27	3/16/96					
28	3/27/96			-15.984	-17.139	
29	4/5/96		-17.877	-16.552	-18.107	
30	4/18/96					
31	4/23/96			-13.306	-18.119	
32	4/30/96		-13.516		-17.517	
33	5/6/96		-14.363		-18.123	
34	5/11/96					
35	5/14/96		-14.485		-19.177	
36	5/23/96					
37	5/30/96		-14.309		-16.502	
38	6/6/96		-9.917			
39	6/13/96	-8.31				
40	6/20/96	-10.925				-10.94
41	6/29/96	-11.24				-10.083
42	7/10/96	-11.844				-9.506
43	7/17/96					
44	7/24/96					
45	7/31/96					
46	8/6/96					
47	8/13/96					

Delta O-18 in
Precipitation and Meltwater

Round	Date	P8	M8	C8	CC8	P9
		Rain	Melt	Snow	Snowpac	Rain
48	8/20/96					
49	8/26/96					
50	9/9/96					
51	9/16/96					
52	9/23/96					
53	9/30/96					
54	10/10/96					
55	10/23/96					
56	11/3/96					
57	11/10/96					
58	11/17/96					
59	11/24/96					
60	12/2/96					

Delta O-18 in
Groundwater

Round	Date	GW1	GW2	GW3	GW4	GW5	GW6
12	10/19/95	-10.504	-8.91	-12.06	-11.306	-12.194	-12.51
13	10/26/95	-10.47	-9.75	-11.85	-11.34	-12.05	-11.92
14	11/2/95						
15	11/11/95	-10.733		-11.383	-11.157	-11.914	-11.76
16	11/18/95						
17	11/30/95	-11.158	-10.248	-11.836	-11.094	-11.059	-11.528
18	12/13/95			-11.863	-11.134	-11.071	-11.337
19	12/21/95			-13.313		-11.061	-11.321
20	1/4/96			-11.67		-12.042	-12.035
21	1/15/96	-11.505		-11.747		-11.374	-11.096
22	1/22/96	-12.67		-11.746	-11.075	-11.739	-11.249
23	1/30/96			-12.88	-10.84	-10.963	-11.241
24	2/13/96			-11.85		-10.977	-11.385
25	2/24/96	-15.073		-11.814	-11.186	-12.144	-10.895
26	3/9/96	-11.992		-11.811		-11.06	-11.128
27	3/16/96	-12.446		-11.941		-11.174	-10.933
28	3/27/96	-12.739		-12.674	-11.069	-11.13	-11.581
29	4/5/96	-12.528		-11.782	-10.866	-11.192	-11.015
30	4/18/96	-12.989		-11.336	-11.215	-11.58	-10.912
31	4/23/96	-14.093		-12.763	-11.285	-11.55	-11.182
32	4/30/96	-13.311		-11.785	-11.316	-11.738	-11.162
33	5/6/96	-10.699		-11.791		-11.729	-11.402
34	5/11/96	-13.323		-11.778	-11.304	-11.751	-11.371
35	5/14/96						
36	5/23/96	-13.134		-12	-11.503	-11.996	-11.531
37	5/30/96	-12.817		-11.817	-11.453	-11.859	-11.547
38	6/6/96	-12.73		-11.769	-11.478	-11.881	-11.625
39	6/13/96	-11.869		-11.815	-11.543	-11.805	-11.624
40	6/20/96	-11.944	-11.724	-11.814	-11.468	-11.868	-11.707
41	6/29/96	-11.883		-11.74	-11.476	-11.735	-11.634
42	7/10/96	-11.415		-11.776	-11.51	-11.748	-11.667
43	7/17/96	-12.885		-11.787	-11.584	-11.766	-11.666
44	7/24/96	-11.717		-12.031	-11.596	-11.719	-11.688
45	7/31/96	-11.759		-12.037	-11.582	-11.733	-11.665
46	8/6/96	-11.585		-11.703	-11.571	-11.636	-11.596
47	8/13/96	-11.655		-11.729	-11.591	-11.614	
48	8/20/96	-11.723		-11.789	-11.653	-11.656	-11.644
49		-11.071		-11.766	-11.702	-11.638	-11.6
50	9/9/96	-11.461		-11.774	-11.733	-11.639	-11.621
51	9/16/96	-11.496		-11.776	-11.729	-11.683	-11.623
52	9/23/96	-11.52		-11.791	-11.665	-11.861	-11.581
53	9/30/96	-10.258		-11.801	-11.672	-11.67	-11.638
54	10/10/96	-11.029		-11.785	-11.535	-11.637	-11.319
55	10/23/96	-11.588		-11.769	-11.489	-11.639	-11.65
56	11/3/96			-11.75		-11.332	-11.571
57	11/10/96	-11.101		-11.963	-11.446	-11.758	-11.199
58	11/17/96	-11.85		-11.753	-11.642	-11.902	-11.552
59	11/24/96	-11.576		-12.255	-11.222	-11.262	-11.441
60	12/2/96	-12.108	-11.068	-11.366	-11.213	-11.602	-11.703
61	12/9/96						

Delta O-18 in
Groundwater

Round	Date	GW7	GW7b	GW8	GW9
12	10/19/95	-11.875		-11.337	
13	10/26/95			-11.39	
14	11/2/95				
15	11/11/95	-11.786			
16	11/18/95				
17	11/30/95	-11.85		-11.415	
18	12/13/95	-10.98		-11.394	
19	12/21/95	-12.012		-11.402	-10.883
20	1/4/96			-11.211	
21	1/15/96	-12.504		-11.071	-9.817
22	1/22/96	-11.729		-11.299	
23	1/30/96	-11.575		-11.433	
24	2/13/96	-11.966		-11.416	-10.31
25	2/24/96	-12.106		-12.057	-9.731
26	3/9/96	-11.839		-11.345	
27	3/16/96			-11.334	
28	3/27/96	-11.712		-11.142	
29	4/5/96	-10.781		-11.254	
30	4/18/96	-12.045		-11.268	
31	4/23/96	-12.997		-11.327	
32	4/30/96	-11.669		-11.314	
33	5/6/96	-11.808		-11.256	
34	5/11/96	-11.729		-11.182	
35	5/14/96				
36	5/23/96	-11.803		-11.252	
37	5/30/96	-11.2		-11.607	
38	6/6/96	-11.938		-11.233	
39	6/13/96	-11.808		-11.194	
40	6/20/96	-11.754	-11.537	-11.184	
41	6/29/96	-11.624		-11.102	
42	7/10/96	-11.63		-11.105	
43	7/17/96	-11.657		-10.963	
44	7/24/96		-11.471		
45	7/31/96	-11.695		-11.028	
46	8/6/96	-11.611		-10.939	
47	8/13/96		-11.469	-10.938	
48	8/20/96	-11.854		-10.979	
49		-12.019		-10.929	
50	9/9/96	-11.778		-10.923	
51	9/16/96	-11.744		-10.997	
52	9/23/96	-11.799		-11.045	
53	9/30/96	-11.878		-10.853	
54	10/10/96	-11.555		-10.853	
55	10/23/96	-11.591		-11.392	
56	11/3/96	-12.035		-10.794	
57	11/10/96		-11.317	-10.881	
58	11/17/96	-11.654			
59	11/24/96		-11.269	-11.598	
60	12/2/96		-11.411	-10.8	
61	12/9/96				

Delta 2-H (Deuterium) and Delta 18-O in Rain (P6) and Groundwater (GW1,3,5)

Round	Date	P6 18O	P6 2H	GW1 18O	GW1 2H	GW3 18O	GW3 2H
1	7/19/95	-6.171					
2	7/27/95	-6.769					
3	8/3/95	-4.215					
4	8/11/95	-6.243					
5	8/18/95	-7.376					
6	8/25/95	-8.618					
7	9/7/95	-7.295					
8	9/14/95	-7.391					
9	9/24/95	-11.251					
10	10/5/95	-9.78					
11	10/12/95	-13.038					
12	10/19/95	-9.384	-60.92	-10.504	-69.68	-12.06	-81.1
13	10/26/95	-8.114		-10.47	-67.01	-11.85	-81.26
14	11/2/95	-11.537					
15	11/11/95	-12.813	-83.55	-10.733	-69.87	-11.383	
16	11/18/95	-9.946					
17	11/30/95	-16.116	-111.93	-11.158	-73.52	-11.836	-80.73
18	12/13/95	-11.249				-11.863	
19	12/21/95	-18.129	-124.94			-13.313	-81.58
20	1/4/96	-20.631				-11.67	
21	1/15/96	-20.091	-143.13	-11.505	-76.85	-11.747	-80.82
22	1/22/96	-11.108		-12.67	-83.77	-11.746	
23	1/30/96	-13.415	-82.28			-12.88	-81.13
24	2/13/96	-21.162				-11.85	
25	2/24/96	-12.432		-15.073	-87.860	-11.814	-80.92
26	3/9/96	-21.415	-154.72	-11.992	-80.49	-11.811	
27	3/16/96	-18.43		-12.446	-81.58	-11.941	-81.39
28	3/27/96			-12.739		-12.674	
29	4/5/96	-13.8	-104.95	-12.528	-82.95	-11.782	-81.34
30	4/18/96	-17.383		-12.989		-11.336	
31	4/23/96	-13.613	-98.51	-14.093	-96.94	-12.763	-81.23
32	4/30/96	-9.538		-13.311		-11.785	
33	5/6/96	-10.23	-68.75	-10.699	-70.21	-11.791	-81.37
34	5/11/96	-7.226		-13.323	-90.05	-11.778	-81.16
35	5/14/96	-17.272	-130.92				
36	5/23/96			-13.134		-12	
37	5/30/96	-8.386		-12.817	-86.93	-11.817	-80.88
38	6/6/96	-7.277		-12.73		-11.769	
39	6/13/96	-7.822		-11.869	-80.04	-11.815	-80.99
40	6/20/96	-9.664	-60.81	-11.944		-11.814	
41	6/29/96	-9.412		-11.883	-79.31	-11.74	-81.01
42	7/10/96	-9.874	-67.77	-11.415		-11.776	
43	7/17/96	-11.561		-12.885	-80.36	-11.787	-80.98
44	7/24/96	-10.76	-75.2	-11.717		-12.031	
45	7/31/96	-11.222		-11.759	-78.7	-12.037	-81.55
46	8/6/96	-9.937	-64.9	-11.585		-11.703	
47	8/13/96	-4.752		-11.655	-79.08	-11.729	-80.41

note: Samples measured from Round 31 and 33 at P6 were meltwater samples

Delta 2-H (Deuterium) and Delta 18-O in Rain (P6) and Groundwater (GW1,3,5)

Round	Date	P6 18O	P6 2H	GW1 18O	GW1 2H	GW3 18O	GW3 2H
48	8/20/96	-8.255	-53.57	-11.723		-11.789	
49	8/26/96	-5.739		-11.071	-74.04	-11.766	-81.13
50	9/9/96	-8.715	-59.79	-11.461		-11.774	
51	9/16/96	-9.547		-11.496	-76.19	-11.776	-81.15
52	9/23/96	-9.552	-62.02	-11.52		-11.791	
53	9/30/96	-10.446		-10.258	-71.97	-11.801	-80.71
54	10/10/96	-17.954	-129.28	-11.029		-11.785	
55	10/23/96	-14.784		-11.588	-78.63	-11.769	-81.07
56	11/3/96	-9.026	-51.94			-11.75	
57	11/10/96	-6.952		-11.101	-74.24	-11.963	-81.15
58	11/17/96	-18.582	-127.64	-11.85		-11.753	
59	11/24/96	-18.943	-135.88	-11.576	-78.8	-12.255	-81.54
60	12/2/96	-13.888	-94.11	-12.108		-11.366	

Delta 2-H (Deuterium) and Delta 18-O in Rain (P6) and Groundwater (GW1,3,5)

Round	Date	GW5 18O	GW5 2H
1	7/19/95		
2	7/27/95		
3	8/3/95		
4	8/11/95		
5	8/18/95		
6	8/25/95		
7	9/7/95		
8	9/14/95		
9	9/24/95		
10	10/5/95		
11	10/12/95		
12	10/19/95	-12.194	-82.63
13	10/26/95	-12.05	-82.44
14	11/2/95		
15	11/11/95	-11.914	-80.65
16	11/18/95		
17	11/30/95	-11.059	-74.32
18	12/13/95	-11.071	
19	12/21/95	-11.061	-74.68
20	1/4/96	-12.042	
21	1/15/96	-11.374	-73.65
22	1/22/96	-11.739	
23	1/30/96	-10.963	-76.23
24	2/13/96	-10.977	
25	2/24/96	-12.144	-74.38
26	3/9/96	-11.06	
27	3/16/96	-11.174	-75.47
28	3/27/96	-11.13	
29	4/5/96	-11.192	-76.14
30	4/18/96	-11.58	
31	4/23/96	-11.55	-78.54
32	4/30/96	-11.738	
33	5/6/96	-11.729	-79.95
34	5/11/96	-11.751	-80.54
35	5/14/96		
36	5/23/96	-11.996	
37	5/30/96	-11.859	-81.31
38	6/6/96	-11.881	
39	6/13/96	-11.805	-80.89
40	6/20/96	-11.868	
41	6/29/96	-11.735	-81.09
42	7/10/96	-11.748	
43	7/17/96	-11.766	-81.08
44	7/24/96	-11.719	
45	7/31/96	-11.733	-80.66
46	8/6/96	-11.636	
47	8/13/96	-11.614	-80.06

Delta 2-H (Deuterium) and Delta 18-O in Rain (P6) and Groundwater (GW1,3,5)

Round	Date	GW5 18O	GW5 2H
48	8/20/96	-11.656	
49	8/26/96	-11.638	-80.22
50	9/9/96	-11.639	
51	9/16/96	-11.683	-79.7
52	9/23/96	-11.861	
53	9/30/96	-11.67	-80.34
54	10/10/96	-11.637	
55	10/23/96	-11.639	-80.31
56	11/3/96	-11.332	
57	11/10/96	-11.758	-80.62
58	11/17/96	-11.902	
59	11/24/96	-11.262	-81.39
60	12/2/96	-11.602	

Tritium measurements in Groundwater
6/20/96 Round 40

Location	Tritium, T.U. from 6/20/96 (Round 40)	laboratory precision (+/-) per mil
GW1	15.8	1.3
GW2	15.9	1.3
GW3	26.7	1.9
GW4	14.6	1.2
GW5	15.9	1.2
GW6	15.2	1.2
GW7	6.5	0.7
GW7b	14.7	1.2
GW8	15.4	1.2

Mount Mansfield Fracture Measurements 10/20/96

strike from N 0 E	dip (right hand)		strike from N 0 E	dip (right hand)		strike from N 0 E	dip (right hand)
129	54		79	78		319	64
150	60		103	88		116	-72
159	31		142	-75		130	30
159	27		82	90		62	88
192	85		86	-87		62	88
194	24		22	62		12	-76
152	16		90	90		58	90
152	89		62	88		60	70
210	-89		70	90		80	87
300	-60		302	90		36	72
340	-72		310	90		44	90
39	90		75	90		3	-40
40	74		345	66		140	16
60	-68		72	78		8	-50
38	85		62	76		8	70
22	90		68	67		20	-40
38	90		12	90		113	-58
39	-89		154	-60		30	90
3	-86		178	90		43	90
82	90		142	90		78	90
0	90		118	90		358	20
96	-78		100	-85		76	90
102	85		185	90		350	-62
50	90		80	-70		65	90
91	90		350	65			
100	90		30	-58			
358	58		143	78			
0	55		110	-68			
328	90		78	85			
72	82		172	-65			
62	90		113	68			
342	-82		175	87			
42	90		120	90			
95	75		100	90			
17	70		108	90			
72	-80		198	-65			
2	-84		102	90			
312	-52		22	74			
342	50		42	67			
55	65		78	90			
90	90		342	58			
355	68		67	-60			
90	-89		97	90			
129	89		11	39			
349	79		99	90			
55	82		172	60			
72	-82		63	90			

APPENDIX B - MODEL DOCUMENTATION

Printouts of the documentation for the STELLA model described in Chapter 4 of this thesis are included. The documentation contains the governing equations for each model relationship, as well as brief text descriptions of each component. This information can be used by others to add their own findings in an effort to improve this model, or to apply the model to other settings.

Stella Documention

Stocks and Flows

Local_Recharge(t) = Local_Recharge(t - dt) + (Local_Cover_Transport) * dt
INIT Local_Recharge = 0
Represents the cumulative infiltration of water to bedrock near the well.
INFLOWS:
Local_Cover_Transport = .1*Local_Soil_Sat-Local_Sed_Thick
Water infiltration to bedrock in the vicinity of the well. Controlled by the saturation of soil and the thickness of overlying sediments. This flow is transferred to the groundwater mixing model to represent shallow flow to the well.

Local_Snowpack(t) = Local_Snowpack(t - dt) + (Local_Snow - Local_Snowmelt) * dt
INIT Local_Snowpack = 100
Accumulation of snow. Controlled by temperature, balance between falling snow and melting in the vicinity of the well.
INFLOWS:
Local_Snow = IF (Temp_Record<=0)
THEN
(Precip_Record*(1+(.01*(800-Local_Elev))))
ELSE 0
The amount of precipitation falling as snow. Based on temperature at the well elevation.
OUTFLOWS:
Local_Snowmelt = IF
Local_Snowpack>0
AND
Temp_Record>0
THEN (.1*Local_Snowpack)
ELSE
0
Controlled by temperature. Depletes the snowpack stock in the vicinity of the well.

Local_Soil_Sat(t) = Local_Soil_Sat(t - dt) + (Local_Rain + Local_Snowmelt - Local_Cover_Transport - Local_Soil_Losses) * dt
INIT Local_Soil_Sat = 50
Degree of saturation of the soil in the vicinity of the well. Controls infiltration and runoff.
INFLOWS:
Local_Rain = IF (Temp_Record>0)
THEN
(Precip_Record*(1+(.01*(800-Local_Elev))))
ELSE 0
The amount of precipitation falling as rain. Based on temperature at the elevation of the well.

Local_Snowmelt = IF
Local_Snowpack>0
AND
Temp_Record>0
THEN (.1*Local_Snowpack)
ELSE
0
Controlled by temperature. Depletes the snowpack stock in the vicinity of the well.
OUTFLOWS:
Local_Cover_Transport = .1*Local_Soil_Sat-Local_Sed_Thick
Water infiltration to bedrock in the vicinity of the well. Controlled by the saturation of soil and the thickness of overlying sediments. This flow is transferred to the groundwater mixing model to represent shallow flow to the well.
Local_Soil_Losses = .8*(Local_Runoff+.4*(Local_Tree_Uptake)+.5*Local_Evap)
Sum of runoff, tree uptake and evaporation. Represents the water that does not enter the bedrock in the vicinity of the well.

Upld_Recharge(t) = Upld_Recharge(t - dt) + (Upld_Cover_Transport) * dt
INIT Upld_Recharge = 0
Represent the cumulative infiltration of water to bedrock from the upland recharge area or areas.
INFLOWS:
Upld_Cover_Transport = .1*Upld_Soil_Sat-Upld_Sed_Thick
Water infiltration to bedrock in the area of upland recharge. Controlled by the saturation of soil and the thickness of overlying sediments. This flow is transferred to the groundwater mixing model to represent deep flow to the well.

Upld_Snowpack(t) = Upld_Snowpack(t - dt) + (Upld_Snow - Upld_Snowmelt) * dt
INIT Upld_Snowpack = 100
Accumulation of snow in the area of upland recharge. Controlled by temperature, balance between falling snow and melting.
INFLOWS:
Upld_Snow = IF (Temp_Record<=0)
THEN
(Precip_Record*(1+(.014*(1330-Upld_Rech_Elev))))
ELSE 0
The amount of precipitation falling as snow. Based on temperature at the upland recharge elevation.
OUTFLOWS:
Upld_Snowmelt = IF
Upld_Snowpack>0
AND
Temp_Record>0
THEN (.1*Upld_Snowpack)

ELSE
0
Controlled by temperature. Depletes the snowpack stock in the area of upland recharge.

Upld_Soil_Sat(t) = Upld_Soil_Sat(t - dt) + (Upld_Rain + Upld_Snowmelt - Upld_Cover_Transport - Upld_Soil_Losses) * dt
INIT Upld_Soil_Sat = 50
Degree of saturation of the soil in the area of upland recharge. Controls infiltration and runoff.
INFLOWS:
Upld_Rain = IF (Temp_Record>0)
THEN
(Precip_Record*(1+(.02*(1330-Upld_Rech_Elev))))
ELSE 0
The amount of precipitation falling as rain. Based on temperature at the upland recharge elevation.
Upld_Snowmelt = IF
Upld_Snowpack>0
AND
Temp_Record>0
THEN (.1*Upld_Snowpack)
ELSE
0
Controlled by temperature. Depletes the snowpack stock in the area of upland recharge.
OUTFLOWS:
Upld_Cover_Transport = .1*Upld_Soil_Sat-Upld_Sed_Thick
Water infiltration to bedrock in the area of upland recharge. Controlled by the saturation of soil and the thickness of overlying sediments. This flow is transferred to the groundwater mixing model to represent deep flow to the well.
Upld_Soil_Losses = .8*(Upld_Runoff+.4*(Upld_Tree_Uptake)+.5*Upld_Evap)
Sum of runoff, tree uptake and evaporation. Represents the water that does not enter the bedrock in the area of upland recharge.

Well(t) = Well(t - dt) + (Deep_Transport + Shallow_Infiltration - Pumping - Flowthrough) * dt
INIT Well = 0
Sum of water entering the well from deep bedrock flow and local infiltration. The deeper water has resided for perhaps several years in the bedrock and has a fairly constant 18O signature, while local infiltration may occur rapidly (days), affecting the 18O of the well.
INFLOWS:
Deep_Transport = Upld_Cover_Transport*Aquifer_Conductivity
The flux of deep water through bedrock and to the well. Determined from the upland recharge model.
Shallow_Infiltration = Local_Cover_Transport

The flux of water though shallow fractures in the bedrock and to the well. Determined from the local recharge model.

OUTFLOWS:

Pumping = .2*Well

Withdrawal of water from the well for residential use.

Flowthrough = Well-Pumping

Water not used may continue through the well and downgradient through bedrock.

Converters

Aquifer_Conductivity = 1

The hydraulic conductivity of the bedrock aquifer. Initially entered based on literature values.

Deep_18O_Flux = Well_Mean_18O*Upld_Cover_Transport

The influence of deep flow on groundwater 18O in the well. Based on the mean 18O, which is believed to be the deep signature, and the flux of deep water from the upland recharge model.

Local_Elev = 742

The local recharge elevation, represents the elevation of recharge to groundwater in the vicinity of particular well. This value is entered as the elevation of the well.

Local_Evap = IF Temp_Record>=0
THEN .01*(800-Local_Elev)*Temp_Record
ELSE 0

Evaporation in the area near the well. Function of temperature.

Local_Runoff = Local_Rain+Local_Snowmelt-(100-Local_Soil_Sat)

Sum of rain and snowmelt that cannont infiltrate in the vicinity of the well. Function of soil saturation.

Local_Sed_Thick = .01*(800-Local_Elev)

Thickness of sediments overlying bedrock near the well. Changes according to the elevation of the well.

Local_Tree_Type = (800-Local_Elev)

The predominant tree type in the area near the well. Determined by elevation. Controls rates of transpiration.

Local_Tree_Uptake = IF Temp_Record>12
THEN 3*(3*(Temp_Record)+.5*Local_Tree_Type)*(1-15/Temp_Record)
ELSE 0

Withdrawal of water from soil and/or interception of falling rainin the vicinity of the well. Function of tree type, temperature.

Shallow_18O = (.14*Temp_Record-12.9)+2
The approximate 18O value of locally recharging water, based on the relationship between temperature and 18O in precipitation (from literature, or as observed in study area)

Shallow_18O_Flux = Local_Cover_Transport*Shallow_18O
The influence of local flow on groundwater 18O in the well. Based on the 18O of precip, and the flux of shallow water from the local recharge model.

Upld_Evap = IF Temp_Record>=30
THEN .01*(800-Upld_Rech_Elev)*Temp_Record
ELSE 0
Evaporation in the upland recharge area. Function of temperature.

Upld_Rech_Elev = -398.422*Well_Mean_18O-4002.55
The upland recharge elevation, represents a minimum elevation of recharge to groundwater supplying a particular well. Calculated based on the relationship between precipitation 18O and elevation.

Upld_Runoff = Upld_Rain+Upld_Snowmelt-(100-Upld_Soil_Sat)
Sum of upland rain and snowmelt that cannont infiltrate. Function of soil saturation.

Upld_Sed_Thick = .01*(800-Upld_Rech_Elev)
Thickness of upland sediments overlying bedrock. Changes according to elevation.

Upld_Tree_Type = (800-Upld_Rech_Elev)
The predominant tree type in the upland recharge area. Determined by elevation. Controls rates of transpiration.

Upld_Tree_Uptake = if Temp_Record>10 then
(3*(Temp_Record)+Upld_Tree_Type)
else 0
Withdrawal of water from soil and/or interception of falling rain in the upland recharge area. Function of tree type, temperature.

Well_18O_Record =
(.5*Shallow_18O_Flux+Deep_18O_Flux)/(.5*Local_Cover_Transport+Upld_Cover_Transport)
The combined influence of deep flow and local infiltation flow on groundwater 18O in the well. The parameter, calculated during each simulation, results in a temporal record of simulated well 18O. This can be compared to actual measurements in order to calibrate the model.

Well_Mean_18O = -12.147

Must be input for each simulation. Based on actual monitoring of temporal 18O in wells.

Time Series Inputs

Precip_Record = GRAPH(TIME) (day, precip. in mm)
(1.00, 0.5), (2.00, 0.5), (3.00, 1.02), (4.00, 0.92), (5.00, 0.78), (6.00, 0.78), (7.00, 0.78), (8.00, 0.06), (9.00, 0.12), (10.0, 0.22), (11.0, 0.22), (12.0, 0.32), (13.0, 0.78), (14.0, 1.18), (15.0, 1.18), (16.0, 1.24), (17.0, 1.14), (18.0, 0.68), (19.0, 0.22), (20.0, 4.94), (21.0, 4.94), (22.0, 4.94), (23.0, 4.94), (24.0, 5.34), (25.0, 2.44), (26.0, 2.48), (27.0, 2.48), (28.0, 8.58), (29.0, 8.18), (30.0, 6.20), (31.0, 6.10), (32.0, 6.10), (33.0, 0.00), (34.0, 0.00), (35.0, 0.00), (36.0, 0.00), (37.0, 0.06), (38.0, 0.06), (39.0, 0.06), (40.0, 0.56), (41.0, 2.84), (42.0, 2.78), (43.0, 3.38), (44.0, 3.44), (45.0, 2.94), (46.0, 0.72), (47.0, 0.72), (48.0, 0.22), (49.0, 0.22), (50.0, 0.52), (51.0, 0.46), (52.0, 0.46), (53.0, 0.96), (54.0, 1.00), (55.0, 0.7), (56.0, 2.68), (57.0, 5.06), (58.0, 4.46), (59.0, 4.36), (60.0, 6.08), (61.0, 4.10), (62.0, 1.78), (63.0, 1.78), (64.0, 2.14), (65.0, 0.42), (66.0, 1.28), (67.0, 1.68), (68.0, 1.68), (69.0, 1.32), (70.0, 1.32), (71.0, 0.46), (72.0, 0.00), (73.0, 0.00), (74.0, 0.00), (75.0, 0.00), (76.0, 0.00), (77.0, 0.00), (78.0, 0.00), (79.0, 0.86), (80.0, 1.26), (81.0, 1.98), (82.0, 2.18), (83.0, 2.18), (84.0, 1.32), (85.0, 2.08), (86.0, 1.36), (87.0, 1.16), (88.0, 1.16), (89.0, 1.16), (90.0, 0.00), (91.0, 0.16), (92.0, 0.92), (93.0, 0.92), (94.0, 0.92), (95.0, 0.92), (96.0, 0.76), (97.0, 0.96), (98.0, 3.40), (99.0, 3.50), (100, 5.54), (101, 6.50), (102, 5.80), (103, 5.08), (104, 7.52), (105, 5.94), (106, 9.30), (107, 13.7), (108, 12.1), (109, 9.56), (110, 9.40), (111, 9.20), (112, 5.50), (113, 11.5), (114, 13.5), (115, 13.7), (116, 13.1), (117, 13.2), (118, 7.06), (119, 5.12), (120, 8.92), (121, 5.42), (122, 4.36), (123, 5.94), (124, 8.32), (125, 4.46), (126, 4.46), (127, 4.46), (128, 2.88), (129, 0.4), (130, 4.68), (131, 10.7), (132, 15.6), (133, 15.7), (134, 15.7), (135, 11.0), (136, 5.08), (137, 0.16), (138, 3.04), (139, 3.70), (140, 3.70), (141, 6.30), (142, 6.30), (143, 3.56), (144, 3.16), (145, 3.16), (146, 0.46), (147, 0.46), (148, 0.32), (149, 2.44), (150, 3.30), (151, 3.30), (152, 3.30), (153, 3.24), (154, 1.06), (155, 0.56), (156, 0.56), (157, 0.56), (158, 7.26), (159, 7.32), (160, 7.02), (161, 7.12), (162, 7.12), (163, 1.90), (164, 8.54), (165, 8.68), (166, 8.78), (167, 8.78), (168, 7.30), (169, 0.4), (170, 0.2), (171, 0.00), (172, 0.66), (173, 2.34), (174, 3.10), (175, 3.16), (176, 5.34), (177, 4.68), (178, 4.42), (179, 3.66), (180, 3.70), (181, 2.84), (182, 2.84), (183, 1.42), (184, 2.34), (185, 12.8), (186, 12.2), (187, 12.6), (188, 12.6), (189, 12.3), (190, 3.36), (191, 4.52), (192, 4.16), (193, 4.16), (194, 5.98), (195, 5.84), (196, 5.38), (197, 5.64), (198, 5.84), (199, 3.36), (200, 5.54), (201, 6.26), (202, 6.00), (203, 5.80), (204, 6.56), (205, 2.90), (206, 1.32), (207, 5.54), (208, 6.46), (209, 6.62), (210, 6.62), (211, 6.12), (212, 1.96), (213, 2.82), (214, 4.38), (215, 4.38), (216, 4.32), (217, 4.26), (218, 2.48), (219, 0.00), (220, 0.00), (221, 0.00), (222, 0.56), (223, 0.56), (224, 0.56), (225, 0.56), (226, 0.56), (227, 0.00), (228, 0.00), (229, 0.06), (230, 0.22), (231, 0.22), (232, 0.22), (233, 0.22), (234, 8.90), (235, 8.74), (236, 9.34), (237, 9.34), (238, 9.34), (239, 1.20), (240, 1.60), (241, 1.00), (242, 1.00), (243, 1.00), (244, 0.4), (245, 0.00), (246, 0.00), (247, 0.00), (248, 0.00), (249, 0.00), (250, 0.00), (251, 0.2), (252, 1.68), (253, 3.76), (254, 4.12), (255, 4.12), (256, 3.92), (257, 2.70), (258, 1.18), (259, 0.82), (260, 0.82), (261, 0.82), (262, 0.56), (263, 0.00), (264, 0.00), (265, 0.00), (266, 0.86), (267, 1.32), (268, 2.90), (269, 2.90), (270, 2.90), (271, 6.92), (272, 7.72), (273, 6.20), (274,

6.20), (275, 6.20), (276, 3.50), (277, 2.24), (278, 2.18), (279, 2.18), (280, 2.18), (281, 0.16), (282, 0.16), (283, 0.16), (284, 0.16), (285, 0.16), (286, 0.00), (287, 11.7), (288, 13.3), (289, 13.5), (290, 13.5), (291, 13.5), (292, 1.72), (293, 0.2), (294, 6.90), (295, 6.90), (296, 6.90), (297, 7.86), (298, 7.86), (299, 0.96), (300, 1.26), (301, 7.62), (302, 7.52), (303, 7.58), (304, 7.68), (305, 8.20), (306, 2.44), (307, 4.02), (308, 3.96), (309, 3.86), (310, 3.04), (311, 4.02), (312, 1.64), (313, 1.80), (314, 1.86), (315, 2.32), (316, 8.16), (317, 8.10), (318, 8.00), (319, 8.04), (320, 7.58), (321, 0.16), (322, 0.16), (323, 0.1), (324, 0.00), (325, 0.00), (326, 0.00), (327, 0.1), (328, 0.1), (329, 0.1), (330, 0.1), (331, 0.2), (332, 0.6), (333, 0.6), (334, 0.6), (335, 2.08), (336, 2.08), (337, 2.08), (338, 2.90), (339, 3.00), (340, 1.78), (341, 1.74), (342, 1.24), (343, 1.24), (344, 1.64), (345, 1.38), (346, 1.32), (347, 1.32), (348, 1.06), (349, 0.72), (350, 0.98), (351, 1.28), (352, 1.28), (353, 0.88), (354, 1.38), (355, 2.84), (356, 3.14), (357, 3.24), (358, 3.34), (359, 3.34), (360, 1.98), (361, 1.68), (362, 1.58), (363, 1.52), (364, 0.96), (365, 0.8)

Actual record of daily precipitation from the study area. This is data from the Proctor Maple Research Center in Underhill.

Temp_Record = GRAPH(TIME) (day, temp. in celcius)
(1.00, -6.86), (2.00, -8.82), (3.00, -11.1), (4.00, -14.6), (5.00, -18.4), (6.00, -20.5), (7.00, -21.2), (8.00, -21.5), (9.00, -19.5), (10.0, -17.3), (11.0, -15.5), (12.0, -12.8), (13.0, -9.92), (14.0, -8.82), (15.0, -6.88), (16.0, -7.56), (17.0, -8.04), (18.0, -5.60), (19.0, -2.18), (20.0, -0.96), (21.0, 0.36), (22.0, 0.86), (23.0, -0.68), (24.0, -2.84), (25.0, -3.04), (26.0, -3.44), (27.0, -3.42), (28.0, -2.90), (29.0, -5.00), (30.0, -7.72), (31.0, -6.30), (32.0, -7.74), (33.0, -11.2), (34.0, -11.6), (35.0, -13.6), (36.0, -16.5), (37.0, -16.8), (38.0, -16.2), (39.0, -14.9), (40.0, -10.9), (41.0, -7.02), (42.0, -4.96), (43.0, -2.42), (44.0, -4.84), (45.0, -8.88), (46.0, -11.0), (47.0, -12.4), (48.0, -14.2), (49.0, -12.6), (50.0, -11.3), (51.0, -11.0), (52.0, -8.00), (53.0, -4.52), (54.0, -2.08), (55.0, 1.26), (56.0, 3.98), (57.0, 3.28), (58.0, 1.04), (59.0, 0.14), (60.0, -0.4), (61.0, -3.78), (62.0, -4.80), (63.0, -6.32), (64.0, -7.16), (65.0, -8.80), (66.0, -8.92), (67.0, -10.4), (68.0, -11.0), (69.0, -9.54), (70.0, -9.58), (71.0, -8.88), (72.0, -4.82), (73.0, -0.42), (74.0, -0.44), (75.0, -0.18), (76.0, 1.34), (77.0, 0.42), (78.0, 0.12), (79.0, 0.7), (80.0, 2.20), (81.0, 2.26), (82.0, 0.6), (83.0, -1.54), (84.0, -0.36), (85.0, -0.52), (86.0, -1.86), (87.0, -1.48), (88.0, -0.44), (89.0, -2.54), (90.0, -2.40), (91.0, 0.72), (92.0, 1.40), (93.0, 0.66), (94.0, 0.34), (95.0, -0.02), (96.0, -1.14), (97.0, -0.86), (98.0, -0.52), (99.0, 0.02), (100, -0.14), (101, 0.3), (102, 0.9), (103, 1.30), (104, 1.54), (105, 2.60), (106, 2.38), (107, 1.56), (108, 1.96), (109, 4.32), (110, 6.76), (111, 8.90), (112, 11.5), (113, 13.0), (114, 10.7), (115, 8.76), (116, 8.98), (117, 7.08), (118, 5.66), (119, 6.62), (120, 7.14), (121, 6.20), (122, 7.54), (123, 8.84), (124, 9.36), (125, 9.06), (126, 8.40), (127, 8.58), (128, 9.02), (129, 10.0), (130, 10.8), (131, 11.3), (132, 9.54), (133, 7.70), (134, 6.36), (135, 6.60), (136, 7.10), (137, 9.12), (138, 11.7), (139, 14.3), (140, 16.3), (141, 17.5), (142, 18.4), (143, 17.8), (144, 15.5), (145, 12.4), (146, 11.0), (147, 10.4), (148, 10.6), (149, 10.1), (150, 10.0), (151, 10.7), (152, 11.8), (153, 12.9), (154, 15.1), (155, 17.1), (156, 17.7), (157, 17.3), (158, 16.3), (159, 16.1), (160, 16.3), (161, 16.9), (162, 18.2), (163, 19.6), (164, 20.0), (165, 20.1), (166, 19.8), (167, 18.3), (168, 17.7), (169, 17.9), (170, 17.8), (171, 17.7), (172, 18.3), (173, 17.7), (174, 16.9), (175, 16.5), (176, 15.7), (177, 14.4), (178, 13.8), (179, 13.7), (180, 13.9), (181, 14.6), (182, 16.3), (183, 18.0), (184, 18.7), (185, 18.4), (186, 18.4), (187, 17.5), (188,

16.8), (189, 17.4), (190, 18.0), (191, 17.3), (192, 17.5), (193, 17.8), (194, 17.2), (195, 17.6), (196, 19.1), (197, 19.6), (198, 19.7), (199, 20.6), (200, 20.3), (201, 18.5), (202, 17.7), (203, 17.4), (204, 16.9), (205, 17.2), (206, 18.9), (207, 19.3), (208, 18.9), (209, 18.4), (210, 17.7), (211, 17.3), (212, 17.3), (213, 17.0), (214, 16.8), (215, 17.1), (216, 17.3), (217, 17.7), (218, 18.9), (219, 20.4), (220, 21.6), (221, 22.3), (222, 22.2), (223, 21.0), (224, 19.0), (225, 17.8), (226, 17.0), (227, 16.6), (228, 17.4), (229, 18.5), (230, 18.6), (231, 18.4), (232, 18.2), (233, 18.3), (234, 18.5), (235, 19.0), (236, 19.4), (237, 19.7), (238, 19.5), (239, 18.9), (240, 17.9), (241, 17.5), (242, 17.5), (243, 16.2), (244, 16.4), (245, 17.2), (246, 17.5), (247, 17.9), (248, 19.3), (249, 19.9), (250, 20.1), (251, 20.0), (252, 19.1), (253, 18.5), (254, 17.7), (255, 17.0), (256, 16.6), (257, 16.4), (258, 15.7), (259, 15.0), (260, 14.4), (261, 13.7), (262, 13.3), (263, 13.2), (264, 13.5), (265, 13.5), (266, 12.5), (267, 11.6), (268, 10.2), (269, 8.94), (270, 8.54), (271, 10.0), (272, 10.8), (273, 11.3), (274, 12.3), (275, 13.1), (276, 10.5), (277, 8.44), (278, 7.36), (279, 6.38), (280, 5.80), (281, 7.86), (282, 10.3), (283, 12.2), (284, 13.1), (285, 13.8), (286, 15.2), (287, 16.1), (288, 15.2), (289, 13.3), (290, 10.9), (291, 9.52), (292, 8.02), (293, 9.14), (294, 11.2), (295, 11.9), (296, 11.8), (297, 13.1), (298, 11.8), (299, 10.4), (300, 11.0), (301, 10.7), (302, 7.96), (303, 6.24), (304, 4.76), (305, 3.20), (306, 2.74), (307, 4.28), (308, 4.50), (309, 4.34), (310, 4.36), (311, 3.30), (312, 1.14), (313, -0.38), (314, -0.54), (315, 1.14), (316, 0.26), (317, -0.36), (318, 1.22), (319, 2.02), (320, -0.28), (321, -0.78), (322, -0.72), (323, -1.20), (324, -1.62), (325, -0.96), (326, -0.62), (327, -0.5), (328, -1.56), (329, -2.66), (330, -3.32), (331, -2.80), (332, -2.60), (333, -3.16), (334, -4.06), (335, -4.16), (336, -6.02), (337, -6.62), (338, -4.96), (339, -4.20), (340, -4.54), (341, -4.18), (342, -6.12), (343, -7.38), (344, -8.56), (345, -10.6), (346, -11.9), (347, -11.7), (348, -12.1), (349, -10.4), (350, -8.32), (351, -7.02), (352, -6.56), (353, -7.64), (354, -9.74), (355, -11.5), (356, -11.4), (357, -10.2), (358, -8.60), (359, -7.28), (360, -6.80), (361, -7.52), (362, -8.06), (363, -8.06), (364, -7.58), (365, -6.48)

Actual record of daily air temperature (daily average) from the study area. This is data from the Proctor Maple Research Center in Underhill.